THE UNIVERSITY OF SHEFFIELD

Pounding Response of buildings under Earthquake Motions

Nava Farhadzadeh

A thesis submitted in partial fulfilment for the degree of

Doctor of Philosophy

The University of Sheffield

Faculty of Engineering

Department of Civil and Structural Engineering

Submission Date: 03/03/2023

To the kindest dad, I've ever seen…

Words can-not express how grateful I am that you are my dad and for everything you've given me, for courage, bravery, and a life full of great experiences…

To my loving mom…

For every sacrifice you've made for our family, for standing strong against every bitter moment of life we all went through and for keeping us a family

To Ava…

For your compromises, love, support, and for everything you went through alone when I should've been there…

To my best friend Behnam

For standing by my side, giving me hope & support, and for making my Ph.D. journey possible …

To Sogand

For always supporting me by being there by my side, I don't know what I would have done without you…

I love you all dearly…

Dedicated to my parents

تقدیم به پدر و مادر عزیزم که بزرگترین دلگرمی زندگی من هستند

تا برده رنج گنج میسر نمی شود مزد آن گرفت جان برادر که کار کرد

$$\mathcal{Nawa} = \int_{1988}^{2006} \int_{2006}^{2014} \int_{2014}^{2023} \int_{2023}^{?} life\ dt.dt.dt.dt$$

Abstract

Structural pounding occurs when two or more structures with insufficient separation distances in between collide under earthquake loading. It occurs as a result of out-of-phase responses of structures due to differences in their dynamic properties. Seismic pounding damage has been observed in several earthquakes such as Mexico City earthquake in 1985 (Rosenblueth and Meli, 1986), Loma Prieta in 1989 (Kasai and Maison, 1997), and more recently Gorkha earthquake in 2015 (Shrestha and Hao, 2018).

The extent of seismic pounding damage ranges from minor crushing to catastrophic collapse of the colliding structure, even though recent design codes provide guidance on mandatory separation gaps to prevent pounding; still, in dense metropolitan areas with growing populations and constructors willing to make the maximum use of available lands, structural pounding is becoming a significant matter that needs attention in the design of new buildings.

Over the past decades, simulating structural pounding and assessing the resultant pounding forces have attracted the attention of many researchers. Simulating pounding between two structures and the extent of pounding damage started from a simple model that could only estimate the elasticity and plasticity of a damage using the pre- and post-impact velocities.

The research gradually evolved to analytical force-based models called contact element models (other names are impact element or gap friction element models) that simulate pounding between structures idealised as lumped masses. These models have been widely used and modified numerous times; however, they suffer from a lot of uncertainties associated with their contact parameters (i.e contact stiffness, coefficient of restitution, and damping ratio) as proper methods/formulas to calculate the parameters for contact between flat surfaces do not exist.

Progressively, these force-based models were implemented in commercial software as gap elements to model structural pounding. In this method of modelling, the gap elements were placed between the colliding structures to measure contact forces. Within the gap element approach, contact parameters have to be defined in advance and be inputted into the gap element before the start of the simulation, and yet the uncertainties with selecting suitable contact parameters persist. The selection of contact parameters influences the pounding response of the structures significantly. Therefore, diverse results are obtained from the existing methods of modelling pounding (Khatiwada and Chouw, 2014).

This research work intends to develop a methodology that properly simulates building pounding using the Finite Element Method (FEM). In this methodology, pounding between buildings is modelled using a penalty-based method. Using the proposed FE method, there is no need to define/ or assume contact parameters in advance and the reliability of the simulation is based on the material models used in the simulation. Unlike the existing lumped mass contact models with pre-defined contact points and limited locations to extract data, in the FE model the contact surface area, time of contact and the duration of contact can be obtained anywhere on the colliding buildings. Satisfactory data such as force, displacement, velocity, and acceleration-time histories at every microsecond of the seismic motion is easily accessible.

To develop this methodology that leads to a more accurate FE model, contact phenomena at material level (i.e concrete and steel) has been studied using direct impact Hopkinson Pressure Bar (HPB) experiments. Direct HPB numerical simulations were validated against the experiments in LS-DYNA. The results of the investigation at the material level were taken onto the structural level and were combined with numerical simulations of shaking table tests validated against shaking table experiments conducted by Garcia et al. (2010).

At a later stage, the findings of the experiments and the numerical simulations are combined into a final FE model that can simulate pounding with more accuracy compared to the existing methods of pounding simulation demonstrating the magnitude of the contact forces and the extent of damage in the colliding concrete buildings. The developed approach allows better insights into the structural and material response mechanisms during earthquake events. Also, more reliable contact parameters can be extracted from the developed FE model and be implemented onto the existing pounding models.

Declaration

Please ensure that the following is included in your declaration:

I, Nava Farhadzadeh, confirm that the Thesis is my own work. I am aware of the University's Guidance on the Use of Unfair Means (www.Sheffield.ac.uk/ssid/unfair-means). This work has not previously been presented for an award at this, or any other, university.

Acknowledgments

I would like to thank my PhD supervisors, Dr Zuhal Ozdemir, Professor Andrew Tyas, and Dr Mihail Petkovski for their guidance, help and support throughout my PhD study. I have learnt many great things from you all in my research career. This PhD would have not been possible without you. In addition, I would like to say that I deeply appreciate Andrew Tyas' generous guidance and continuous motivation through all my efforts and struggles which I will never forget. I have learnt many great things about impact from you.

I would like to thank my director at my workplace AECOM for being understanding and for allowing me the time I needed to spend on my PhD thesis. I miss my greatest friends Dr.Sheyma Kennedy and Dr.Nicoletta Sanvitale who gave me the courage to continue my path. More importantly, I would like to extend my thanks to my amazing friend Sogand for being a great confidant. I had amazing time at the University of Sheffield along with my good friends, Dr Neda Nabid and Dr Soheil Khoshkholghi.

I am thankful to Kieran Nash and Paul Blackbourn for their help in providing the equipment I needed in the laboratory and to help me prepare my samples, and to the technicians at Buxton laboratory.

I am forever in debt of my parents for financing my study and my life in the UK. Finally, I would like to thank my husband Behnam for being patient and standing by myside through-out my years as a PhD student and making this journey possible. I am looking forward to starting our new life journey together in our new home.

Nava Farhadzadeh

22nd April 2022

Table of content

List of Figures

Appendix-A Figures

List of Tables

Appendix-A tables

Abbreviation

A	Area
C	Damping constant
CSCM	Continuous surface cap model
DABS	Dynamic analysis bridge system
DIF	Dynamic increase factor
E	Young modulus
EOS	Equation of state
EPDC	Elasto-plastic damage cap model
F	Force
FEM	Finite element method
FPZ	Fracture process zone
FHWA	Federal highway administration
GF_c	Compressive fracture energy
GF_t	Tensile fracture energy
GF_s	Shear fracture energy
H	Hertz damped model
HPB	Hopkinson pressure bar
HSV	High speed video
K & C	Karagozian & Case
L	length
LVE	Linear viscoelastic model
LSTC	Livemore software technology corporation
PGA	Peak ground acceleration
MLVE	Modified linear viscoelastic model
MDOF	Multi degree of freedom
NLVE	Non-linear viscoelastic model
R	Radius
SDOF	Single degree of freedom

Notation

K	contact stiffness
f_C	Compressive strength
f_t	Tensile strength
m	mass
ρ	Density
ζ	Damping coefficient
$\dot{\boldsymbol{\delta}}$	Velocity
δ	Displacement
R	Radius
π	Pi
$\mathbf{v}'$	Post-impact velocity
v	Velocity
v	Poisson's ratio
c	Wave velocity

Chapter 1

1. Introduction

In this PhD thesis work, a technique based on the Finite Element Method (FEM) is developed to model structural pounding with higher accuracy than existing modelling methods of structural pounding. This chapter provides an outline of the thesis structure as well as the aim and objectives of the research.

1.1 Research background and motivation

Structural pounding is a complex phenomenon that occurs between closely spaced structures with out-of-phase responses during earthquake events. When the adjacent structures collide, forces are generated which leads to plastic deformations, local cracking and may cause total failure of the structure. Over the past decades, modelling structural pounding has attracted the attention of many researchers. However, there are still uncertainties with the existing models of structural pounding which is mainly associated with their parameters such as contact stiffness. The purpose of this Ph.D. work is to develop a methodology that can reliably model pounding of buildings and overcome the limitations of the existing pounding models. Since physically testing pounding behaviour of buildings under earthquake is very expensive and time-consuming, analytically and numerically simulating the structures are preferred methods.

Research on the modelling of seismic structural pounding started from simple analytical models called stereomechanics approach (Goldsmith, 1960) that could predict the degree of plasticity of an impact using closing and residual velocities. The ratio of the residual or post impact velocity over the closing or initial velocity is called the coefficient of restitution shown as (*e)*. If the value of restitution coefficient is 0, the impact is plastic and if it is 1, the impact is elastic. Methods of modelling pounding improved over time and evolved into analytical

models that could predict the magnitude and duration of an impact by idealising structures as point mass models.

However, the existing analytical contact models suffer from uncertainties in contact parameters such as contact stiffness and damping ratio. One of the limitations is the lack of a proper formula to calculate contact stiffness for flat surfaces and in a lot of times, its value is based on assumption/or estimation. A contact model consists of a spring that is placed between masses, and the stiffness property of that spring (called contact stiffness and is denoted by "K") is estimated based on small impact experimental findings. Mostly the contact stiffness is taken equal to the axial stiffness of a member of the structure in investigations carried out by researchers such as Maison and Kasai, (1997); Zhu et al. (2002); Watanabe and Kawashima, (2004); Ye et al. (2009); Khatiwada and Chouw, (2014); Raheem et al. (2018); Chenna and Ramancharla (2018); Raheem et al. (2019); and Godbole et al. (2021). However, this method ends up in diverse results and different conclusions for different impact cases. Such models with great disadvantages are unable to predict what happens to buildings when they come into contact multiple times. Dashpots were later added to the analytical models to account for plastic deformation and energy loss and still, their values are based on assumption due to lack of robust formulas. The contact parameters are functions of material, impact velocity, mass and the geometries of the colliding bodies.

The FEM combined with contact element model is an alternative method to model pounding between adjacent structures. Contact in between two adjacent structures is defined using contact elements/or gap friction element. Yet, the contact element properties have to be defined in advance and still the contact parameters are assumed. Diverse results about structural pounding behaviour in earthquake are concluded from these methods. Apart from that, modelling impact using the previous methods have several uncertainties associated with it, the pounding behaviour of buildings is still not very well understood (Khatiwada and Chouw, 2014).

The developed FEM within this PhD offers significant advantages over the existing approaches particularly that in such a method contact is explicitly modelled using the penalty method instead of using gap elements and defining the contact parameters in advance which is no longer needed. However, such a method requires confidence that the FEM can model impact/pounding with higher accuracy compared to the existing methods of modelling pounding. In the developed FE models, concrete material model plays a significant role in increasing the accuracy of the FE models. In the developed methodology, two concrete material models called Continuous Surface Cap Model (CSCM or MAT_159), and Karagozian and Case (K&C or MAT_72R3) were considered. Firstly, physical and numerical

Hopkinson Pressure Bar (HPB) tests were carried out on concrete and steel samples to investigate impact at material level as well as calibrating the numerical model parameters. HPB findings were transferred onto a greater model at structural level. Numerical simulations of shaking table tests conducted on a full-scale individual building were carried out and were validated against experimental work conducted by Garcia et al. (2010). Finally, full-scale FE models of buildings were developed to investigate building pounding. The current method developed within this Ph.D. work, makes it possible for researchers to investigate the pounding behaviour of buildings in much more detail including cracking/spalling and crushing of concrete. The contact location unlike the existing methods of pounding is not pre-defined, therefore, it is possible to study where the buildings come into contact at first. Finally, the approach developed here allows better insight into the mechanisms of structural and material response during pounding events.

Using this tool, (1) unlike the gap friction elements that are placed at certain locations in the existing methods, there is no need to define contact location neither any contact parameters are determined in advance, (2) buildings with different geometries can be studied including contact between flat surfaces, (3) variable histories such as force-time, acceleration-time, etc. can be obtained anywhere on the building, (4) concrete cracking and crushing and building deformation can be observed during pounding, (5) structural pounding response can be studied in great detail including the first and subsequent points of contacts between buildings can be identified, as well as the contact duration and contact forces magnitudes, and finally (6) the proposed FE method can be used as a tool to calculate more reliable contact parameters such as contact stiffness and the coefficient of restitution.

1.2 The aim and objectives of the work

In investigating collision between two adjacent structures, researchers are faced with some challenges with the main one being the lack of large/small-scaled experiments on pounding of concrete buildings to compare and validate against numerical or analytical simulations. Experimental work can offer valuable and clear insight into the behaviour of concrete buildings during and after collision. However, these experiments are very expensive and time consuming particularly pounding tests on large concrete buildings. Therefore, numerical methods are preferred, however, they require reliable computational resources.

The aim of this Ph.D. work is to develop a methodology that can reliably model pounding of buildings. In this methodology, the FEM is employed in LS-DYNA to investigate building impacts using a penalty-based method step by step with the aid of experimental work and

numerical validation against the experiments starting from material level to structural level. The penalty-based algorithm automatically calculates contact forces when it detects penetration and in this method the reliability of such a model is based on the choice of material model. The proposed FE method has laid a reliable foundation to provide accurate modelling of building pounding. This powerful method aids in better understanding of the fundamental principles of structural collision in details. Often, in structural pounding, the exact location of the first contact, how and where the first damage initiates and how it propagates in the structure remain unknown. However, it is essential to gain an understanding of the effect of pounding on buildings.

To fulfil the aim of this research, the objectives of the work are to:

- Investigate the impact/contact behaviour of concrete and steel materials using direct HPB tests and determine whether the chosen concrete models predict the experimental results well
- Validate the direct HPB FE simulations against the direct HPB experiments
- Develop and validate the numerical simulation of a two-storey building under earthquake motions physically tested on a shaking table test conducted by Garcia et al. (2010) including investigating the building's dynamic behaviour/response under earthquake motions
- Examine the capabilities of the two common robust concrete material models, Continuous Surface Cap Model (CSCM or MAT_159) and Karagozian and Case (K&C or MAT_72R3) available in LS-DYNA to model impact and to select the most suitable material model through their validation against both direct HPB and shaking table experiments
- Examine the capability of the concrete material models in capturing plastic deformation in concrete by means of erosion
- Incorporate all the findings of the simulations carried out into one final FE model of building pounding
- Investigate the applicability of the incorporated FE model in simulating pounding between buildings using two case studies: (1) slab to slab pounding, (2) mid-column pounding particularly with flat contact surface geometries independent of pre-determining/assuming contact parameters in advance, as well as concrete cracking/crushing. Also obtaining in-depth detail/output data such as

displacement/velocity/acceleration/force-time histories, time of contact, number of contact and their locations etc.

1.3 Outline of thesis chapters

The outline of the dissertation can be summarised as follows:

- **Chapter 2** presents a literature review on the theoretical background and previous research on structural pounding. Research on structural pounding have been reviewed, discussed and gaps have been identified.

- **Chapter 3** presents physical and numerical FE simulations of direct Hopkinson Pressure Bar (HPB) tests. A set of direct Hopkinson pressure bar tests on concrete and steel samples have been undertaken in laboratory. Specimens made of concrete and steel in different sizes were tested under variable impact velocities. FE simulations of direct HPB were validated against the experimental data in LS-DYNA (LS-DYNA, 2018). The suitability of two most popular concrete material models, CSCM (MAT_159) and K&C (MAT_72R3) available in LS-DYNA were studied through parameter sensitivity analysis and data calibration. The results of both validations were discussed.

- **Chapter 4** presents the results of FE simulations of a full-scale building under shaking table tests. The FEM was employed to simulate a two-storey building subject to variable seismic motions. The FE analysis results were validated against shaking table tests conducted by Garcia et al. (2010) in France. The calibration process was carried out using two robust material concrete models called CSCM and K&C. Capabilities of these models in simulating shaking induced crushing/cracking of concrete have been assessed and recommendations have been made.

- **Chapter 5** presents the results of monotonic push-over analysis on a two-storey frame to evaluate capability and accuracy of the material models in modelling inelastic seismic response of the building. A static non-linear procedure called push-over analysis was used to determine the capability and reliability of the material models in capturing concrete crushing by means of erosion. This technique assisted in better understanding of crushing/crack modelling in numerical simulations.

- **Chapter 6** presents the final FE pounding simulation of buildings which is the combined model of the previously validated FE simulations of direct HPB and the shaking table simulations. The methodology developed for numerical and experimental investigation of pounding behaviour at material level and structural level is incorporated into final models of building pounding. The information and knowledge obtained from the well calibrated models in chapters 3, 4 and 5 were gathered to construct these final simulations that involve pounding between two buildings' slabs as well as pounding of a building's slab onto another building's column.

- **Chapter 7** presents conclusions of this study. This chapter summarises the key findings of the research carried out and draws statements as a conclusion based on the findings and it makes suggestions on how this research can be further developed and evolve into a comprehensive reference guide for future researchers of seismic building pounding.

Chapter 2

2. Literature review

This chapter provides a background to what structural pounding is and what causes pounding to happen. It reviews cases where pounding was catastrophic for structures and how researchers took initiative to model pounding and understand this complex phenomenon better. The focus of this chapter is to provide a theory background on the previous and current methods of investigating structural pounding. These methods include analytical and numerical modelling of structural pounding as well as experimental work carried out to solve the uncertainties associated with understanding structural responses when subjected to impact/pounding. An overview of the disadvantages and advantages of the previous works is given, and the gap that this thesis work fulfils, is highlighted. By reviewing the background information pertinent to this thesis subject, it is apparent that the current research on structural pounding lacks not only a detailed method that combines Finite Element Modelling with experimental work to investigate pounding/impact, but also a reliable method that can be used to model pounding between any types of buildings with any geometry.

2.1 What is pounding and why does it happen?

Structural pounding or in another term structural collision is a phenomenon that happens to structures that are closely spaced to each other and have out of phase responses when subject to seismic motions. In many cities due to poor structural design and their lack of compliances with Earthquake Design Codes in providing enough gap between two structures, pounding of structures is inevitable and can lead to catastrophic events. Due to lack of knowledge, financial difficulties, and shortage of lands in populated areas, many buildings are built with small space or none at all. For example, according to (Dogan and Gunaydin, 2009) 64% of buildings in

Eskisehir city in Turkey are built with insufficient gaps in between. Figure 2.1 illustrates three tall buildings that have been built very closely and are susceptible to pounding. Also, in cities such as Thessaloniki in Greece (Anagnostopoulos, 1988), Taiwan (Jeng & Tzeng, 2000), Wellington (Bothara et al., 2008), and Gorkha in Nepal (Shrestha and Hao, 2018), buildings have been built with no separation gap in between. In the Author's home country, Iran, there are so many structures built with almost no separation gap, some even share a brick wall or adjoining structural element. Even after introducing the compulsory requirement for having gaps between newly built structures in the building codes, frequently revising these codes can mean some of these buildings may not comply with the current codes anymore (Chouw 2002).

Figure 2.1 Adjacent buildings in Eskisehir city with insufficient gap as shown with red circle (Dogan and Gunaydin, 2009)

As a result of the out of phase responses of structures in earthquake, collision happens between them. Once they collide, large impact forces are produced on both structures resulting in concrete crushing, spalling, and yielding of reinforcements leading to local or global failures. What happens to these structures during impact is dependent on so many factors such as the dynamic characteristics of the structures which causes their out of phase responses, ground condition as well as the characteristics of the earthquake such as its magnitude, and how closely the structures are built.

2.1.1 Pounding observed in previous earthquakes

Structural pounding has frequently been observed and reported during the past earthquakes. For example, the most recent structural pounding observed was during the Nepal earthquake also known as Gorkha earthquake in 2015 as shown in Figure 2.2. Based on a field investigation report, pounding was observed several times in different areas in Gorkha and was the main reason for these concrete and masonry buildings to catastrophically fail (Wijeyewickrema et al., 2015).

Figure 2.2 Collapse of buildings due to pounding in Bhaktapur during Gorkha earthquake in 2015 (Wijeyewickrema et al., 2015)

De Carlo hotel is another example of structural failure due to pounding in Mexico City. In the 1985 Mexico City earthquake, which resulted in some of the most extensive pounding damage seen to date, pounding was very evident in 15% of structural damages or failures. Overall, pounding somehow influenced 40% of the budilings' failures/damages in the Mexico City earthquake (Brown and Elshaer, 2022). After the earthquake, it was estimated that around

10,000 people lost their lives, 50,000 were affected by injuries, and 250,000 lost their homes (Miari et al., 2019).

Also in San Fernando earthquake of 1971, the Olive View hospital's main building collided against it's adjacent stairway tower which resulted in the stairway tilting away from the main building for sometime and then it gradually collapsed (see Figure 2.3). A survey on 1989 Loma Prieta earthquake reported pounding occurrence in 236 cases of every 500 structures (Kasai and Maison, 1997).

Figure 2.3 Olive view hospital pounding- the stairway collapsed sometime after the earthquake (Mahin and Bertero, 1976)

Pounding is not only limited to buildings; it has been frequently observed in bridges particularly at their expansion joints. Expansion joints are beneficial in mitigating shrinkage and thermal changes in bridges, however, they put bridges at great risk of seismic induced pounding between decks, or deck and abutment as shown in Figure 2.4 (Miari et al., 2019). Pounding damages in bridges were observed in USA Sen Fernando earthquake in 1971 (Jennings PC 1971), USA Northridge earthquake in 1994 (Moehle et al., 1995), USA Loma Prieta in 1989 (Priestley et al., 1996) Japan's Kobe earthquake in 1995 (Bruneau et al., 1996; Bruneau 1998), Taiwan's Chi Chi earthquake in 1999 (Bruneau et al., 2000), the Yogyakarta earthquake in Indonesia in 2006 (Elnashai et al., 2007), and the New Zealand's Christchurch earthquake in 2011 (Chouw and Hao, 2012).

Also damage as a result of pounding between Shipshaw bridge deck and its abutments occurred during the 1988 Saguenay earthquake in Quebec Canada (Miari et al., 2019).

Figure 2.4 Earthquake induced pounding between bridge decks (Miari et al., 2019)

2.1.2 Structural Design Codes Recommendations on minimum separation between buildings

Nowadays, there is compulsory requirement for minimum separation gap to be placed between structures. Most of the world countries have specified these requirements in their structural seismic codes. In Eurocode 8: Design of structures for earthquake resistance, minimum gap between buildings is taken as SRSS (square root of the sum of the squares) expressed as follow:

$$\text{SRSS} = \sqrt{S_1^2 + S_2^2}$$

S_1 is the maximum horizontal displacement of the first building and S_2 is the maximum horizontal displacement of the second building (EC 8, 1988). The second method used to determine the minimum gap is the maximum plastic displacement of the taller building which compared to the SSRS rule is less conservative (Favvata, 2017).

In Iran, the minimum distance is taken from Standard 2800 which states for buildings less than 8 floors high, $d = H \times 0.005$. H is the height of the building, and d is the horizontal displacement response of the structure. The gap between the buildings is both buildings' displacements responses added together as shown in Figure 2.5. For buildings taller than 8

floors, d is the non-linear lateral displacement response of the taller building's top floor multiply by 0.007 (Iranian 2800 Standard, 1988).

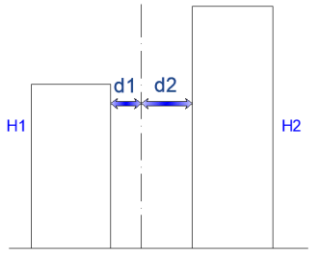

Figure 2.5 Schematic drawing of structural minimum displacement required based on their height

Even after the introduction of mandatory earthquake code provisions in Iran, in 1990 Rudbar's earthquake, many buildings collapsed and took the lives of many people (Ibrion et al., 2015). A lot of buildings were built before the mandatory requirements with no gap in between, some of them are even connected with a share structural part such as a wall. Still, even if buildings comply with codes, frequently revising these codes could mean that the existing buildings do not comply with their current version. Also, structures could still be prone to pounding if foundation conditions are not taken into account in the design stage (i.e buildings lateral displacement is more on soft soil) (Khatiwada, 2014).

2.2 Modelling method of structural pounding

As previously shown, pounding can lead to considerable damages to structures. It is very difficult to fully understand and justify the responses of the structures when they impact. Subsequently, the differences in the characteristics of structural dynamics, gorund condition as well as the earthquake characteristics make it very difficult to simulate real structural pounding behaviour. Over recent decades, many different methods have been used for modelling impact. A simple method is the stereomechanics approach (Goldsmith, 1960). This approach is based on the conservation of momentum law and is only able to determine the post impact velocities of the colliding objects. The approach was an incomplete attempt to model structural pounding. In the approach, contact/pounding forces could not be obtained, therefore the theoratical model was unable to detect the deformation of the colliding bodies. Contact duration was neglected as collision was assumed to be a sharp instant impact with no duration.

2.2.1 Contact element approach (simplified contact models)

To estimate forces in models of structural pounding, it is necessary to explicitly model the contact mechanics, mapping the forces generated over the time of impact. This can be modelled using contact element models. It was from the 1980s that the application of contact models became very popular in simulating structural pounding.

Research on contact elements started from simulating structures as single degree of freedom (SDOF) systems (Anagnostopoulos, 1988; Athanassiadou et al., 1994; Davis, 1992; Wolf and Skrikerud, 1980) and quickly progressed on to idealising these buildings as multi-degree-of-freedom (MDOF) systems as shown in Figure 2.6 (Anagnostopoulos and Spiliopoulos 1992). In these models idealised as lumped masses, the mass of every floor is assumed as lumped mass concentrated at one point. When subject to seismic motions, these masses start to have out of phase movements and at some point, may come in to contact. In these models, it is assumed that the whole structural mass comes into contact with the other structure.

In Figure 2.6, the contact element model, also called gap friction element or in another name the link elements are placed at every floor between the two structures consist of an elastic (tensionless) spring with certain stiffness noted as K as well as a gap in between the masses. These contact element models simulate the contact force-time histories of structures during single collision or in earthquake events. As soon as contact takes place, structures start to displace and at some point, they collide and depending on the structural material and the geometry of the contact area, these collisions have different contact stiffness and as a result contact/impact forces are generated (relationship is expressed in Equations 2.1-2.4). Once all these happen it is said that the contact element has become activated. Schematic drawing of collision in terms of displacement- time history between two concrete samples is shown in Figure 2.8. Also, some of the common contact/link elements are discussed in the following pages.

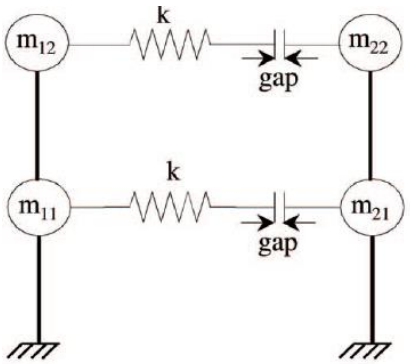

Figure 2.6 Structures idealized as Lumped mass models with multi-degrees of freedom (Khatiwada and Chouw, 2014)

The most classical theory of contact is the elastic Hertzian model which is based on a linear spring-with stiffness- model. This model describes that the deformation in the colliding body is proportional to the contact force (see Equation 2.1- 2.4). The assumption of this theory is based on a perfect collision between either, two spherical surfaces, or a spherical and a flat surface (Goldsmith, 1960). This approach is more accurate compared to the stereomechanics approach as it considers the deformation of the colliding bodies as well as the duration of the impact.

$$F = K_e \times \delta^n \qquad 2.1$$

$$K_e = \frac{4}{3\pi}\frac{1}{h_1 + h_2}\sqrt{\frac{R_1 R_2}{R_1 + R_2}} \qquad \text{(Impact of two spherical surfaces)} \qquad 2.2$$

$$K_e = \frac{4}{3\pi}\sqrt{R}\frac{1}{h_1 + h_2} \qquad \text{(impact of a sphere surface against a planar surface)} \qquad 2.3$$

$$h_i = \frac{1 - v_i^2}{\pi E_i} \qquad 2.4$$

Where F is contact force, K_e is the elastic stiffness and δ is the displacement and n is the power to the displacement which is either 1 for linear or 3/2 for non-linear, h_1 and h_2 are the material parameters. R_1 and R_2 are the radiuses of both spheres, m is the mass and v is Poisson's ratio and E is the young modulus.

The Hertz model can be used to simulate linear or non-linear behaviour of colliding objects; however, the greatest drawback of the model is the lack of energy dissipation consideration in

the model which ultimately results in prediction of large contact forces compared to the experiments.

Since, the Hertz contact model has been improved over time by adding a dashpot to the original linear spring model to account for plastic deformation (see section 2.2.2 to 2.2.5) by Hunt and Crossley (1975) and was modified again later by researchers such as Muthukumar and DesRoches (2006) and Jankowski (2007). The relationship between the damping ratio and coefficient of restitution (expressed in Equation 2.7), as well as the damping constant (C) formulas (Equations 2.6, 2.13, and 2.17) within the model have all been modified numerous times by different researchers such as Mahmoud (2008), Ye et al., (2009(b)), and Barros and Khatami (2012). The advantage of these models is that they can be implemented into the commercial structural analysis software without the need of great programming modifications effort (Khatiwada, 2014). Some of these primary contact models have been described in the following sections.

2.2.2 Linear viscoelastic model (LVe)

In the linear viscoelastic model or Kelvin-Voight model, a linear spring is placed parallel with a viscous damper as shown in Figure 2.7 and the contact element/model is expressed as follow:

$$F = K\delta + C\dot{\delta} \tag{2.5}$$

Where F is the contact force, K is the contact/impact stiffness, δ is the relative displacement, $\dot{\delta}$ is the velocity, and C is the damping constant and ζ is the damping ratio expressed as:

$$C = 2\zeta\sqrt{K\frac{m_1 m_2}{m_1+m_2}} \tag{2.6}$$

$$\zeta = \frac{\ln(e)}{\sqrt{\pi^2+\ln(e)^2}} \qquad e = \frac{v'_2 - v'_1}{v_1 - v_2} \tag{2.7}$$

Where v_1' and v_2' are the post impact veloities of the colliding structures 1 and 2, v_1 and v_1 are the initial velocities of the structures, and e is the coefficient of restitution. The ratio of the post-impact velocity to the initial velocity is called the coefficient of restitution. This coefficient is an indication of the loss in kinetic energy of the impacting bodies. The kinetic energy loss is the result of impact waves travelling in the bodies causing viscoelastic changes

or permanent deformation (Seifried, et al., 2010). If the value of *e* is equal to 1, the impact is an elastic impact, and the closer it gets to 0, the more plastic the impact becomes. Apart from the impact velocities, this value is also dependent on the mass, and the material properties of the structures. The main disadvantage of the linear viscoelastic contact model is that it produces meaningless tensile forces near the end of the force-time histories. Some modifications to the damping formulas of the model have also been carried out to amend the false idea of constant uniform damping throughout the whole contact duration in the contact model.

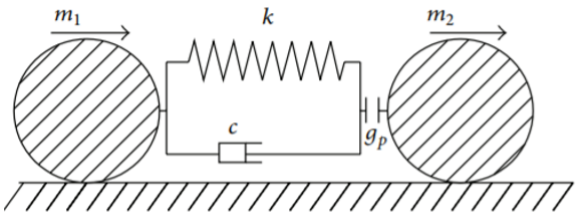

Figure 2.7 schematic drawing of a contact element placed between two colliding bodies with a linear spring and a dashpot to account for energy dissipation (Zhao and Liu, 2016)

2.2.3 Modified linear viscoelastic model (MLVe)

The relationship between the damping constant and the damping ratio of the linear viscoelastic model was first modified and improved by Mahmoud (2008) as expressed in Equations 2.9-2.10.

$$F = K\delta + C \qquad \delta > 0: \dot{\delta} > 0 \qquad \text{(Collision approach period)} \qquad 2.9$$

$$F = K\delta \qquad \delta > 0: \dot{\delta} < 0 \qquad \text{(Collision restitution period)} \qquad 2.10$$

In modified linear viscoelastic contact model as expressed in Equations 2.9 and 2.10, there are two phases during the contact: (1) approach phase (Equation 2.9), and (2) restitution phase (Equation 2.10). As shown in the Equations, the displacement is greater than zero meaning the relative displacement or the gap between colliding bodies is closed and contact has taken place as shown in Figure 2.8.

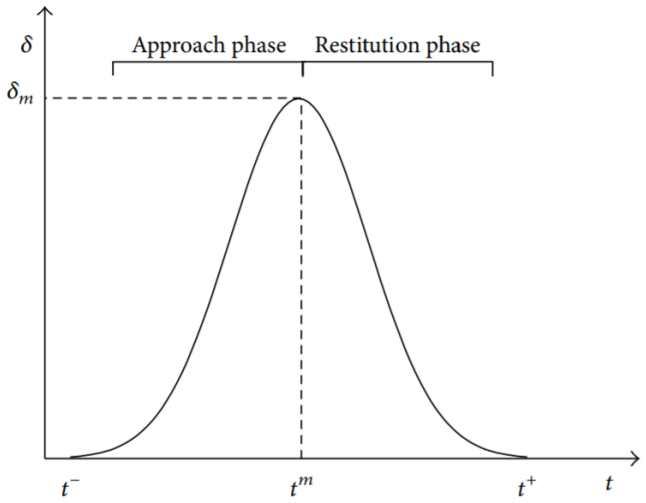

Figure 2.8 Schematic drawing of the two "approach and restitution" phases of interpenetration during collision (Zhao and Liu, 2016)

In this contact element model, the damping constant is calculated using the same formula expressed in Equation 2.6 but a few years later a new formulation was introduced by Mahmoud and Jankowski (2011) for the damping ratio part of the Equation 2.6. The modified damping ratio expression is illustrated in 2.11.

$$\zeta = \frac{1}{\pi}\left(\frac{1-e^2}{e}\right) \qquad 2.11$$

2.2.4 Hertz Damped Model (HD)

Hertz damped model is an improved version of Hertz model which accounts for energy dissipation. It includes the displacement and its rate of change. The model's linear damping constant was replaced with a non-linear damper and the model's energy loss is accounted for by a damping that depends on the deformation of the bodies and its rate of change as expressed in Equations 2.12- 2.14 (Muthukumar and DesRoches, 2006).

$$F = K\,\delta^n + C\dot{\delta} \qquad 2.12$$

$$C = \zeta\,\delta^n \qquad 2.13$$

$$\zeta = \frac{3k\,(1-e^2)}{4(v_1-v_2)} \qquad 2.14$$

The Hertz-damped model proposed by Muthukumar and DesRoches (2006) was found to be significantly inaccurate in simulating pounding by Ye et al. (2009(b)).

2.2.5 Non-linear viscoelastic model (NLVe)

To eliminate the shortcomings of the linear viscoelatic model which was the existence of the meaningless tensile forces in the time histories, and the non-linear elastic models with no damping or uniform damping throughout the whole duration of the contact, Jankowski (2005) proposed a new model similar to the modified linear viscoelastic model that includes a non-uniform viscous damping that changes with the deformations of the impacting bodies (Khatiwada 2014).

$$F = K\,\delta^{3/2} + C\dot{\delta} \qquad \dot{\delta}_{(t)} \geq 0 \qquad 2.15$$

$$F = K\,\delta^{3/2} \qquad \dot{\delta}_{(t)} < 0 \qquad 2.16$$

$$C = 2\zeta\sqrt{K\sqrt{\delta}\left(\frac{m_1 m_2}{m_1+m_2}\right)} \qquad 2.17$$

$$\zeta = \frac{9\sqrt{5}}{2}\frac{1-e^2}{e[e(9\pi-16)+16]} \qquad 2.18$$

Damping ratio for this model can also be calculated using the Equation 2.11. Jankowski (2006) found the NLVe to perform slightly better in simulating the contact forces of a ball impacting a rigid surface than the MLVe. However, he has stated the fact that all these models give very rough estimate of the actual complex behaviour of structural pounding, particularly, for objects with more complex impact geometries.

Khatiwada (2014) stated that the main advantage of the NLVe model compared to the other models is its ability in simulating force-time histories, providing reliable contact stiffness and damping values are inputted onto the contact model. However, the greatest disadvantage is that these values can not be determined in advance and can only be obtained iteratively if

reliable force-displacement data are available. Also, it is very difficult to determine the value of the contact stiffness for every pounding scenarios. In the absence of such data the accuracy of the model is compromised.

Despite all the great effort to research structural pounding using the contact models and all the factors influencing structural pounding behaviour such as the contact surface geometry, structural stiffness and mass, structure-soil interaction, and the ground motions characteristics, etc., simulation of structural pounding still suffers from many uncertainties as in some of the existing research it is found that one model can reasonably simulate contact force-time response of a structure in one impact scenario while the same model did not work for a different impact case. It was observed that the performance of every model is very different to each other when applied to the same impact case (Khatiwada, 2014). Figure 2.9 shows the performance of three different contact models for one impact case where a concrete pendulum strokes a concrete pile (Jankowski, 2005).

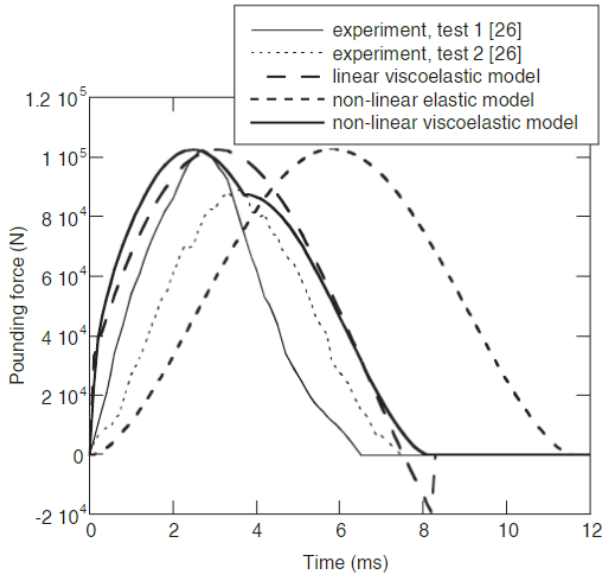

Figure 2.9 Comparison of the performance of LVe, NLe, and NLVe contact models with experimental results of a pendulum striking a concrete pile (Jankowski, 2005)

Even the models' parameters found to have diverse influences; for instance, Muthukumar & DesRoches (2006) found the response to be sensitive to the coefficient of restitution value whereas the contrary was found by Anagnostopoulos (1988). On the other hand, contact stiffness has been found to always influence the simulation by a great amount. As incorrect estimation of the contact stiffness value leads to over-estimating or underestimating the contact forces. It has been mentioned previously that only Hertz model suggest contact stiffness formula for impact of two spherical objects, or one spherical and one planar. Some

of the researchers such as Maison and Kasai (1990) and Muthukumar and DesRoches, (2006) take contact stiffness value equal to the axial stiffness of the structural element ($\frac{EA}{L}$). Only limited number of studies such as VanMier et al. (1991) attempted to determine contact stiffness for concrete-to-concrete impacts using small concrete samples and suggested a range between 2 KN/mm$^{3/2}$ to 80 KN/mm$^{3/2}$ which are not applicable to large scale pounding cases.

An experimental and numerical study by Guo (2012) on pounding of steel bridge decks found that the contact stiffness obtained from the analytical contact models significantly over-estimates the contact forces due to the limitation with the assumptions of these models compared to reality. Khatiwada and Chouw (2014) findings also agree with the study by Guo (2012) confirming there are great discrepancies in the existing contact stiffness theoretical methods and the current identified values. As Khatiwada (2014) stated that these issues have made the identification of a correct model very difficult and as a result the practicality of these models has been rigorously impacted by such uncertainties.

The limitation of the analytical contact element models and the uncertainties associated with their application has made them unsuitable to investigate pounding any further using their current versions. Apart from lumped mass models, in the existing pounding simulation methods, FEM has been combined with link element models (Jankowski, 2008) that were placed between two FE structures, however even in this method contact parameters must be defined in advance and the issue with pounding simulation persists.

To overcome uncertainties associated with the methods of researching structural pounding, the Finite Element Modelling is suggested. However, in the suggested FEM, contact is modelled with penalty method rather than placing link element models between the colliding structures and assuming contact parameters or spring properties. In this method, the reliability of the FEM is depending on the chosen material model. FEM combined with experiments provides much more reliable method to model structural pounding without dealing with the limitations of the existing methods of structural pounding.

Contrary to the existing lumped mass models that idealise buildings as lumped masses, it is capable of considering damping, induced-contact stress waves responsible for local concrete cracking and crushing as well as global structural damage. Also, any geometry with any complexity can be constructed and pounding can be monitored locally which is not possible in the existing lumped mass modelling methods. The effects of material parameters as well as reinforcement detailing can be modified based on the user needs, and any data such as stress, force, displacement, etc can be obtained anywhere in the model.

Without proper methods of pounding analysis, researchers remain with the choice of either investigating pounding/impact experimentally themselves or use the suggested contact parameters values existing in the literature. The pounding phenomena is complex by nature and there have always been problems with modelling approaches. For several decades, using the existing modelling methods of structural pounding (e.g contact element models) researchers have been unable to correctly identify structural pounding responses. Even those who went on to use numerical simulations instead of analytical models struggled to find suitable contact parameters to model impact effectively because in most numerical modelling software such as OpenSees and Sap2000, contact model parameters (e.g contact stiffness and damping) have to be defined and implemented onto the gap elements (an example of a gap element is shown in Figure 2.7) that are placed between the colliding structures.

2.3 Numerical Modelling of structural impact/contact in LS-DYNA using different Concrete Material Models

One of the early researches on 3D Finite Element Modelling of contact was conducted by Agardh and Laine (1999). Impact of a steel cylindrical shape projectile with velocity of 1500 m/s onto a steel fibre-reinforced concrete slab was simulated in LS-DYNA software. MAT_SOIL_CONCRETE known as MAT_78 used for modelling concrete was applied to model the slab, and the reinforcing bars were modelled as solid steel. The numerical results were compared with the same impact test done by Bryntse (1997), and it was observed that the model was capable of capturing the damage occurred in the slab. A few years later, a similar study was published by Sadiq et al. (2014) who studied the impact response of nuclear power plants against aircraft attacks. Reinforced concrete panels as shown in Figure 2.10 to Figure 2.12 was simulated in LS-DYNA using Continuous Surface Cap Model (CSCM MAT_159) and Winfrith (MAT_84) (bi-linear elastic- plastic model) material models.

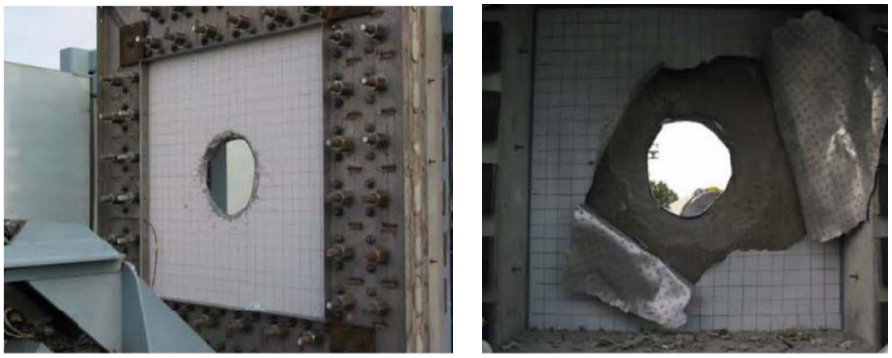

Figure 2.10 Experiments on the impact of aircraft to concrete panel (Sadiq et al., 2014)

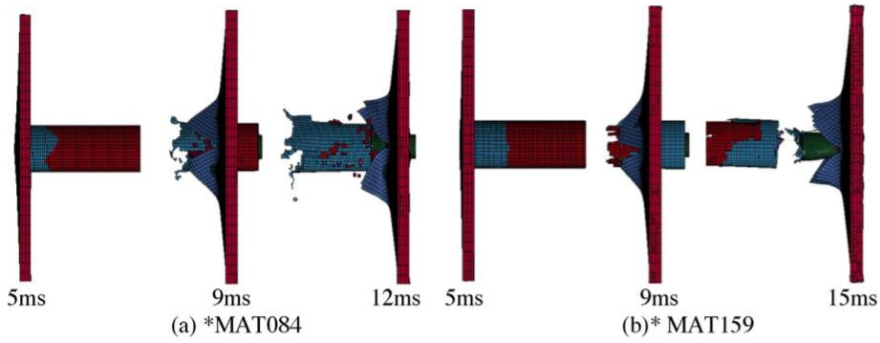

Figure 2.11 Simulation of concrete panel's crushing/damage using Winfrith (MAT_84) and CSCM (mat_159) (Sadiq et al., 2014)

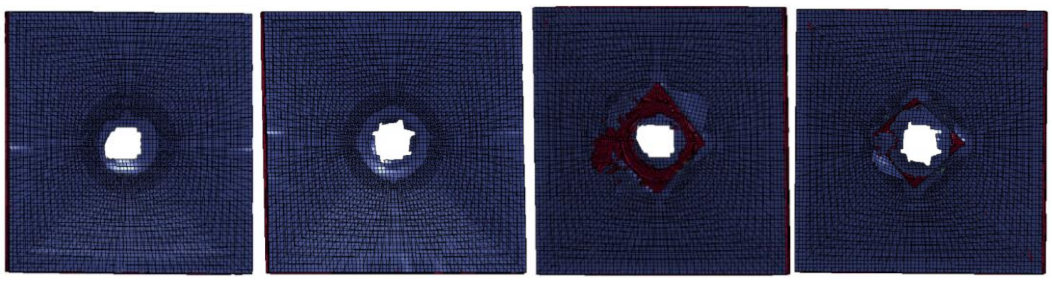

Figure 2.12 LS-DYNA simulation of front and back faces of the concrete panels after impact; starting from first photo on the left (i) front face response using MAT_84 (ii) front face response using MAT_159 (iii) back face response using MAT_84 (iv) back face response using MAT_159 (Sadiq et al., 2014)

To model damage, Winfrith material model was used along with *MAT_ADD_EROSION, but CSCM was used on its own as the model has an in-built erosion feature. *MAT_ADD_EROSION is a command that is used along with material models to introduce erosion to the program. Erosion means element deletion and the main purpose of this command is to prevent mesh tangling by deleting elements that have lost strength and no longer contribute to the model. In the study, both material models exhibited reasonable responses, however, for large deformations due to very high strain rate dynamic impacts, Winfrith (MAT_84) was found to perform better. However, when Winfrith (MAT_84) is used with *MAT_ADD_EROSION, a parametric study should be conducted to find suitable erosion criteria. Erosion or element deletion in a model can be set to occur based on a particular criterion, for example based on maximum principal strain, maximum principal stress, or shear stress, etc. It is suggested that before simulating this type of impact using any of the concrete material models available, a proper methodology for validation of these impact analyses particularly for the type of material models used, should be compared against experimental work and reliable published data.

Ranjan et al. (2014) also studied the effect of missile impact and aircraft attacks onto the concrete walls and slabs of nuclear power stations. The CSCM material model was chosen to model concrete in LS-DYNA (LS-DYNA, 2018). Reinforcement bars in the slabs and walls with steel yield strength of 428 MPa and ultimate failure strength of 581 MPa was modelled using the Symonds-Cowper model. Elastic response of the slabs and walls were modelled with missile velocity of 1 m/s, and the velocity was increased up to 215 m/s to obtain plastic deformations. In every case the missile rebounded with a lower velocity, e.g for impact velocity of 215 m/s, it rebounded with residual velocities of 55.20 m/s. In the model, erosion was set to occur when the maximum principal strain surpassed by 20%. Contrary to the study by Sadiq et al. (2014), it was observed that the FE model using the CSCM closely predicted the contact forces and the damage/crushing and spalling of the concrete compared to the experiments. Contrary to the findings of the study by Ranjan et al. (2014) that found CSCM to perform reasonably well; Kim et al. (2011) found that CSCM underestimated the force-displacement response of the concrete plates subjected to missile impact. Such observation in Kim's study has been said to be due to several possibilities such as strain rate over estimation, modelling method used in the study and its effect on the boundary conditions, and material model parameters. Chung et al. (2015) researched the effect of missile crush onto concrete slabs as part of a nuclear safety program of Korean institution. *MAT_PLASTIC_KINEMATIC material model was used to model the steel reinforcements and *MAT_PIECEWISE_LINEAR_PLASTICITY was used to model steel missile. Due to the symmetry in the specimen, only $1/4^{th}$ of it was modelled in LS-DYNA. Three concrete

material models were used: CSCM (MAT_159), Winfrith (MAT_84), and Karagozian and Case (K&C or MAT_72R3). Winfrith model showed the most similar displacement pattern compared to the tests. But CSCM best resembled realistic damage patterns and reasonably predicted the maximum displacement responses. This was due to the fact that CSCM has an in-built erosion system, and no additional erosion is needed, however, the other two material models require *MAT_ADD_EROSION to show element erosion and reflect a similar damage observed in the experimental work. K&C found to under-perform when used with default values and as a result two of the parameters were calibrated. It was stated that element erosion was an incredibly important factor that influenced their simulation result. However, a study by Remennikov and Kong (2012) on steel-concrete-steel sandwich panels subject to hammer impact did not include the eroding parameter of the CSCM for the core concrete in the panel as they believed it led to under-estimating the maximum load-bearing capacity of the panel.

Sangi and May (2009) modelled reinforced concrete slabs in LS-DYNA using K&C and the Winfrith material models and subjected the slabs to drop weight of 98 kg; the slabs were subjected to impacts in several locations as shown in Figure 2.13. *Constrained_lagrange_in_solid keyword in LS-DYNA is used to bond concrete to the reinforcements; such keyword assumes perfect bonding between the concrete and the reinforcement bars.

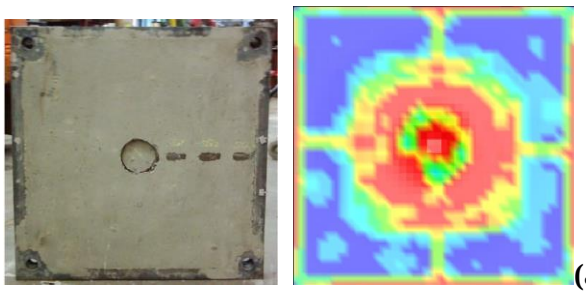
(a)

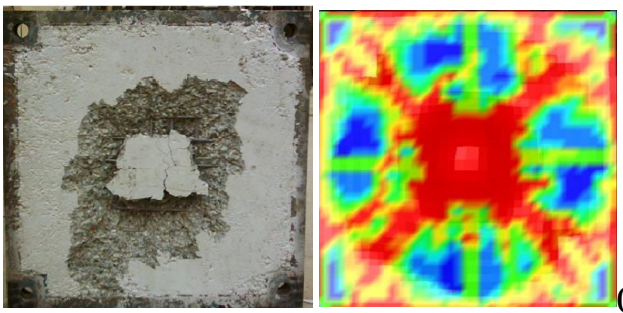
(b)

Figure 2.13 Comparison of LS-DYNA simulation results using Karagozian & Case with experimental work, (a) the front face of the slab in the experiment as well as the numerical simulation, (b) the back face of the slab in the experiment and the numerical simulation (Sangi & May, 2009)

It was found that the K&C model was not able to properly capture the response of the peak impact force. On the other hand, Winfrith concrete model performed better in capturing the peak forces and was able to resemble the damage and concrete crushing observed in the tests.

Apart from simulating missile impacts in LS-DYNA, modelling of vehicle crush onto concrete is also popular. Kang and Kim (2017) investigated the impact of eight-tonnes truck with velocity of 40-50 km/h onto a steel column held by a concrete plinth. Abu-Odeh (2015) conducted an experiment on a bogie crashing onto bridge concrete barriers with a velocity of 24 km/h as shown in Figure 2.14. He simulated the crash in LS-DYNA using three different material models, CSCM, Karagozian & Case, and Winfrith known as Mat_084. The models were used with their short input initial basic parameters without any calibration. The purpose was to observe and assess the performances of the models using their basic parameters.

Figure 2.14 Experimental work on the impact of bogie against the concrete barrier (b) numerical simulation of bogie test in LS-DYNA (Abu-Odeh, 2015)

CSCM and Winfrith models were able to model some of the crack patterns similar to the experiment. Also contact forces were predicted reasonably close to reality when using CSCM and Winfrith compared to the Karagozian and Case model. Similar test was repeated with higher velocity of 32 km/hr; CSCM was the only model correctly resembling the concrete crushing and spalling observed in the test.

Their findings agree with Magallanes (2008) simulation of a blast impact on a concrete wall using four different concrete material models in LS-DYNA; Holmquist Johnson Cook (HJC), brittle damage concrete (BDC), CSCM, and K&C. In his single element simulation, it was observed that only CSCM and K&C were able to capture the real volumetric expansion behaviour of concrete meaning they simulated a more ductile behaviour compare to the other two, particularly compared to BDC that showed a linear behaviour followed by a brittle failure. Also, HJC was not accurate in simulating the tensile fracture of concrete.

He also conducted a blast test on a concrete column and simulated it in LS-DYNA using the same concrete models. While HJC and BDC underestimated the behaviour substantially, K&C modelled the column deformation reasonably well. Despite some irregularity CSCM exhibited during compression softening, it produced sensible results in general. The only other downside to the performance of CSCM was the appearance of shear failure at about $1/4^{th}$ of the height of the column that was not detected in the test.

Based on the author's experience with erosion formulation implemented in the CSC model in this PhD work, one of the reasons for such erroneous behaviour is the choice of a parameter value called ERODE within CSCM. As described previously, this parameter oversees deleting elements when their strength approaches zero and the numerical time steps becomes increasingly small. To avoid mesh tangling, the analysis needs to rid of the offended elements. As a result, it might delete elements when their maximum principal strain becomes greater than the specified value by the user (if the maximum principal strain is the chosen erosion criteria). Therefore, elements get deleted in unexpected locations. To overcome such an issue, the user should compare a range of reasonable values to simulate element erosion mainly based on trial and error. The simulation will have to be compared to an experiment that the simulation is based on and a suitable value should be selected upon the experimental damage observations.

Jaime (2011) simulated rock drilling in LS-DYNA using CSCM and investigated erosion occurring when cutter interacted with rock. Reasonable range was selected for the ERODE parameter of CSCM, and the results of the simulations were compared to her experiment and a final ERODE value was chosen based on its capability in modelling the real damage behaviour i.e rock cracking and chipping observed in the experiment.

Bi and Hao (2013) simulated 3D finite element modelling of a two span simply supported bridge in a Canyon site. They studied pounding between superstructure parts of concrete bridges using Karagozian and Case model as well as Pseudo Tensor (Mat 16) in LS-DYNA. To reduce computational time, mesh was only refined at impact locations. An advantage of simulating pounding of bridges over buildings is that pounding point is more obvious i.e between two decks where expansion joints are located. For the parts with refined mesh, Karagozian and Case model was employed and for the other parts with greater mesh, smear crack model (Mat_16) was used. The reason for using two models was the fact that Mat_16 models softening behaviour of concrete based on fracture energy release in the analysis and for such model small elements can cause numerical instability therefore the model was used for greater size elements. The behaviour of smear crack models such as CSCM is described in detail in Chapter 3.

Most of LS-DYNA concrete models do not include in-built erosion algorithms including MAT_16 and K&C models. Therefore, *MAT_ADD_EROSION was used to delete elements. They applied 0.15 as the maximum principal strain criteria that was taken from a study by Tang and Hao (2010) on cable stayed bridge response to blast impact. Such value is an ad hoc value and cannot be used for other models. In general, all erosion values are ad hoc values. For other simulations, comparison must be done to select the most suitable erosion value for that particular simulation. For example, Jaime (2011) found 0.05 to be the most suitable value to model element erosion/damage when using Karagozian & Case model in rock cutting simulation. It is not clear whether any other erosion value could have been better suited for the analysis done by Bi and Hao (2013) as the authors did not run any comparison.

He et al. (2017) conducted an experimental work on pounding of two prototype bridge decks with the same concrete strength as a real bridge. The pounding took place at the expansion joints between decks that were secured onto different foundation types. Same scenario was modelled in LS-DYNA using Karagozian & Case model for the superstructure of the bridge, and the elastic material model was used for the footings. Erosion was set to occur when the principal strain of concrete reached 0.15 in the model. This value was taken from a study by Tang and Hao (2010) which the value was also used in a study by Bi and Hao (2013) when simulating pounding of concrete bridges. Contrary to the previous findings on pounding response of buildings, stiffer deck's acceleration was more responsive to pounding. It was found that when decks pounded, the piers were less affected by the earthquake motions. When a soft foundation was modelled, decks pounded severely, and the displacement of the bridge members were amplified.

Wenchen earthquake happened in 2008 in the central mountains of Sichuan. Many bridges were severely affected by the earthquake, and Gaoyuan concrete bridge is an example of these bridges. As shown in Figure 2.15, Gaoyuan Bridge failed due to pounding between the expansion joints as well as the abutments. Hu et al. (2019) simulated the failure response of Gaoyuan concrete bridge using solid-beam coupling method in LS-DYNA. In this method, the nodes of beam elements are master nodes, and the nodes of the solid elements are slave nodes. Rotational and translational movements of the solid part (concrete) is controlled by the beam elements as shown in Figure 2.16 and it is used to save computational time. In the model, CSCM was used to model the piers of the bridge whereas JOHNSON_HOLMQUIST_CONCRETE (HJC) model known as MAT_111 was used to model the concrete girders.

Figure 2.15 Gaoyuan Bridge pounding failure at expansion joints (Lin et al., 2010) as well as pounding of deck against abutments in Wenchen earthquake (Hu et al., 2019)

The FE model in LS-DYNA successfully captured the local and global responses of the bridge particularly the damages observed in the expansion joints and was very time efficient. The damage simulated by the CSCM material model was very close to the damage observed in the bases of the piers during the earthquake as illustrated in Figure 2.16.

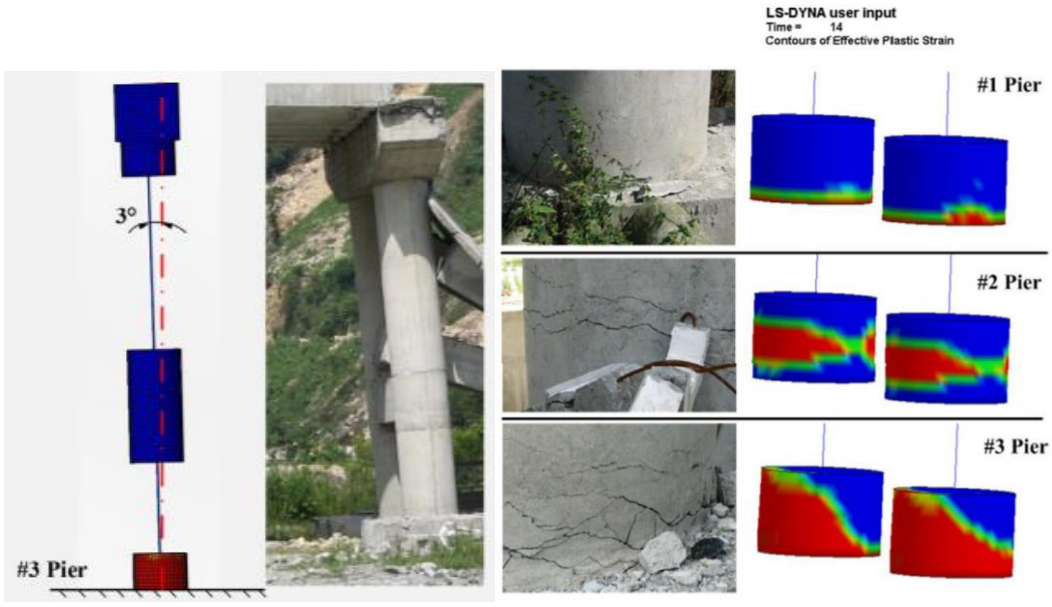

Figure 2.16 Concrete cracks in the bases of the piers were captured reasonably by CSCM material model (Hu et al., 2019)

Despite reasonable findings, it is not clear if the original CSCM short input parameters have been used or the full parameters. In the study, no investigation was made on the influence of the model's key parameters on the response of the bridge.

According to the existing research, concrete structures behaviour has been modelled using the CSCM mainly for progressive collapse (Pham et al., 2017; Yu et al., 2018), impact of a dropping weight (Adhikary et al., 2012; Adhikary et al., 2013), and vehicle crash/impact (Saini & Shafei, 2018; Sainin & Shafei, 2019; Auyeung et al., 2019). Yu et al., (2018) used CSCM to model the behaviour of concrete beam-slab substructure when a column was removed (e.g for refurbishment or replacement of structural elements) and concluded that the model successfully resembled the cracks and concrete failure observed in the experiments. Saini and Shafei (2019) looked into the low velocity impact of vehicles against concrete structures as well as impact of waterborne and windborne debris as well as rock fall. The CSCM, an elasto-plastic damage cap model (EPDC), K&C, and Winfrith material models were compared. They subjected concrete beams and steel tubes filled with concrete to drop hammer test and simulated the same scenario in LS-DYNA. The CSCM and particularly K&C found to perform better than the other two models. CSCM was also found to perform reasonably well in research conducted by Fan et al. (2020) on the impact of barge (transport boat) on concrete bridge piers.

Bentata et al. (2020) experimentally and numerically investigated the impact response of fibre reinforced retrofitted concrete beams impacted by a dropping steel ball of 0.70 kg. K&C model was used to predict the impact forces, maximum displacements, crack pattern, and stress distribution. Teng et al. (2008) also studied the behaviour of steel fibre reinforced concrete slabs under projectile impact with very high velocities. K&C model was used along with an Equation of State (EOS). EOS describes the hydrostatic/bulk behaviour of materials based on pressure and volumetric strain. Dynamic Increase Factor (DIF) was also included within the material model. It is a ratio of dynamic over static enhancement/strength proportional to the strain rate. Using the MAT_ADD_EROSION, a plastic strain criterion was set for the elements which commanded elements to fail as soon as they reached a strain value of 0.9. This value usually is achieved by trial and error. This value can be set differently for different parts of a model. It was observed that the numerical simulation was successful in capturing the correct damage pattern caused by the projectile.

Levi-Hevroni et al. (2018) experimentally and numerically investigated the dynamic tensile loading of concrete (Figure 2.17) using split Hopkinson bar test. Numerical simulation of the Hopkinson bar test was carried out in LS-DYNA, and concrete with a strength of 50 MPa was modelled using MAT_72R3 (Karagozian & Case) and MAT_159 (CSCM) as shown in Figure 2.17 .

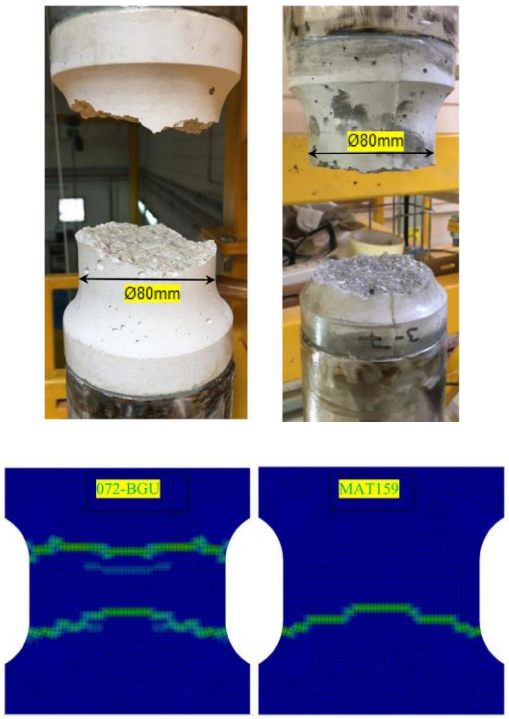

Figure 2.17 (Top) Tensile fracture in concrete specimens after HPB tensile test, (bottom) Comparison of the performances of the modified Mat 72R3 and Mat 159 in simulating cracking/crushing in the tensile test

Both material models were calibrated to optimize the results; CSCM has 49 parameters, five of these parameters have been calibrated to produce better results as shown in Table 2.1. In Table 2.1, G_{fc}, G_{ft}, and G_{fs} are the compressive, tensile, and shear fracture energies; η_{0T} and η_T are the rate effects for uniaxial tensile stresses. On the other hand, K&C has 50 parameters in total plus an Equation of state (EOS). In the numerical study, damage parameters (λ) were calibrated, as well as tensile damage factor (b_2) and stretch factor (s). To avoid over-whelming with large number of tables and data, only a small version of the table is presented below in Table 2.2.

Table 2.1 Calibrated CSCM parameters

	G_{fc}	G_{fs}	G_{ft}	η_{0T}	n_T
MAT159	7.4956	7.06E−2	7.06E−2	6.17E−5	**0.48**
Modified 159	10.57	0.1	0.04	20E−5	**1.25**

Table 2.2 Calibrated K&C parameters

	s	b_2	f_t'(MPa)
072-BGU	0	7.06E-2	4
Modified 072-BGU	5	4.20	2.8

In general, CSCM or the calibrated version of MAT_159 performed better than the K&C model or its modified version. As shown in Figure 2.17 several tensile plastic strains occurred when modelling with MAT_72R3. However, MAT159 showed the tensile plastic strain to occur at the bottom which was the case in the experiments (Levi-Hevroni et al., 2018). It was observed that after the calibration, tensile stress pulse agreed with the data measured from the concrete bar.

Concrete material models have also been used in modelling concrete structural response against detonations/explosive materials. Ganel et al. (2016) modelled reinforced concrete slabs with two different concrete material models, CSCM (MAT 159), and K&C (MAT 72R3), and subjected the specimens to blast load. They found that CSCM performed reasonably better compared to K&C model. Hong et al. (2017) used K&C model along with tensile DIF values calculated from the CEB- FIP model code to model concrete slabs' behaviour against explosion in LS-DYNA. They found that the DIF values suggested by the code underestimates the real behaviour of the slab. CSCM was also used in modelling structural concrete subject to dynamic loadings in several research by Coughlin et al. (2010), Chen et al. (2015), Olmati et al. (2016), Gomathi et al. (2020).

2.4 Previous experimental and numerical research on structural impact/pounding

One of the early generations of experimental studies on concrete-to-concrete impacts is conducted by VanMier et al. (1990). The motivation behind their study stemmed from investigating impact occurring between the concrete units of breakwater armour. Several factors such as the contact surface geometry of the colliding bodies, the mass of the colliding objects, the quality of concrete, and the impact velocities were studied.

In these tests, a concrete striker with a specimen glued to its tip, impacts a concrete pile of 20m length with diameter of 250 mm x 250 mm as shown in Figure 2.10. Two sets of specimens with sizes of 200mm and 400mm were impacted with velocities of 0.5 m/s and 2.5 m/s. Two types of strikers with weight of 290 kg and 570 kg were used to impact specimens. Striker specimens with different geometries were used as shown in Figure 2.11. Impact was tested between specimens with following geometries (1) spherical-planar, (2) conical-planar, (3) truncated conical-planar, and (4) spherical-corrugated. Impact repeatedly took place until extensive plastic deformation was observed as shown in Figure 2.20 (a-c).

Force-time histories were recorded using an accelerometer attached to the middle of the bar. Peak force-time histories were in similar range for the first few impacts until it decayed. It was found that the contact force-time histories were depending on the contact surface geometry of the specimen as well as the striker velocity and mass as shown in Figure 2.13. The contact stiffness of the spherical to planar contact was calculated to be 44 kN/mm$^{3/2}$ which compared to the stiffness value of 201.73 kN/mm$^{3/2}$ obtained by the Hertz theoretical formula is significantly small. (Khatiwada 2014, Muthukumar and DesRoches 2006).

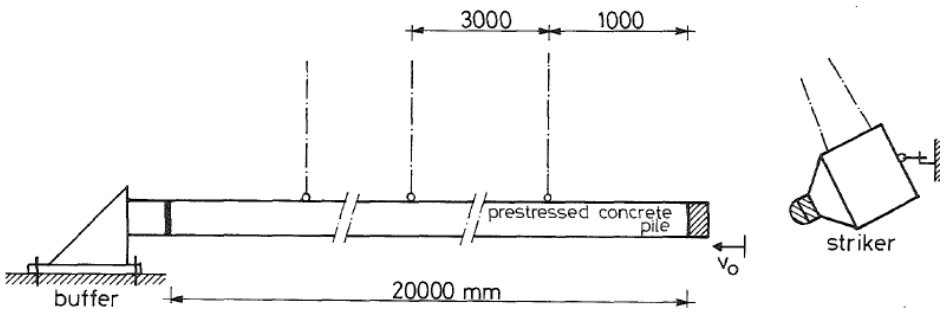

Figure 2.18 Impact test apparatus (VanMier, 1991)

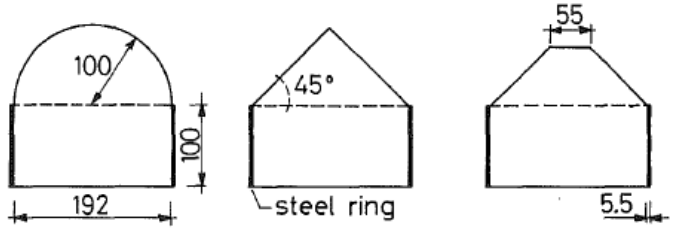

Figure 2.19 Striker specimens with different geometries (VanMier, 1991)

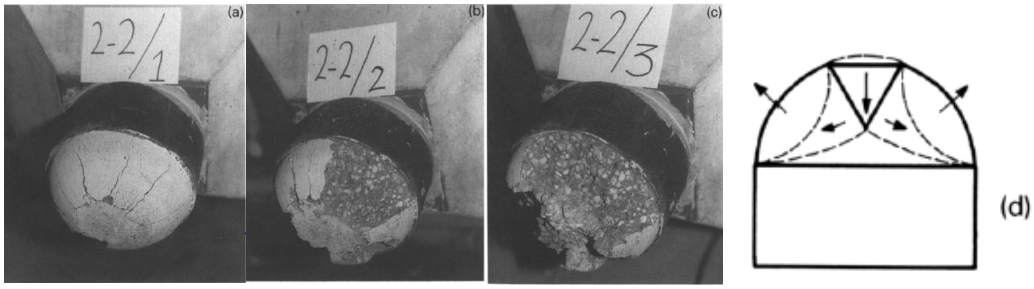

Figure 2.20 (a-c) Plastic deformation in the specimens attached to the striker, (d) assumption of mechanism of fracture and stress propagation in the concrete specimen with spherical shape (VanMier, 1991)

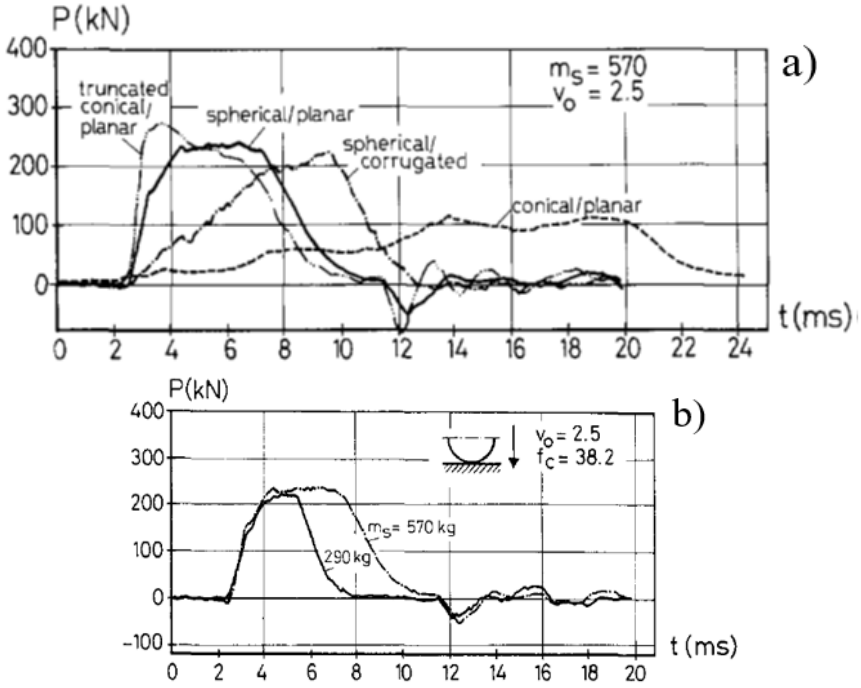

Figure 2.21 (a) Effect of contact surface geometry on the impact forces, (b) the influence of striker's mass on the impact forces; impact between sphere and a flat surface with impact velocity of 2.5 m/s (VanMier, 1991)

It can be observed from Figure 2.13(a) that for impacts that involve larger contact areas, a higher stress pulse with longer duration is achieved. This is due to the fact that larger surfaces stay in contact for a longer period of time as there is great friction between them. Whereas for other cases such as the conical-planar impact case, as soon as contact takes place, the conical specimen's peak breaks, therefore a low contact force is obtained, then the striker continues to crush the specimen with more or less similar magnitude of force and during the whole time the specimen remains in contact with the striker and that is the reason the contact duration is so lengthy.

It can be observed from Figure 2.13(b) that the mass of the striker influenced the duration of the impact rather than its peak. A heavy striker takes more energy and as a result more time to bounce back and separate from the specimen after the impact. It crushes the specimen harder compared to a lighter striker and the damage is more severe. As a result, the post impact velocity is small because the heavy striker does not bounce back as much resulting in a lower coefficient of restitution value (towards value of 0 indicates plastic deformation) indicating greater damage. The effect of striker's velocity is not presented here, however, the experimental results indicated that impacts with higher velocities induce substantial increase in the contact forces. For example, in spherical-flat impacts with velocities of 0.5m/s, 1m/s, and 1.5m/s, the contact forces were 290 kN, 500 kN, and 700 kN. Therefore, impact velocity was found to be directly influencing the magnitudes of the contact forces. Khatiwada et al. (2013) studied the pounding behaviour of two concrete slabs hanging as pendulums. He varied the geometry, velocity and the mass of the colliding bodies. For some of the trials the impact was tested between spherical and flat surfaces and for the rest between flat surfaces. His results also agree with VanMier et al. (1990) study confirming that the impact intensity was depending on the pendulum striker's velocity. The difference between the pounding cases was that in VanMier et al. (1991) study one of the impacted bodies was stationary and the other one moving, whereas in Khatiwada's research both were moving and coming into contact at some point and that made a difference in the severity of the impact and whether the lighter mass hit the heavier one first or vice versa. Damage was most observed when the heavier slab hit the lighter one. Peak acceleration was found to increase linearly with increase in the impact velocity but was independent of the striker mass.

Liebovich et al. (2012) studied the pounding behaviour of two circular concrete bars experimentally (as shown in Figure 2.22) with lengths of 1000 mm and 500mm.

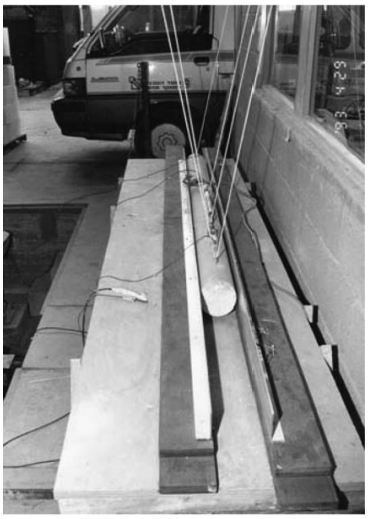

Figure 2.22 Concrete rods hanging by ropes of 5m height

They observed that impact between the rods was not a perfect impact meaning there was misalignment between the colliding rods. This is a frequent event that happens in impacts of rods which disagrees with Hertz theory that is based on perfect alignment between surfaces. Goldsmith (1960) has stated that in real life experiments perfect alignment during collision is very hard to achieve. Irregularities on the surface of the materials contributes to this problem as well. As the contact velocity increased, the peak acceleration increased as well, but the duration of the impact was smaller in the shorter bar. It is stated in their study that impact duration is dependent on the bar length. This statement is true for elastic impacts only. Such statement could be wrong for high velocity impacts and can-not be generalised for all cases. Impact duration is also dependent on the intensity of the impact.

If the impact is soft the objects slide over one another for a longer period of time and the stress pulse duration is longer. However, if the impact is stiff and there are a lot of plastic deformations then the time the two objects are in contact is minimised making the stress pulse duration small. In such experiment the conductor has to make sure the rod length is just about enough for stress pulses to travel freely to the end of the bar and return without coinciding. Otherwise, the results are inaccurate and misleading. Jankowski (2010) conducted two sets of experimental work; (1) dropping a ball onto a rigid surface made of different materials such as steel, ceramic, timber, and concrete, (2) two steel towers vibrating and pounding on a shaking table test. In his dropping ball experiment, he found that the coefficient of restitution value was not sensitive to the ball mass, but rather depending on the starting velocity; the coefficient of restitution decreased when the initial velocity increased. He introduced Equations (polynomial functions) by fitting experimentally determined restitution coefficients and initial velocities for different material impacts. His shaking table test showed that

pounding amplified the structural response. However, in some cases pounding was beneficial and helped to restrain the movement of the building and prevented severe damage particularly for more flexible buildings.

Shrestha and Bi (2016) stated that shaking table tests were conducted in attempt to gain a better understanding of structural pounding/impact. However, due to being very expensive particularly large experiments, these tests are conducted mainly in a way that permanent plastic deformations were avoided, therefore, local damage was not very much explored. To observe the influence of pounding on the inter-storey-drifts of two buildings, one stiff and the other one flexible, Crozet, et al. (2019) conducted shaking table tests on two storey composite buildings (as shown in Figure 2.23) with steel grades of S355 and S275.

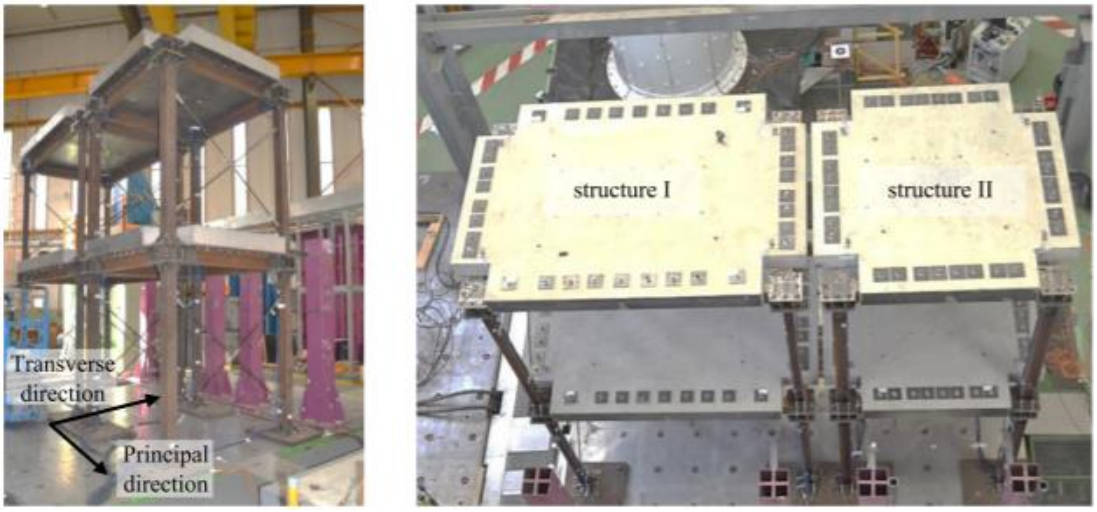

Figure 2.23 Composite structural test set-up (Crozet et al. 2019)

Numerical simulation of the shaking table test illustrated in Figure 2.23 was simulated in a FE code called Cast3m by Crozet et al. (2019). They found that the inter-storey drift did not increase very much if the earthquake severity was mild or if soft small multiple impacts occurred. In their experiment, despite their best effort in constructing the buildings properly with only small discrepancies, still there was imperfect alignment between the buildings during impact. To mitigate such effects of pounding, a firm link was used to connect the buildings to enable them to move in phase. However, it was observed that the stiffer building's inter-storey drift was increased for the duration of the earthquake. The link found to be very effective in reducing the response of the more flexible building. They concluded that despite the differences between their FE model and their experiment, the correlation between the two was satisfactory.

There are other shaking table experiments carried out over the past years, for example Filiatrault (1996) carried out shaking table tests on two, eight and three- stories buildings that either had no separation gap in between or a separation gap of 15mm. Chau et al. (2003) subjected two steel towers to El-Centro earthquake. These buildings had different masses and dissimilar natural frequencies due to the differences in their dynamic characteristics such as mass and stiffness. However, a common disadvantage of their work was that by using a load cell or pounding head they directed the impact to occur at a particular pre-defined location on the surface of the buildings. It is very obvious that such method is unrealistic when it comes to real structural pounding behaviour as in reality it is unclear at which location of the structure pounding occurs first.

To verify whether this hypothesis of pre-defined pounding location introduced by those researchers is realistic, Zhu et al (2002) carried out tests on the pounding of concrete bridge decks, as well as deck to abutment. He then simulated 3D version of the bridge in his own computer code called Dynamic Analysis Bridge System (DABS) and used a linear link element with linear dashpot to investigate the ponding behaviour of a steel bridge that consisted three spans. However, the location of impact was not defined in advance and was arbitrary, therefore, nodes of any parts could have come into contact. Impact parameters such as the coefficient of restitution was obtained from his experiments and was included in the link element. His model proved satisfactory, and it was concluded that pounding can-not be pre-defined.

Jia et al. (2019) simulated pounding between decks of a railway bridge in SAP2000 using gap elements. The first two vibrational modes were found to be most critical making the bridge decks more susceptible to pounding. The inputted contact parameters found to be very important in the pounding response of the structures. In their simulation, they used an impact stiffness value of 9.9×10^9 (N/m) given in a study by Wang et al. (2004) which found the impact stiffness to be half of the axial stiffness of the shorter bridge deck. They examined several other close values such as 9.8×10^9 (N/m), and 1.0×10^{10} (N/m) in different case studies with different gap openings to find which value produces the worst pounding force and damage to the bridges. It was found that the input contact parameters' value i.e contact stiffness plays a significant role in generated pounding forces. A range of contact stiffness values were implemented in SAP2000 to assess the change in the pounding forces. They also assessed the effect of initial separation gap between the decks ranging from 0.10-0.14m. Pounding forces severely changed with variable contact stiffness values. The most critical pounding force of 9.62×10^7 N was obtained when the gap between the joints was 0.14m with an impact stiffness of 9.9×10^9 N/m as shown in Figure 2.16. In Figure 2.24 (a) at times where the blue pick displacement response has passed the red dash line, the decks have come into

contact which means the deck displacement has exceeded the initial separation gap of 0.14m and as a result pounding forces were generated at those time shown in Figure 2.24 (b).

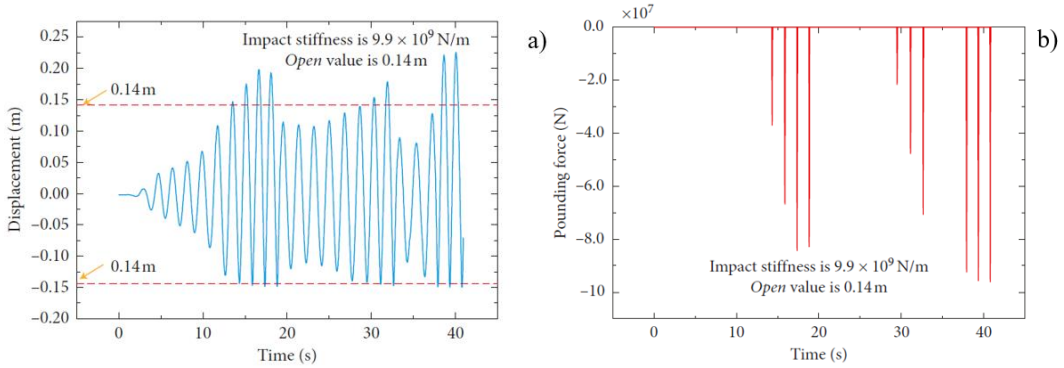

Figure 2.24 longitudinal displacement response of bridge decks (Wang et al., 2004)

This study also confirms the dependability of contact models on the correct choice of contact parameters which is very hard to find. Even those used in previous simulation and seemed to work might not be suitable for another problem. Contact stiffness depends on the geometry of the impacted bodies (surface of the contact) and how rough or smooth their surfaces are, the material type as well as the velocity of the impacted bodies. Therefore, the choice of the right contact parameters always remains a challenge in this type of pounding modelling. Kang et al. (2021) simulated the impact behaviour of concrete columns subject to hammering, as well as barge impacts onto concrete bridge piers in OpenSees (Mazzoni et al., 2007). A link element with elastic spring and viscous damper was used in the analysis. Force-displacement data were used to obtain the contact stiffness values of 2×10^9 N/m and 4×10^9 N/m for hemispherical and flat contact areas. As the contact stiffness is a function of contact area, the latter is higher value because the contact area was greater. Variable contact stiffness values were assumed for different geometries based on those values. The author has claimed the method to be reliable in investigating pounding and has stated the efficiency in the computational time in analysing such problems. However, explicit algorithms in OpenSees (Mazzoni et al., 2007) needs improvement and OpenSees exhibits convergence issues particularly in implicit analysis when dealing with strong dynamic nonlinearities (Lu et al., 2019).

Abdel Raheem et al. (2018) employed 3D Finite Element analysis of structural pounding between three RC buildings in a row with different heights subjected to eight different earthquakes in ETABS. A simple concrete model with 30 MPa strength was used; ETABS has an internal library of basic standard section properties of different materials that users can use with minimal input parameters (Structural Software for Building Analysis and Design,

ETABS, 2021). A linear damped contact/gap element was defined between the adjacent structures. For such modelling with application of contact models, contact stiffness has to be pre-defined; a contact stiffness value equal to the axial stiffness of the impacting floors was taken from a similar study done by Watanabe and Kawashima (2004). Overall, three factors were identified as the major effective parameters in pounding: (1) structural period, (2) earthquake characteristics, and (3) position of the structure to the neighbouring structures. The analysis showed that pounding was beneficial to the middle building because the building benefited from being restricted by the other two buildings on each side and as a result was not damaged by the earthquake motions. The taller building had the maximum displacement response and showed a whiplash behaviour. Even though the author claimed that the findings of such a study can help in revising the recommendations made by building codes and mitigating pounding risks, it is unclear whether the contact forces that were generated during the pounding are over-estimated or under-estimated. Contact forces are responsible for damages observed in the analysis and these forces are the results of contact parameters such as contact stiffness. Other estimation of such value can actually lead to different conclusion.

The second disadvantage with their method of modelling is that the location of the contact/impact elements are defined by the user. The user usually places them where the slabs come into contact. Such assumption could be wrong as during pounding any part of the building may come into contact that could be the start of pounding damage. Besides, during collision of two structures, two greater areas may come into contact and not just a single point on the body of the structure.

A similar study by Lopez-Almansa and Kharazian (2018) on pounding of 2D three-storey and five-storey buildings, with different number of bays, as well as buildings with aligned slabs was carried out as shown in Figure 2.25. Kelvin-Voight contact element model (Linear Viscoelastic Model- LVe described in section 2.2.2) was selected in SeismoStruct software to measure pounding forces. Contact stiffness was taken equal to the axial stiffness of the floors for each pounding case ranging from 211.1 to 21109 kN/mm. They compared the results of pounding cases with varied separation gaps between the buildings.

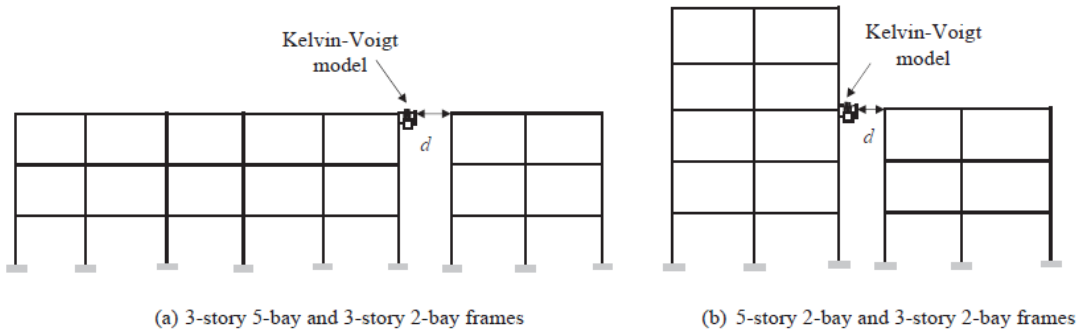

Figure 2.25. 2D simulation of pounding frames in SeismoStruct with gap elements placed in between the buildings (Lopez-Almansa and Kharazian, 2018)

They modified the damping parameter (C) of the Kelvin-Voight model while keeping the damping ratio either 0 or 0.05, the damping parameter was hand calculated using their new formulation. Contact stiffness values, coefficient of restitution, initial separation gap, percentage of energy dissipation, and the severity of the impact were identified as influential parameters on the pounding response of the buildings (Lopez-Almansa and Kharazian, 2018).

A research on 3D structural pounding by Polycarpou and Komodromos (2012) considered impact between equal height buildings modelled as linear multi- degree freedom systems (MDOF) using their own coded program. In that study, floors were modelled as rigid plates, and contrary to the previous studies, contact was assumed between areas rather than points. Impact was considered as a small area on the centroid of the impacted polygon plates as shown in Figure 2.26.

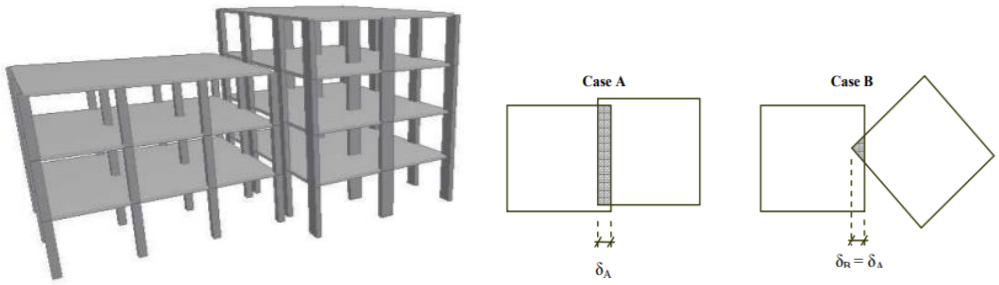

Figure 2.26 Simulation of pounding between floors including schematic drawings of central contact area between floors modelled as rigid plates (Polycarpou and Komodromos, 2012)

A penalty contact method in FEM was used to calculate impact forces along with a dashpot that accounts for energy dissipation. The advantage of their work over the previously mentioned research is that using a penalty method eliminates the possibility of wrong estimation of contact forces as a result of choosing incorrect contact parameters. However, in

such a method, the reliability lies on the choice of concrete material model. The greatest advantage of this approach is its computational efficiency which makes parametric study (study to define reasonable contact stiffness, damping ratio, i.e) time saving. However, it is not mentioned in their investigation whether or not they have validated the performance of their simulation particularly the concrete behaviour against any experiments or any other software/codes. Also, the concrete material parameters were not stated.

One of the disadvantages of their simulation was that their model was a linear elastic model incapable of simulating damages particularly at the contact point. Also, the floors were modelled as rigid plates which again is not a good representative of building pounding in real world. Also, the authors have claimed that they developed a new code for their own purpose because they did not find a suitable software that could include penalty method and take into account the influence of the impacted bodies' geometries. To the best of this PhD author's knowledge, LS-DYNA (developed by John Hallquist in 1976) is an excellent software to analyse structural dynamic behaviour.

Jankowski (2008) simulated the pounding that occurred between olive view hospital's main building and its stairway tower during the 1971 San Fernando earthquake (as shown previously in Figure 2.3). During the event, the lighter building (the stairway) was hammered a few times by the main building and tilted but completely failed after a few days. He conducted 3D FE modelling of the pounding. He used a plasticity concrete material model that assumes tensile and compressive stresses as the main failure mechanisms in concrete. A gap friction element was placed between aligned nodes of the buildings as shown in Figure 2.27.

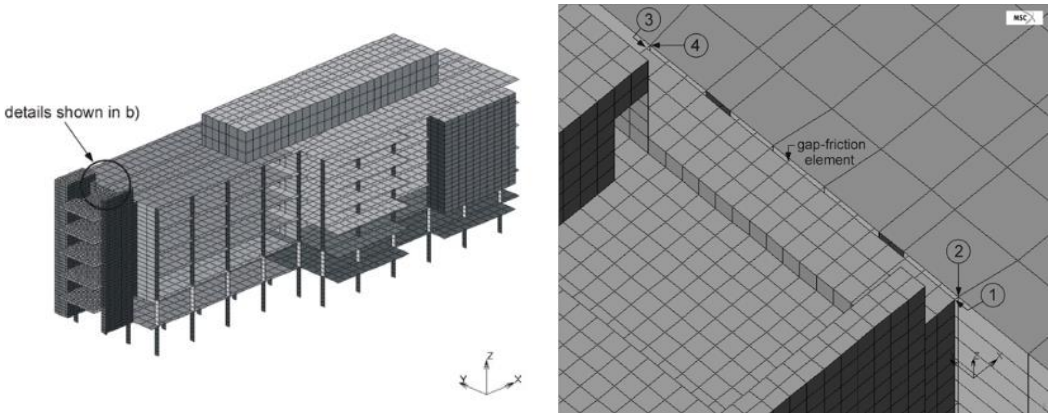

Figure 2.27 FE simulation of Olive View hospital in MSC Marc software (Jankowski, 2008)

From the analysis, displacement histories were obtained, and pounding was spotted when the lines interacted. As an example, displacement-time history of node 1 is presented in Figure 2.28.

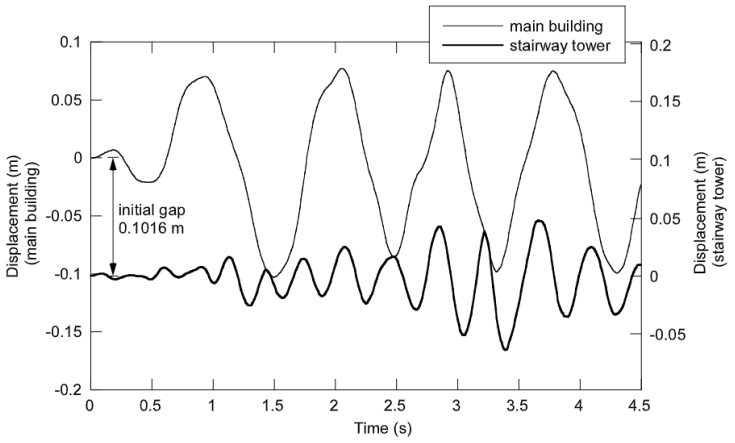

Figure 2.28 Displacement-time histories of the main building and the stairway (Jankowski, 2008)

The first impact between the structures occurred within 1.5 seconds of the seismic motion. The following impacts were observed at 2.5 seconds, and 3.3 seconds where the buildings stayed in contact for a longer period of time (approx.100 milliseconds). The main building experienced a lot of plastic damage and Jankowski (2008) concluded that the main reason identified was the shear failure of the ground floor's columns in the main building. However, due to the flexibility of the lighter building pounding amplified its response which seconds the findings of (Crozet, et al 2019). Such effect could have been prevented if the buildings were designed with similar periods or if sufficient separation distances was provided. On contrary, the stiffer building's response was not influenced by pounding very much, however, the occurrence of plastic strains in the bases of the columns was the result of the earthquake shakes severity.

Mahin et al. (1976) conducted an extensive research on Olive View hospital. He also re-produced the same scenario using a simplified inelastic model and modelled the light building as a rigid structure. They found that torsion was not influential in the destruction of the hospital; however, Jankowski (2008) disagreed with that, and stated that torsional effects were significant. The findings of a study by Mavronicola et al. (2020) on the pounding of multiple storeys based-isolated buildings (BIBs) show that mass eccentricities in the buildings causes torsional effects that are very harmful to based isolated buildings. This accompanied with a misaligned impact between the buildings during earthquake result in severe increase in the displacement response and shear forces in the buildings.

The model in Mahin et al. (1976) study was very stiff and did not represent the real behaviour of the staircase, neither could it consider the plastic deformations in the bases of the columns. It is concluded by Mahin et al. (1976) in his extensive report on the Olive View hospital that the buildings were over-designed, however, the first two stories were built with insufficient detailing. Both studies agree that the main building was not affected much by pounding. It should be noted that one of the disadvantages of Jankowski's work is that spalling and crushing of concrete was not considered in his model.

Fatahi, et al. (2018) used 3-D finite element analysis in ABAQUS to investigate pounding between three adjacent 15-storey reinforced concrete buildings on pile foundation with variable separation gaps under Northbridge (1994) and Kobe (1995) earthquakes. As part of the research, interaction between pile foundation and soil was also studied. It was observed that pounding increased the shear force in the columns particularly for the middle building that was confined by the other adjacent structures and as a result this effect was transferred down to the pile group and exerted extra pressure onto the pile. This effect is usually detrimental and causes building failure. In such buildings with pile foundations, engineers must pay attention to the interaction between the piles and soil at the same time and not treat them separately as pounding is always damaging in these cases. It is concluded that the minimum gap must be increased for structures with shallow foundations.

The focus of this chapter, so far, has been on what structural pounding is, and how researchers started to investigate pounding between bridges, buildings, etc using simplified models first, and then gradually research on pounding evolved into more advanced methods of modelling using variable computational tools that use force-based models. Still uncertainties persist in modelling of structural pounding and because of the incompetency of the previous methods, a lot of their findings can-not be applied onto other pounding cases.

It is shown that researchers either used contact link elements (force-based models) with their own chosen contact parameters to simulate structural pounding in different software, or they looked at large FE models of buildings with several floors and looked into their global behaviour. None has taken a more robust method to model simpler structures with fewer stories and an in-depth approach to investigate structural pounding. Still remains a question whether pounding at all influences structures globally, or locally, or both.

It is apparent that only a few researchers such as VanMier et al. (1990) have carried out experimental work on impact/contact of materials as a first step to understand concrete behaviour and impact mechanism and damage progression in structural materials. It is crucial to apply a more accurate approach in simulating structural pounding by understanding contact at material level first, and once a deeper knowledge of concrete behaviour at material level is

gained, then all that knowledge can be transferred onto understanding contact/pounding between more complex geometries such as actual structures that include members such as reinforcement bars.

The topic of structural pounding is a very broad topic that involves interesting areas with wide range of influential factors that contribute to the complexity of pounding. It was not the purpose of this section of the literature study to review all the existing and current studies in this field of structural pounding. It has rather aimed for the readers to become up to date with the important narrative of the research, and it has highlighted the gap in the knowledge that requires further attention, or where existing assumptions are not accurate. The remainder of this chapter focuses on those research that have been conducted in LS-DYNA in particular, to model contact/impact using variable concrete material models and it highlights a gap in the literature showing the lack of a robust material model that can be used for simulating pounding of buildings.

2.5 Summary

As described in the review of the previous research, to this date large number of numerical studies as well as experimental work have been carried out to investigate structural pounding. It started from analysing structures using simple analytical contact models that were numerously modified over several decades, and gradually research on structural impact was moved towards modelling simplified structures in engineering software tools by placing a gap element in between the contact location to obtain contact forces and displacements. However, all those methods, as described in the body of literature, have great uncertainties and limitations. In the newest studies, researchers have started analysing structural pounding using the Finite Element Method. Application of FEM using penalty method removes the uncertainties associated with pre-defined contact locations and the choice of contact parameters, however, introduces another challenge which is the choice of material model used for the modelling.

To this date, research work on modelling and analysing building pounding is very limited and identifying a material model that is suitable to model pounding between buildings is required. The research on the seismic building pounding contrary to bridge structures is very much limited and the numerical simulations have not been validated against any experiments, and yet, the pounding mechanism is still not very well understood. Even in pounding of bridges where research on impact/pounding is more advanced, particularly pounding of decks where the location of impact is obvious, still understanding the pounding mechanism remains a challenge.

To overcome the limitations and uncertainties associated with the existing methods of simulating pounding described in the body of literature, a new method is developed using detailed FE modelling that offers significant advantages over the existing approaches. Particularly, since the contact is modelled using penalty method and estimation of contact parameters and the uncertainties associated with choosing suitable parameters such as spring properties, or the damping ratio which is a function of coefficient of restitution are no longer of concern.

In this method, the suitability of material models and their accuracy in predicting the real structural behaviour is examined through two most robust material models called Continuous Surface Cap Model (CSCM or MAT_159) and Karagozian and Case (K&C or MAT_72R3). In this thesis, the performances of both models are examined at material level using direct Hopkinson Pressure Bar (HPB) experimental tests and numerical simulations. Afterwards, the concrete models were examined at structural level using shaking table simulations and their

validation against shaking table experiment carried out by Garcia et al. (2010). Lastly, the findings of both simulations were incorporated into an overall structural pounding FE model.

The recommendation on the use of material models made herein helps researchers to select a suitable model for simulating building pounding/impact events that take place between any two concrete buildings made of different geometries. As mentioned by Shrestha and Bi (2016) simulation of arbitrary pounding/impact between closely spaced structures considering local damage as well as global damage is still a very challenging subject to explore. Also, despite the fact that there are available simulation tools that have the required capacity to simulate structural pounding, still the accuracy and reliability of such simulation greatly depends on the choice of the material models.

The incorporated FE detail model of building pounding has made it possible to investigate the pounding mechanism further as the two buildings are free to come into contact at any point therefore impact location is not pre-defined. Number of contacts contact forces magnitudes, their duration, etc can be obtained from anywhere in the FE model.

Determination of contact parameters (i.e contact stiffness and damping ratio) based on assumption/estimation is no longer required or as such that exists in the gap contact element formulation. Also, buildings with flat surface geometries can be modelled, and most importantly the FE model can consider variable range of low strain rate to high strain rate dynamic problems.

Chapter 3

3. Physical and numerical direct HPB tests on concrete and steel samples

To establish a reliable methodology for simulating structural pounding, it is important to understand the contact behaviour of structural materials first before transferring that understanding onto something more geometrically complex such as the pounding of multi-storey buildings. Lack of robust simulations that can consider a wide range of strain rates and that are based on experiments to reliably model pounding/impact behaviour at material level between flat surface geometries is the motivation behind this chapter of the PhD study which led to establishing a numerical method for the researchers and engineers to employ for modelling structural pounding in the future.

A series of direct impact Hopkinson Pressure Bar (HPB) tests was conducted at the University of Sheffield Blast & Impact research laboratory at Harpur Hill, Buxton, Derbyshire to observe the behaviour of concrete and steel at plain material level during impacts. The impact arrangements differed for each test, for example in some cases impact took place between a concrete specimen and a steel striker, or between two steel bars, or a concrete specimen and a concrete striker. The intensity of impact for every case was different as the striker velocity changed for every test ranging from 0.58 m/s to 26.60 m/s. The key principle underlying the design of the test programme was that of deriving high quality experimental data from tests with carefully controlled boundary conditions, such that the resulting data could be used to validate numerical modelling approaches. Direct HPB impact tests rather than the more usual Split HPB tests were conducted because the aim was not to characterise the material strength at high rate, it was rather to extract quantitative data of what is effectively a structural impact problem. In direct impact tests, the key quantitative data obtained is visual imagery of the

deformation and failure of the specimen, obtained through high-speed video (HSV) footage, and measurement of the stress versus time passed into the HPB by the face of the specimen in contact with it. Numerical models of the experimental tests have been conducted using CSCM and K&C in order to identify the most promising approaches for capturing the elastic and inelastic response of the concrete observed in the tests.

The finite element software LS-DYNA (LS-DYNA, 2018) is used for carrying out the entire numerical analyses in this PhD study. Livermore Software Technology Corporation (LSTC) has developed LS-DYNA for the purpose of simulation of non-linear finite element problems. It is capable of analysing a vast number of complex FE models from static problems to high strain rate dynamics with strong visual capabilities. The program has been optimised for FE modelling of non-linear transient dynamic analysis and it is suitable for capturing large deformations of FE models with wide ranges of strain rates during impact/blast analysis and it has wide range of material models available. For such advantages, LS-DYNA is chosen to simulate the direct HPB models.

The reliability of the numerical simulation enormously depends on the choice of material models. Due to the extreme non-linearity in concrete behaviour, great effort is required to calibrate the chosen material models against the experiments. Continuous Surface Cap Model (CSCM or MAT_159), and Karagozian and Case (K&C or MAT_72R3) in LS-DYNA were used in the HPB simulations and calibrated to resemble the concrete behaviour observed in the tests.

Inelastic deformations caused by the impact waves in the specimens were studied in more detail using both material models, and the performance of CSCM was compared against K&C. Both material models exhibited excellent correlation with the tests in general with less than 10% difference (i.e peak stress), except that the model with CSCM exhibited a softer impact, whereas the model with K&C showed a stiffer response. Also visualising realistic concrete crushing was possible for both material models when element erosion or deletion of elements (based on the maximum principal strain) was set to 1.09 for CSCM and 0.07 for K&C.

3.1 Direct HPB experiments

For many years, direct Hopkinson Pressure Bar (HPB) tests or Kolsky bar have been used to determine the dynamic properties of materials. The direct HPB tests in this study consist of three cylinders; HPB, specimen, and striker as shown in Figure 3.1. The HPB used in this study is a long cylindrical bar made of steel and it is subjected to impact loading from one

end. There are two conditions for the other end: (1) the other end is fully fixed, or (2) the other end is completely free. The HPB in this study had a free end.

Pressure pulses are generated by striking one side of the long bar by a steel or concrete striker bar. The concrete/steel striker bar is inserted onto a pressure gas gun. The gas gun itself is screwed onto a pressure reservoir with a thin brass disc in between them. During the test, the disc bursts and rapidly releases the pressure from the reservoir onto the back of the striker bar which accelerates the striker bar.

As soon as impact occurs, a uniformly distributed pressure is exerted onto the face of the specimen. During the impact, the generated strain pulses propagate along the bar and are recorded at a reasonable distance away from the face of the impact to avoid interaction between the outgoing and incoming pulses (Tyas & Watson, 2000). In the experiment conducted for this thesis, once the impact occurs, axial strain is recorded by strain gauges placed at 1m away from the face of the HPB, and from the strain recorded axial stress is calculated.

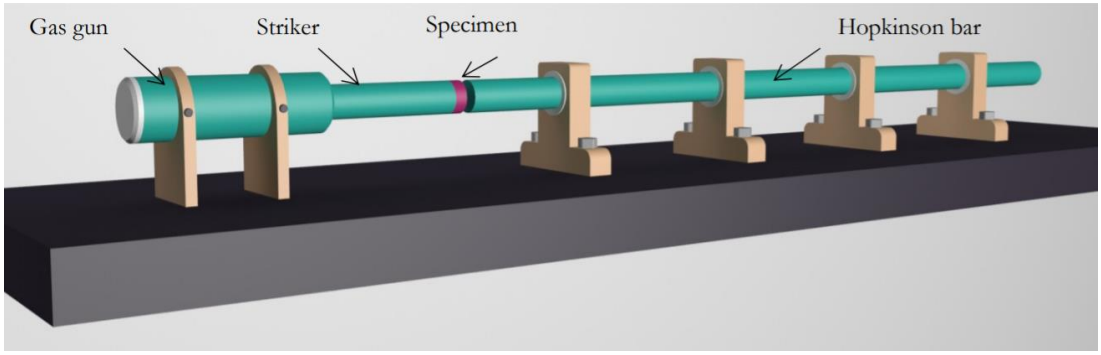

Figure 3.1 Hopkinson Pressure Bar set-up

3.1.1 Test set-up and sample sizes

Several impact tests were conducted at the Blast and Impact Laboratory of the University of Sheffield in Buxton. Impact was generated with four arrangements: (1) impact of steel striker to steel sample, (2) concrete striker against concrete sample, (3) steel striker against concrete sample, and (4) concrete sample against the steel HPB. The HPB used in this work was formed of a 0.0492m diameter cylinder on EN24 (T) steel, with Kyowa KSP semiconductor strain gauges used to measure the propagating strain pulses. Geometrical and material properties for the bar are given in Table 3.2. Concrete specimens were 0.05m in diameter, with lengths

varying between 0.025m and 0.05m. Concrete and steel strikers were 0.4m in length and had the same diameter as the specimens 0.05m with a difference of ±0.0001m. It should be mentioned that making the specimens' sizes to 0.05m, particularly, the concrete specimens were very difficult and due to the nature of concrete there were slight differences in the diameter of the concrete specimens. Concrete and steel samples and strikers are illustrated in Figure 3.2 and Figure 3.3.

3.1.1.1 Preparing concrete and steel samples

Concrete samples were casted in strong firm plastic cylindrical tubes made in different sizes. They were measured and cut into different sizes and were glued. A small base was also constructed and was attached to the bottom of the tubes to make them stand. Concrete cubes were also cast to measure the compressive strength of concrete over time as shown in Figure 3.2. Compressive strengths of the cubes and the cylinder specimens were taken as 60 MPa and 48 MPa.

Figure 3.2 photos show steel strikers and samples as well as casting process of concrete in laboratory

Figure 3.3 Steel and concrete samples

3.1.1.2 Hopkinson Pressure Bar tests

The experimental detail such as the specimen size and impact velocity etc., are shown in Table 3.1. As an example, the test apparatus arrangement for Test 1 is shown in Figure 3.4. The specimen is attached to the HPB shown on the left side of the photo and the steel striker is placed against it. The experimental results are shown in forthcoming sections and are further discussed along with comprehensive discussions on the numerical simulations validated with reference to these experiments.

Table 3.1 HPB impact tests detail

Test numbering	Specimen size m	Specimen material	Impact type	Striker velocity m/s
T1	0.025	Concrete	Steel striking concrete specimen attached to HPB	18.88
T2	0.025	Concrete	Concrete striking steel HPB	8.15
T3	0.050	Concrete	Concrete striking steel HPB	8.75
T4	0.025	Concrete	Concrete striking steel HPB	0.58
T5	0.025	Steel	Steel specimen striking steel HPB	19.40
T6	0.025	Concrete	Concrete specimen striking another concrete specimen attached to HPB	26.60
T7	0.050	Concrete	Concrete striking steel HPB	7.0

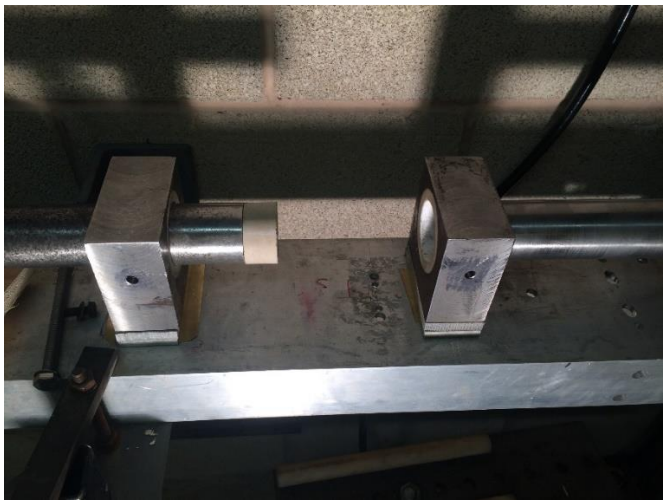

Figure 3.4 Experimental apparatus set-up for test 1

3.2 Finite element modelling of the Hopkinson Pressure Bar

3-D Finite Element modelling was conducted for the HPB experiments explained in section 3.1 using LS-DYNA based on the tests' arrangements conducted at the laboratory. Accurate construction of a FE numerical model is important, however, majority of that accuracy and reliability of such model purely depends on the choice of material models used. By assessing the model's responses at plain material level first (testing plain specimens using experiments such as direct HPB) the capability and suitability of such material models are better assessed.

In this study, two best suitable concrete material models were selected; Continuous Surface Cap Model (CSCM) known as MAT_159, and Karagozian & Case (K&C) known as MAT_72R3, as well as steel material models i.e elastic steel (MAT_001) and simplified Johnson-Cook models (MAT_098) in LS-DYNA. They are chosen based on advantages such as that both material models offer automatic generation of default input parameters. Both models are rate sensitive; CSCM has an inbuilt strain rate formulation and K&C offers tabulated form of the Dynamic Increase Factor (DIF) to be entered by the user. CSCM is capable of modelling strain softening in concrete through fracture energy based on CEB-FIP Model Code 1990 Design Code, and it has an in-built element erosion mechanism that resembles failure of material. K&C has Equation of States (EoS) that takes into account the compaction porosity effects in concrete. Both material models have well-established user-manuals. By the end of this chapter, performances of these two material models have been examined and compared against the experiments using stress histories.

3.2.1 Elastic steel

Linear elastic material model (*MAT_ELASTIC in LS-DYNA) was used to model the HPB. During the actual test in the lab, the direct HPB tests were performed in a way to prevent any permanent damage on the HPB and it remained elastic at all time. Therefore, the same condition is modelled in LS-DYNA. The properties of the steel bar used in the experiment and in the FE model is shown in Table 3.2.

Table 3.2 Elastic steel HPB properties

MID	1
ρ	7850 kg/m^3 (+/-25 kg/m^3)
E	212E+09 (+/- 1.5E+09) (N/m^2)
Poisson's Ratio (v)	0.29
C- One dimensional wave velocity	5194 m/s (+/-13 m/s)
Radius (a)	0.0246 (+/-0.00005m)

3.2.2 Simplified Johnson-Cook material model (MAT_98)

This simplified Johnson-Cook model known as MAT_98 in LS-DYNA was used to model the steel specimens which were grade S355. The input parameters for this model are shown in Table 3.3. The J-C model is a visco-plastic material model that is usually used for modelling metals that have high strain rate dependency (Johnson and Cook, 1983). In such model, the yield strength and the strain hardening are rapidly changing with strain rate while the modulus of elasticity is remaining constant. This material model has been used in different research areas such as FE modelling of steel connections by Rahbari et al. (2014), modelling of steel projectile impact by Borvik et al. (2001), and impact performance and progressive axial failure/collapse of high strength steel columns by Oscar and Eduardo (2008).

The flow stress σ_y in Johnson Cook material is expressed as follows:

$$\sigma_y = (A + B \times \varepsilon^n)(1 + C \ln \acute{\varepsilon}^*) \quad 3.1$$

Where σy is the effective stress, A, B, and C are constants, ε is the effective plastic strain.

n is the work hardening component. $\acute{\varepsilon}^*$ is the normalised effective plastic strain rate. The parameters used in the numerical modelling is expressed in Table 3.3. Failure happens when the effective plastic strain exceeds PSFAIL.

Table 3.3 Simplified-Johnson Cook input parameters (Rahbari et al., 2014)

MID	98
ρ	7850 (kg/m^3)
E	2.07E+11 (N/m^2 or Pascal)
PR	0.3 (Poisson's ratio)
VP	1
A	1.6642E+8 (N/m^2 or Pascal)
B	4.8578E+8 (N/m^2 or Pascal)
N	0.16981
C	0.022
PSFAIL	0.5962
SIGMAX	SIGSAT
SIGSAT	1.0E+28
EPSO	1.0

3.2.3 Continuous Surface Cap Model (CSCM) MAT_159

CSCM (MAT_159) was originally developed with the aim of simulating the failure and crushing/deformation of the roads/motorways' concrete barriers and safety structures as a result of vehicle crash as part of a research funded by the Federal Highway Administration (FHWA). This material model is commonly referred to as smooth continuous surface cap model. Based on damage formulation, this model anticipates strain softening of the material and it considers the ductile and brittle damages separately (Jaimie, 2011). A comprehensive description of the developing process of this model was given by Murray (2007b), and the main equations and key parameters are described herein.

In this material model, concrete is assumed isotropic, and for the elastic part Hooke's law is used to describe the relationship between the elastic stress and elastic strain. This law depends on the shear modulus *(G)* and the bulk modulus *(K).* As soon as the material experiences permanent deformation, following the elastic phase, concrete starts to yield and if the stress continuous to increase, it reaches the failure point. The yield stresses state is defined by a 3-dimensional yield surfaces (Murray 2007b). In the analysis, at every time step, as the strain rate increases, the stress is updated for every step using the Hooke's Law, the updated stress is called the trial elastic stress. If this falls in or on the yield surface, then the plasticity formulation is ignored and the behaviour is elastic, however, if it lies outside the yield surface

then the behaviour is elastic-plastic that possibly includes rate effects, plastic damage, and hardening then the algorithm of plasticity returns the stress state to the yield surface (Murray 2007b). The plasticity algorithm will predict concrete dilation once the stress state has returned to the yield surface. For modelling dilation, a plasticity algorithm is required which is included in the model.

3.2.3.1 Yield surface

CSCM model is a viscoelastic-plastic cap model that includes a smooth continuous curved surface/intersection between the shear failure surfaces, with the hardening compaction surface known as cap. A general figure of the yield surface is illustrated in Figure 3.5 (Jiang and Zhao, 2015). It is for this smooth intersection between the failure surface and the cap that the model is called continuous surface cap model (CSCM). The cap surface can be unity or ellipse. Concrete is typically assumed to be isotropic, and isotropic materials have three stress invariants. For this material model the yield surface is expressed using three stress invariants. They are denoted J_1 (this is the first invariant of the stress tensor), J'_2 (this is the second invariant of the deviatoric stress tensor), J'_3 (this is the third invariant of the deviatoric stress tensor).

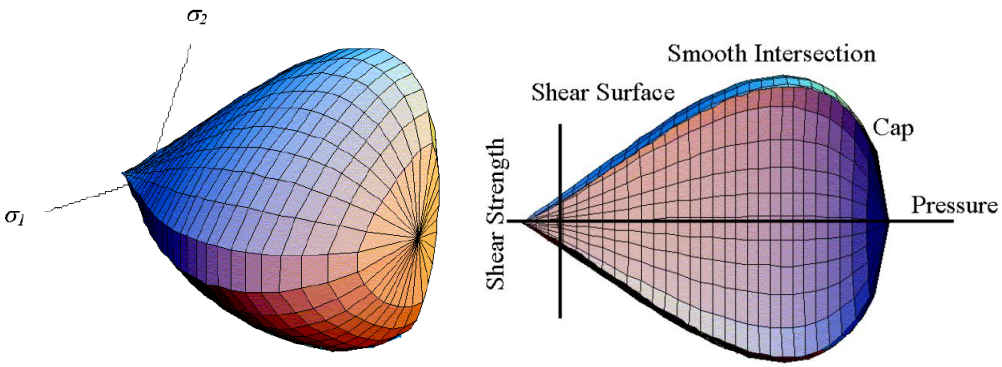

Figure 3.5 General 3-D graphic shape of the yield surfaces of concrete (on the left), on the right is the general 2-D shape of the concrete yield surface

Shear surface is employed to model the concrete strength in the tensile and low confining pressures. The shear surface formulation along the compression meridian is as follow:

$$F_f(I_1) = \alpha - \lambda \exp^{-BI1} + \theta I_1 \qquad 3.2$$

Where the values of α, β, λ, and θ are used to fit the surface of the model to strength measurements from the triaxial compression tests (Figure 3.6) that were carried out on plain

concrete cylinders when developing the material model (LS-DYNA, 2018). The triaxial compression data is shown as principal stress difference versus pressure.

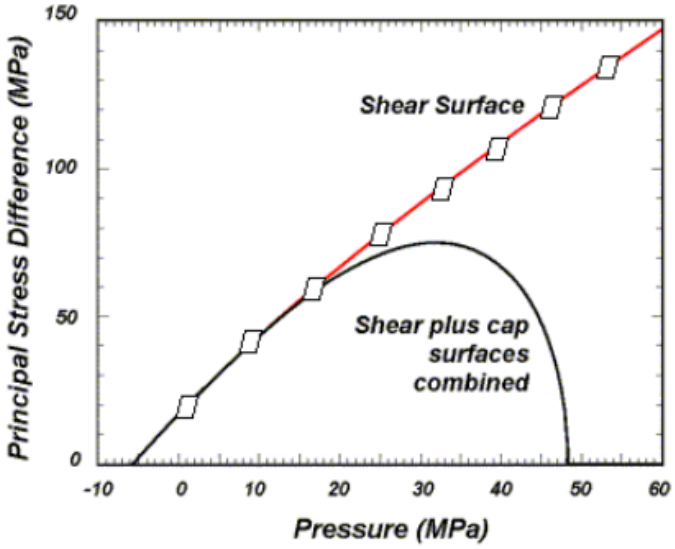

Figure 3.6 Shear failure and cap surface; cap can be unity (in red) or ellipse (in black)

3.2.3.2 Cap hardening surface

The combination of shear surface and the cap are employed to model the concrete strength in the low-to-high confining pressures. The cap is applied for modelling the changes in the plastic volume that is related to pore collapse. Plastic volume changes are modelled by the cap which when it expands, it simulates volume compaction, and when it contracts, it simulates plastic expansion in the volume which is known as dilation. The cap motion forms the hardening shape of the pressure versus volumetric strain curves, and it moves to demonstrate the change in plastic volume and without the motion, the pressure versus volumetric strain curve is perfectly plastic (Murrey, 2007b). The expansion and the contraction of the cap is established on the rule of hardening which is expressed as:

$$\varepsilon^{p}_{v} = W\,(1 - \exp^{-D1\,(x-x0)\,-\,D2\,(X-X0)2}) \qquad 3.3$$

Plastic volume strain is ε_v^p , W is the max plastic volume strain compaction specified by the user, and D_1 and D_2 and X_0 are the initial location of the cap. These five parameters are obtained from pressure versus volumetric strain curves. X_0 demonstrates the pressure at the start of compaction in isotropic compression. Combination of R and X_0 denotes the pressure at the initiation of compaction in uniaxial strain. D_1 and D_2 simulate the pressure versus volumetric strain shape (Murrey, 2007b).

3.2.3.3 Damage in CSCM

Concrete shows softening behaviour in the tensile and low-moderate compressive pressures (reduction in strength). Softening in concrete is demonstrated by a damage formulation which without the damage formulation the cap will be perfectly plastic for tests simulations such as direct pull tests or triaxial compression or tension tests. Such a behaviour is not realistic and despite that concrete behaves perfectly plastic in high confining pressures, this behaviour does not represent concrete behaviour in tension or in lower confinement. Strain softening which is a decrease in strength during progressive straining is modelled via the damage formulation and once the strain-based energy terms (G_f) exceed the threshold damage, damage initiates.

A damage parameter which is scalar and shown as d, transforms σ_{ij}^{VP} known as visco-plastic stress tensor with no damage to stress tensor with damage shown as σ^{d}. Damage accumulation is based on two formulations: brittle damage and ductile damage.

$$\sigma_{ij}^{d} = (1 - d)\, \sigma_{ij}^{VP} \qquad 3.4$$

If the pressure is tensile, brittle damage accumulates and if the pressure is compressive, the ductile damage accumulates. As the damage starts to accumulate, d starts to increase from 0 to 1 using the equations expressed in 3.5 and 3.6.

Ductile damage $$d(\tau_t) = \frac{0.999}{D}\left[\frac{1+D}{1+De^{-C(\tau 1-\tau 0t)}} - 1\right] \qquad 3.5$$

Brittle damage $$d(\tau_c) = \frac{dmax}{B}\left[\frac{1+B}{1+Be^{-A(\tau C-\tau 0C)}} - 1\right] \qquad 3.6$$

The parameters A, B, C, and D are calculated internally in LS-DYNA, and they determine the softening curve shape plotted as stress-strain, or stress-displacement. d_{max} is the maximum damage that can be reached, and the brittle damage is internally set as 0.99.

The softening curve shape plotted as stress-strain or stress-displacement is internally formulated by A and C (softening parameters) and D and B which are the softening shape parameters, as well as the fracture energies denoted by G_f.

3.2.3.4 Fracture energy in CSCM

Fracture energies in CSCM are important properties that form the strain softening part of the concrete response. GF_c is the fracture energy in compression, GF_t is the fracture energy in tension, and GF_s is the fracture energy in shear. The other important parameters are the rate effect (repow) as presented in Table 3.5, and the erosion (ERODE) which occurs when the maximum principal strain is reached. GF_t values are given in Comite Euro-International du Beton (CEB-FIP Model Code 1990), however, there are not any formulations that shear or compressive fracture energies can be calculated from, and instead they are approximated based on tensile fracture energy value. Usually GF_t and GF_s are equal, and GF_c = 100 GF_t with a repow value ranging from 0 to 1.

When shear-based damage or compression-based damage is required, tensile fracture energy can be reduced based on Gfs = ½ GF_t, or compressive fracture energy GF_c = 50 GF_t. If even more damage is required, repow could be reduced to 0.5. Table 3.4 obtained from CEB code shows variable tensile fracture energies for concrete with different compressive strength and aggregate sizes.

Table 3.4 Tensile fracture energies G_{Ft} given in CEB-FIP code (Murray, 2007b)

Unconfined compressive strength MPa (psi)	8-mm (0.31-inch) aggregate KPa-cm (psi-inches)	16-mm (0.62-inch) aggregate KPa-cm (psi-inches)	32-mm (1.2-inch) aggregate KPa-cm (psi-inches)
20 (2.901)	4.0	5.0	6.5
28 (4.061)	5.0	6.0	8.0
38 (5.511)	6.5	7.5	9.5
48 (6.962)	7.0	9.0	1.15
58 (8.412)	8.5	1.05	1.30

1 KPa-cm = 0.05710 Psi-inch

3.2.3.5 Element erosion in CSCM

In a FE model, when an element is severely crushed and has lost almost all strength and no longer contributes to the stability/strength of the model, the time step for that element becomes smaller and smaller. For the analysis to continue, the offended element must be removed and as a result the program deletes that element, therefore, the analysis can continue to run and that is known as erosion (Murray, 2007b). As mentioned d_{max} is the maximum damage that

can be reached and the brittle damage is internally set as 0.99, therefore when the element loses strength, *d* approaches unity and the element erodes when damage exceeds 0.99. ERODE value can be set by the user for a value from 1.01 to 1.10. For example, if an ERODE value of 1.05 is chosen by the user, element erosion occurs at 5% maximum principal strain or in another term the maximum principal strain is 0.05.

3.2.3.6 Rate effects in CSCM

In CSCM, the user can increase the fracture energy and influence damage formulation as a function of rate effects. The formulation of rate effect in a material model is applied in such a way that the increase in strength is proportional to the increase in strain rate. In CSCM, the rate effect algorithm has a power known as repow that can enhance the fracture energy or reduce it by a certain amount. Therefore, when repow is chosen as 0, fracture energy remains constant, and it is maintained independent of rate effects and the response is brittle. However, a repow equal to 1 means fracture energy is increasing (with rate effects) and it is in proportion to the rise in strength (with rate effects) (Murray, 2007b). Therefore, a repow of 1 produces a response with maximum strength.

3.2.3.7 CSCM input data

In Continuous Surface Cap Model (CSCM) named as *MAT_CSCM_CONCRETE, in LS-DYNA, 45 parameters are included, five of which are the salient parameters as expressed in Table 3.5. Extensive parametric study was conducted in this work to observe the influence of some of the CSCM parameters on the response of concrete, however these seven parameters of CSCM are the most influential. Some of these parameters such as REPOW and ERODE were calibrated by fitting the direct HPB test data. CSCM full parameters for concrete cylindrical strength of 48 MPa are expressed in Table 3.6 (sections 1-7) (Murray, 2007b).

Table 3.5 Key parameters of CSCM

PARAMETERS	DESCRIPTION
ERODE	Elements erode when damage goes beyond 0.99 and the maximum principal strain exceed ERODE-1
DAGG	Maximum aggregate size
G_{FC}	Fracture energy in uniaxial compression
G_{FT}	Fracture energy in uniaxial tension
G_{FS}	Fracture energy in uniaxial shear
F'_C	Unconfined compression strength
REPOW	Power increasing fracture energy with rate effects

Table 3.6 Long input parameters for CSCM

Section 1: Control parameters

MID	159
ρ	2340
NPLOT	1
INCRE	0
IRATE	1
ERODE	1.09
RECOV	10
IRETRC	1
PreD	0

(* Units are Newton, meter, kilogram, and seconds, and Pascal)

Section 2: Stiffness parameters

$G_{0\ \text{Shear Modulus}}$	1.340E+10 (Pascal)
$K_{0\ \text{Bulk Modulus}}$	1.468E+10 (Pascal)

Section 3: Shear surface hardening parameters

N_H	1
C_H	0

Section 4: Yield surface parameters

α	1.5980E+07 (Pascal)
θ	0.3575
λ	1.0510E+07 (Pascal)
β	1.9290E-08 (Pascal^{-1} or 1 m s^2/kg)
α_1	0.7473
θ_1	5.5660E-10 (Pascal^{-1} or 1 m s^2/kg)
λ_1	0.1700
β_1	4.6610E-08 (Pascal^{-1} or 1 m s^2/kg)
α_2	0.6600
θ_2	6.6960E-10 (Pascal^{-1} or 1 m s^2/kg)
λ_2	0.1600
β_2	4.6610E-08 (Pascal^{-1} or 1 m s^2/kg)

Section 5: Cap parameters

R	5.0
X_0	1.0150E+08 (Pascal)
W	0.05
D_1	2.5000E-10 (Pascal^{-1})
D_2	3.4920E-19 (Pascal^{-2} or 1 m^2 s^4/kg^2)

Section 6: Damage parameters

b	100
d	0.1
G_{fc}	7.8860E+03 Pascal-meter
G_{ft}	7.8860E+01 Pascal-meter
G_{fs}	7.8860E+01 Pascal-meter
pwrc	5
pwrt	1
pmod	0

Section 7: Rate effects parameters

η_{co}	2.0050E-04
N_c	0.78
η_{to}	8.3020E-05
N_t	0.480
overc	3.2770E+07 (Pascal)
overt	3.2770E+07 (Pascal)
S_{rate}	1.0
repow	1.0

3.3 Karagozian and Case Model (K&C) - MAT_72R3

In civil engineering applications, analyses are performed frequently that involve concrete with no to little information regarding the concrete characterisation. More complex issue involved is the lack of knowledge and formal training on how to obtain the material characterisation parameters and the material responses (Schwer, 2005).

As a result, it is extremely helpful in concrete analyses to have a material model that requires a few basic input parameters to run but projects a reliable representation of concrete response with failure and damage. It is one of the aims of this PhD to make it easy for the users of LS-DYNA dealing with concrete modelling to know in advance which one of the material models is the most suitable for pounding simulation of buildings without having access to concrete material characterisation data or even requiring to carry out tests to find these parameters. As most of the times apart from the required knowledge and training, researchers may not have access to equipped laboratories or the necessary budget to carry out tests.

The Karagozian and Case model (K&C) or the Material type 72R3- Release III is an improved version of the Pseudo-TENSOR Model (MAT_16). The most notable improvement of the original material model is its new capability in generating full default concrete parameters. This model is a three invariant model that includes strain rates, damage, and shear failure surface. Karagozian and Case model, similar to CSCM is a robust material model that has the required capabilities to model concrete structures. However, at this stage it is still uncertain whether it is suitable to be used in modelling building pounding. In this PhD work, the material model has been put to the test using different numerical simulations and its robustness has been examined against experimental data and the findings are presented here in this chapter.

3.4 Compressive shear strength in K&C

As part of the development of concrete and defining the shear surface parameters, the model's shear strength is compared and fitted with data obtained from compressive triaxial tests and α_0, α_1, α_2 are obtained by regression fit against test data. Triaxial test is carried out where a specimen is put in hydrostatic compression loading and the lateral and axial pressures are held equal until the desired confining pressure, σ_2, for example 30 MPa is obtained. Gradually, the axial pressure rises while the two principal stresses on two sides (lateral pressure) are kept constant while the stress on one side goes up to the point of failure (Schwer and Malvar, 2005).

Against this behaviour is exhibited by metal where the pressure against volume response (bulk modulus) is constant. The main difference between these two materials i.e concrete and steel is that the shear strength of concrete increases with confinement but metal is not affected, for example in areas prone to earthquakes, shear reinforcements are provided for columns to increase the shear strength and concrete confinement which also will increase ductility of the structural column.

3.5 Compaction in K&C

Concrete is a brittle material with a lot of porosity that causes the non-linear response of compaction to rise. Karagozian and Case model includes formulation that describes such relationship as pressure against volume strain.

Isotropic compression part of the K&C model comprises an Equation of State (EOS) or as named in LS-DYNA *EOS_Tabulated_Compaction which represents the relationship between pressure and volume strain. Similar to CSCM, the model generates an input file with full parameters based on the initial given compressive strength (f_c) which the parameters can

be altered/modified by the user and place back onto the LS-DYNA input file for a second run if such data is available for a particular concrete.

For K&C model, similar to CSCM, when there is not a proper way of measuring the concrete's tensile strength, the tensile strength (f_t) of concrete can be obtained from one of many codes available for concrete such as the CEB-FIP model code 1990 standard. f_t is expressed as follow:

Unconfined tensile strength $$f_t = 1.58\left[\frac{(f_c^2)}{a_0}\right]^{1/3} \quad (3.7)$$

a_0 is conversion of unit factor. Conversion unit factor is necessary as the material model was originally developed using formulas derived from Standard English units and in order to specify the strength of concrete, it will need to be converted to the standard metric system of units (Schwer and Malvar, 2005).

3.5.1 Karagozian & Case input data and Dynamic Increase Factor (DIF)

Karagozian and Case has 50 parameters along with a tabulated Equation of State (EOS) that describes the relationship between pressure and volume strain as mentioned in the previous sections. Long input parameters for concrete strength of 48 MPa is illustrated in Table 3.7.

Table 3.7 Long input parameters for Karagozian & Case (MAT_72R3) for concrete strength of 48 MPa- (* Units are Newton, meter, kilogram, and seconds, and Pascal)

MID	72
A_0	1.419E+07 (Pascal)
A_1	4.463E-01
A_2	1.683E-09 (Pascal^{-1} or 1 m s^2/kg)
A_{1F}	4.417E-01
A_{2F}	2.465E-09 (Pascal^{-1} or 1 m s^2/kg)
A_{0Y}	1.071E+07 (Pascal)
A_{1Y}	6.250E-01
A_{2Y}	5.365E-09 (Pascal^{-1} or 1 m s^2/kg)
LOCWIDTH (localisation width)	0.0254 (m)
RSIZE (conversion factor)	39.37 (in-m)
UCF (conversion factor)	0.000145 (psi-Pascal)

ρ	2340 (kg/m^3)
PR (Poisson's ratio)	0.2
F_t	3.972E+06 (Pascal)
b_1	1.6
b_2	1.35
b_3	1.15
ω	0.5
S_λ (stretch factor)	100
NOUT (output selector for plastic strain)	2.0
EDROP	1.0
NPTS (Npoints)	13

Apart from those input parameters, dynamic increase factor (DIF) curves can be defined for modelling high strain rate dynamic simulations. Curve in LS-DYNA is the name for any tabulated table with two columns, which the values in the first column are directly proportional to the values of the second column and it is manually inputted in the program as part of the concrete material model. In Karagozian and Case DIF curve, the first column is the strain rate ranging from compressive to tensile, versus a second column that includes the shear strength enhancement. In the LS-DYNA manual, in defining the DIF curve, the compressive values are positive, and the tensile values are negative. The definition of the DIF values for variable strain rate ranges come from formulations expressed in the CEB code model (formulas 3.8 – 3.11) for the DIF values to be calculated manually. However, the most recent versions of LS-DYNA require the user to only input a K&C parameter called LCID as 723 for all DIF values

to be calculated automatically by the program. The program calculates these values based on a study by Malvar and Crawford (1998) on characterising the effect of strain rate in concrete using the expressions given below for compressive DIF values:

$$DIF_c = \left(\frac{\dot{\varepsilon}}{\dot{\varepsilon_s}}\right)^{1.026\alpha_s} \quad \text{For } \dot{\varepsilon} \leq 10^6 \text{ s}^{-1} \quad 3.8$$

$$DIF_c = \gamma_s \left(\frac{\dot{\varepsilon}}{\dot{\varepsilon_s}}\right)^{1/3} \quad \text{For } \dot{\varepsilon} > 10^6 \text{ s}^{-1} \quad 3.9$$

Where $\dot{\varepsilon_s}$ is the static strain rate of 3×10^{-5} s^{-1}.

γ is $10^{6.156\alpha-2}$,

α_s is calculated using $1/ (5+9 f_c/f_{co})$,

f_{co} is 10 MPa,

f_c is the dynamic compressive strength

It is suggested by Magallanes et al. (2010) that the second division of strain rate effects that are expressed in CEB code should be disregarded and according to Crawford and Malvar (1997 & 2011) & Wu et al. (2014) the following branch can be substituted instead of the original CEB formulas to calculate tensile DIF values:

$$DIF_t = \left(\frac{\dot{\varepsilon}}{\dot{\varepsilon_s}}\right)^{\delta} \quad \text{For } \dot{\varepsilon} \leq 1 \text{ s}^{-1} \quad 3.10$$

$$DIF_t = B \left(\frac{\dot{\varepsilon}}{\dot{\varepsilon_s}}\right)^{1/3} \quad \text{For } \dot{\varepsilon} > 1 \text{ s}^{-1} \quad 3.11$$

Where $\dot{\varepsilon_s}$ is the reference strain rate in the range of 10^{-6} s^{-1}

Where B is $10^{6\delta-2}$

$\delta = 1/ (1+8f_c / f_{co})$

For the direct HPB numerical validations, the strain rate enhancement curve was activated, and it was found that the influence of the enhancement in increasing concrete strength using K&C was not very significant in analysing and capturing the concrete impact responses in the direct HPB simulations. An investigation by Schwer (2009) on split Hopkinson Pressure Bar

agrees with disregarding DIF curves when using concrete models such as K&C that does not automatically consider the strain rate effect. The results of his simulation analysis depicted that at low strain rates for example below 10 s^{-1} inertial confinement increase the axial stress by less than 20% in both unconfined and confined compression tests. For higher strain rate ranges for example 100 s^{-1}, the specimens showed non-homogeneous lateral deformations. Shear failure surfaces (stress difference versus mean stress) for low and high strain rate compression tests were compared by Schwer (2009) and it was observed that the specimen exhibited non-uniform deformation under impact. The inertial confinement caused by the outer region made the specimen core to maintain a great stress ~ 30 MPa while the outer surfaces were under lower pressures. Schwer (2009) study confirms the finding of Li and Meng (2003) who conducted numerical and experimental Split Hopkinson Pressure Bar (SHPB) tests using K&C, and their results showed that in high strain rate dynamic impact tests, inertial confinement alone boosted concrete strength instead of the material's strain rate sensitivity. At such a great strain rate particularly above ~ 100/s, the deformation of the specimen is no longer uniform as shown in Figure 3.7. Researchers such as Ma et al. (2006), and Cotsovos and Pavlovic (2008) have stated that the application of DIF to model strain rate effect on structural impact response is not a material property and it leads to over-estimating the strength of concrete material. Hao and Hao (2010) carried out Split HPB tests and numerical analysis to study the compressive behaviour of concrete at different strain rates and they found the increase in concrete strength is the result of inertial effect as well as the effect of material. They have found that the lateral inertial effect is influenced by the increase in strain rate particularly over 200 1/s. They concluded that for lower strain rates the strength of concrete is more defined by the mortar in concrete as the aggregate does not come into surface contact much in the lower velocity impacts. However, for higher strain rate impacts, the crushing extends in the body of the specimen including its aggregate which then contributes to an increase in the strength of concrete.

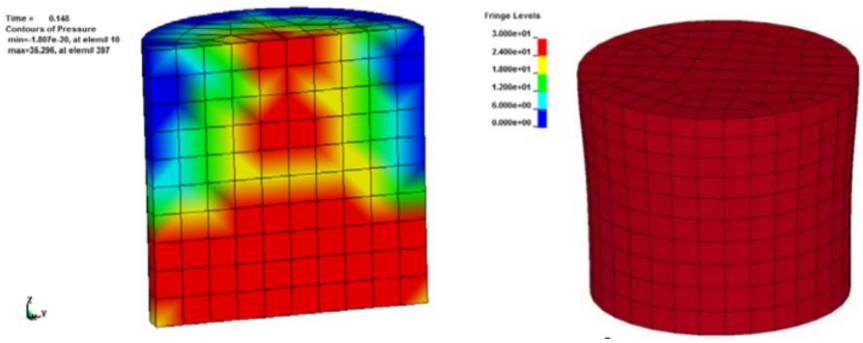

Figure 3.7 Unconfined compression test shows non-homogeneous pressure and deformation (Schwer, 2009)

Controversial findings and observations have made the application of DIF in concrete modelling a grey area. It is difficult to distinguish if it is the influence of DIF or the inertial confinement effect that results in increase in concrete strength. Investigating such a matter requires specific experimental work to observe the influence of inertial effect on the concrete dynamic behaviour which is out of scoop of this study. In this study it was found that K&C model can capture the direct HPB impact response without the application of DIF. Therefore, it was found that the automatic parameter generation works just fine without DIF data to produce meaningful results in the direct HPB simulations.

3.6 Mesh convergence study of HPB numerical simulation using CSCM and K&C

An important part of FE modelling is mesh size as it can significantly affect the final outcome of the analysis. The adequacy of numerical models relies on identifying the right element size. The two material models, K&C and CSCM, have different in-built formulation and are of different type, therefore, separate mesh analysis for each one of them have been carried out for each model. Mesh convergence analysis for both material models are described in further sections using Lagrangian mesh algorithm.

3.6.1 The Lagrangian Algorithm

Lagrange mesh method has been used for all the FE simulations within this research. In this method, mesh grids are attached to the materials and they move with the movement of materials and if the material is crushed and distorted, the grids will be distorted as well. Lagrangian algorithm is a good method to be used for multi-material models because even though the mesh is distorted, the volume and density of material may change but the mass

stays the same therefore the mass is conserved at all times. This is contrary to Eulerian Algorithm in which the mesh is fixed, and the material moves through the mesh. Also, element and material boundaries should be carefully treated in the other meshing methods, such problem does not exist in Lagrangian algorithm. However, in Lagrangian method large deformations can sometimes become problematic if the material is highly crushed, which then element erosion such as *MAT_ADD_EROSION can be used to overcome such a difficulty.

3.6.2 Mesh size regularisation

Mesh regularisation has been explained in more detail in sections 3.6.3 to 3.6.5 which are on determination of suitable mesh size to validate the direct HPB numerical simulations against the experiments. CSCM similar to the other concrete models have to maintain constant fracture energy despite the change in the length of the elements. The energy that causes fracture in concrete is the area under the stress-displacement curve from the peak strength to zero (when concrete fails) with units of force-length/area such as N-m/m^2, MPa-m, or N/m. In most concrete material models, treatment of damages leading to failure is formulated internally and when it is subjected to compression stresses, due to the damages caused, softening occurs. In almost all these models, results are sensitive to element refinement, i.e. variable element sizes produce different stress-displacement responses. Mesh regularisation is a method that is included in the modern material models to overcome this dependency that occurs because of strain softening (Schwer, 2020). This is done to prevent strain localisation in the smallest irregular element in the FE model. However, the material model is developed in a way that the strain at failure is adjusted depending on the element size, measured by the so called “characteristic element length”. The strain at failure and the element characteristic length are related and it is controlled by the fracture energy adjustment internally in every individual element.

Cracks are modelled through fracture energies in CSCM. Basically, as concrete loses strength, it softens and as a result cracks are formed, and energy is released. Therefore, in CSCM, the softening behaviour is represented as fracture energies denoted by symbol G_{ft}, G_{fc}, and G_{fs} for tensile, compressive and shear fracture energies. With this type of material models, the analysis becomes mesh sensitive and despite the model’s developer statement (Murrey, 2007a) on mesh independency of such concrete models, the model response still has to be checked against mesh size sensitivity.

In the mesh convergence analysis process, if the size of the element is too small, fracture energy accumulates within that element which is a numerical artefact. The element reaches

the critical failure stress too fast and as a result fails too quickly. On the other hand, if the element is too large there is more fracture energy needed to be dissipated before failure and sometimes the element might never actually fail because so much fracture energy has to be released to cause element failure and, in that condition, it will never reach the critical stress to do so.

Numerical techniques such as mesh regularisation is usually included internally within the models themselves. The idea behind such a technique is to keep the internal energy constant and independent of the element size. In models such as CSCM, fracture energy regularisation is implemented within the concrete material model internally, but the main difficulty is that for such a technique the element size must be just about large enough to accommodate sufficient energy as very small elements cause instability and introduce errors in the model (Khoe & Weerheijm, 2019).

Another important factor influencing the mesh size is the crack width in concrete. Figure 3.8 shows schematic illustration of a crack zone in concrete. It includes crack area with aggregates and some very small micro-cracks in concrete. This area is called fracture process zone (FPZ). It is very important that the element size is large enough to include the crack zone as shown in Figure 3.8(b). Once such requirement is met, enough fracture energy can be released. Otherwise, if the fracture zone spans over several elements such as Figure 3.8(a), each element releases energy separately (Khoe & Weerheijm, 2019).

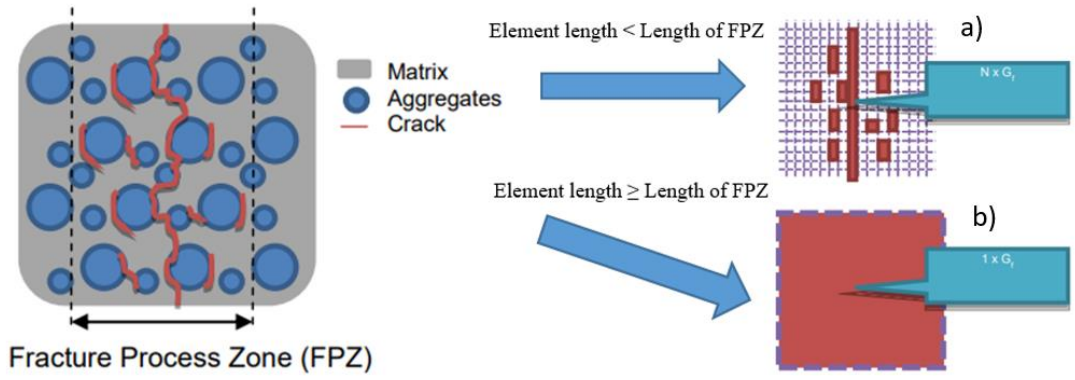

Figure 3.8 Fracture Process Zone (FPZ) in concrete; (a) the length of element is smaller than the length of the FPZ, (b) the length of the element is large enough to include the FPZ (Khoe & Weerheijm, 2019)

3.6.3 HPB cylinder mesh refinement for CSCM and K&C

HPB, striker and the specimen cylinders were meshed with variable number of row elements in the circumferential direction as shown in Figure 3.9. The way the circular cross section is meshed is commonly referred to as butterfly mesh. The mesh element sizes start from approximately 0.725 mm to about 10 mm. There is a range of element sizes for each cylinder. For example, in the bar with 2mm mesh, the smallest element is 1.02 mm (on the inside core of the bar) and then gradually the size goes up to nearly 2mm on the outer surface of the bar. Best effort was made to divide the bars into square meshes, however for simplicity, the element sizes mentioned in the figures have been rounded to the nearest exact value.

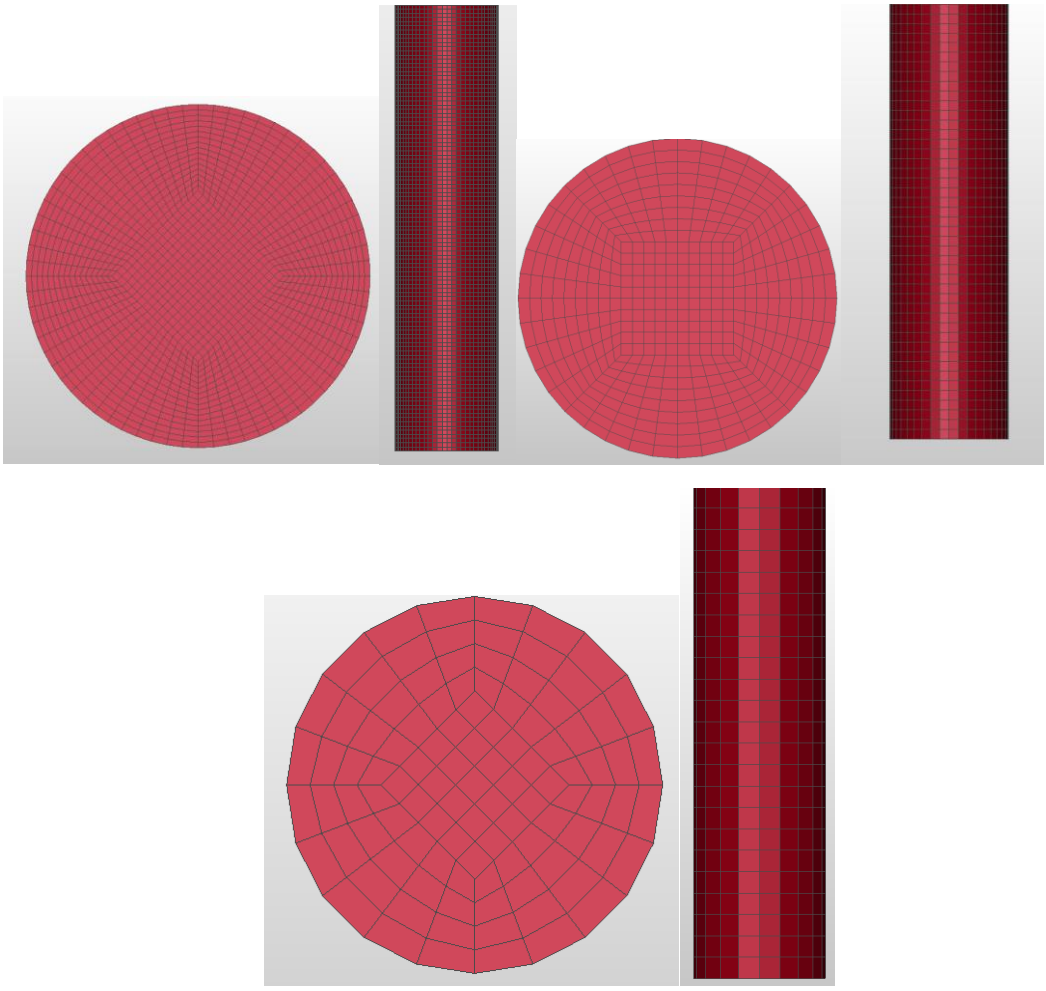

Figure 3.9 Butterfly mesh with different circumferential row elements: (left top) 68 row elements with mesh size of 2mm, (right top) 40 row elements with mesh size of 4mm, and (centre below) 20 row elements with mesh size of 8mm

3.6.4 Mesh study on CSCM

The model used for the mesh convergence analysis of HPB simulations was consisting of a HPB and a concrete specimen attached to it and the specimen was subjected to an impact velocity of 18 m/s as shown in Figure 3.10. Stress- time histories for different mesh sizes obtained from the location of strain gauge have been compared and are illustrated in Figure 3.11.

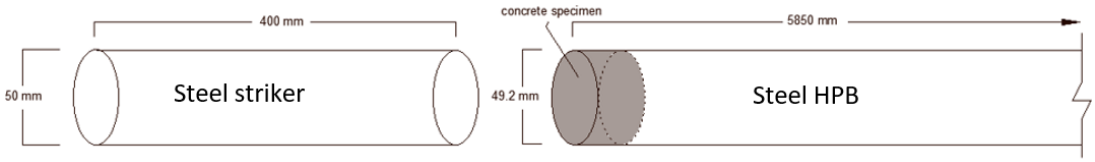

Figure 3.10 Impact arrangement for conducting mesh convergence analysis

Another performed comparison brought to light one other observation, which confirms the accuracy of the mesh analysis and that is most visible in the internal energy evaluation shown in Figure 3.12. The total internal energy is the energy that is taken up by the system and in the compared simulation cases herein everything is the same except for the mesh size that varies in each model. Ideally all the histories should end up with the same internal energy, however that is not completely the case.

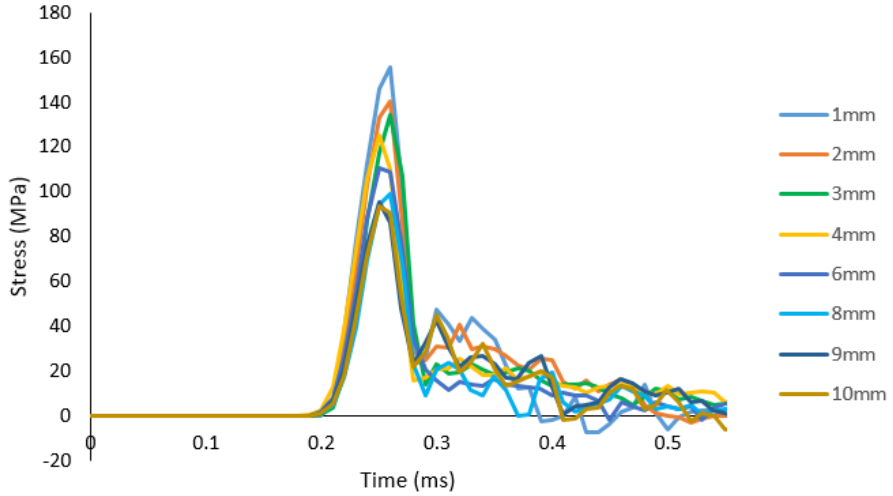

Figure 3.11 Stress histories comparison for CSCM

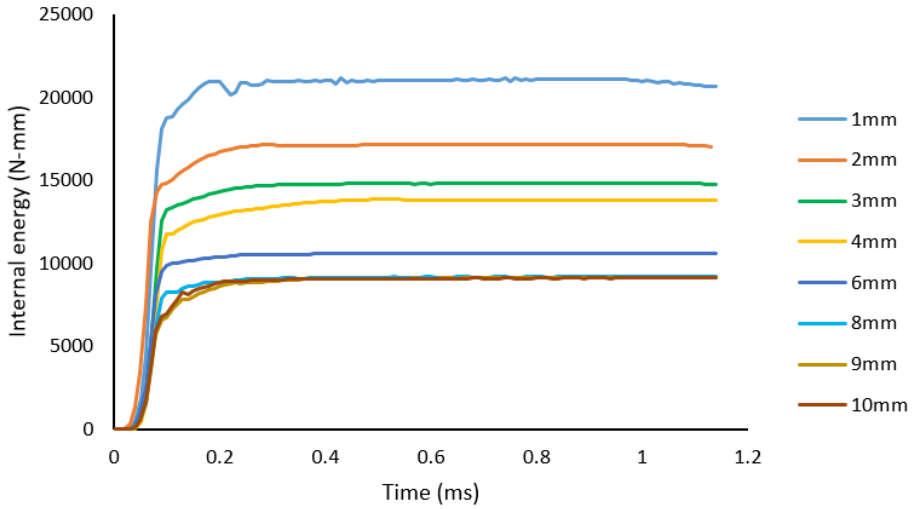

Figure 3.12 Comparison of internal energies for different mesh sizes in CSCM

The observations received in mesh sensitivity analysis using CSCM agrees well with the findings of Alanon et al. (2018) and Khoe and Weerhejim (2019) who also found that the internal energy is mesh dependent. It is important to ensure that the mesh element size fracture energy is fully dissipated in a sufficient area that corresponds to the fracture energy zone Alanon et al. (2018). In the mesh study of CSCM, when large elements were used, larger fracture energy was taken up by the element to reach the failure state whereas for smaller elements it took small amount of energy to fracture. In this study it was found that if at least the size of the element is minimum a similar size to the aggregate size in the concrete mix, there is enough area for the element to dissipate energy and should be able to accommodate damage in the fracture zone. Following the comparison of stress-time curves obtained from different mesh sizes, it can be observed that the analysis converges when mesh is approximately 8-10mm. The aggregate size used in the concrete mix as well as the CSCM model used in the simulation is about 10mm. This verifies the statement that for those concrete models that simulate crack through energy dissipation, the element size should be large enough to accommodate the fracture process zone as well as the maximum aggregate size used in the concrete. The requirement for such large element size in direct HPB simulations is because of larger fracture zones (Bazant, 1998).

3.6.5 Mesh study on K&C including erosion

Mesh convergence analysis for the same direct HPB model arrangement is also conducted with K&C (MAT_72R3) model. The model shows slightly better consistency in terms of mesh

regularisation compared to CSCM (MAT_159). Contrary to CSCM, the analysis converged at a smaller mesh size for K&C as shown in Figure 3.13.

Karagozian and Case model does not include an in-built erosion formulation, therefore an extra command known as *MAT_ADD_EROSION in LS-DYNA (LA-DYNA, 2018) is required to artificially rid of distorted elements in the numerical model as shown in Figure 3.14. As mentioned previously, when an element is crushed or distorted, the time step for that element becomes increasingly small. In order for the solution analysis to continue running, the analysis removes that offended element and that is known as erosion. The erosion parameter is an "ad hoc" value that is determined based on error and trial particularly for this material model that uses *MAT_ADD_EROSION. There is no test to be done to determine this value and in order for the simulation to represent real behaviour (real concrete fracture/crushing or cracking) in terms of erosion, experiments must be at hand. The inability of the K&C model to have an in-built erosion system, disadvantages its powerful capability in modelling concrete, otherwise the material model is a robust useful model capable of modelling concrete behaviour. In erosion studies, principal strain, stress or shear stress can be used as a reference base point for erosion to occur (erosion criterion) and the program must be instructed to remove elements when for example strain in that element reaches a certain value. All erosion studies in this PhD work are based on maximum principal strain and once the specified value of failure strain is reached within the model, elements start to eliminate.

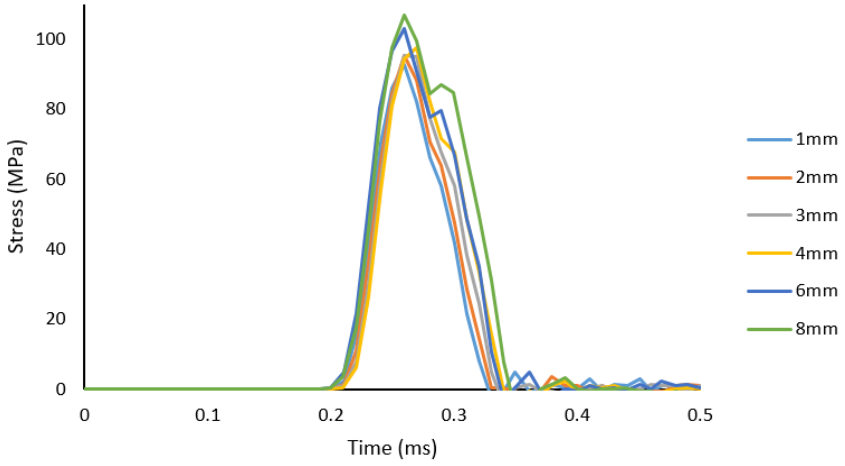

Figure 3.13 Stress histories comparison for K&C

Similar to CSCM, K&C also has an in-built regularisation formulation that should technically make element sizes independent of the fracture energy, however, mesh dependency of fracture energy still exists. In general, mesh regularisation is found to be working better in K&C model particularly for mesh sizes larger than 25.4mm. In direct HPB simulations, even though the

mesh elements were smaller than 25.4m (from 1mm to 10mm), still the implemented mesh regularisation functioned well.

As part of the mesh convergence analysis, along with stress histories comparison, to have the confidence that the model of direct HPB correctly simulates impact, internal energies have also been compared to show that both stress and internal energy histories converge at the same mesh size as shown in Figure 3.15.

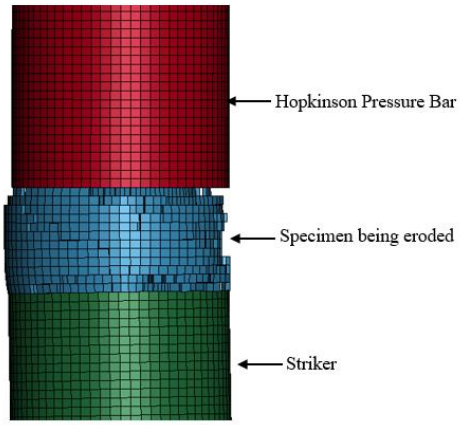

Figure 3.14 Concrete crushing by means of erosion (element deletion) in K&C model

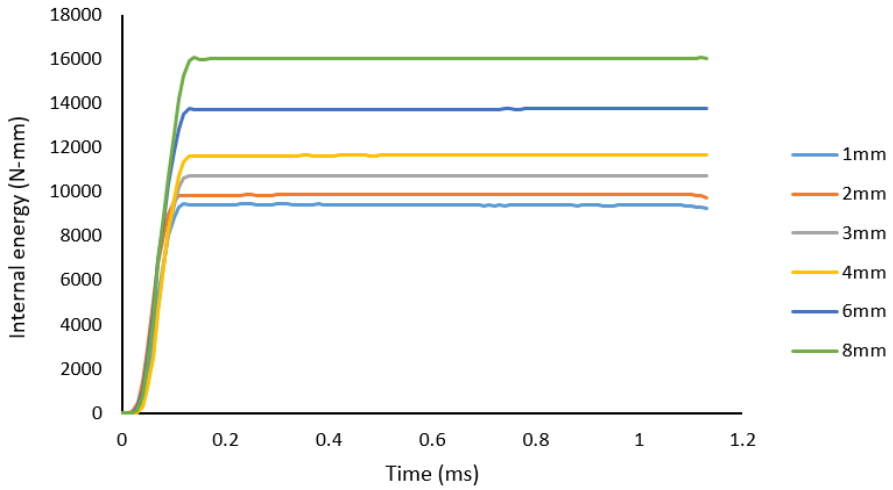

Figure 3.15 Internal energy comparison in K&C model

It should be noted that the purpose of the mesh convergence analyses conducted for both concrete material models is not to get the material models to converge at the same values or

to compare their convergence performances but rather it is just to show how the models each converge separately.

3.7 Validation of FE simulations of direct HPB tests

The arrangement of direct HPB impact tests is illustrated in Figure 3.16. In the photo provided, concrete specimens and strikers are shown in solid grey. The radius of the HPB was 24.6mm (+/-0.05mm) for all tests. The specimens were either 25 or 50 mm and the length of the strikers regardless of the type of material was 400 mm.

Direct HPB impact tests were recorded using a high speed camera at Buxton laboratory (Photos provided on the right side of Figure 3.17 is from the camera recordings) and the model constructed in LS-DYNA is shown on the left side of the Figure 3.17. The whole process of impact and the duration of contact, and the damage it caused to either side was monitored and compared to the FE simulations. As examples, numerical simulations of tests 1 (steel to concrete impact) for CSCM and test 6 (concrete to concrete impact) for K&C and their comparison against the tests are shown in Figure 3.17 and Figure 3.18.

Figure 3.17 (a-f) illustrates the direct HPB and a concrete specimen attached to it in three stages, one photo is taken just microseconds before the impact, and the other two are during impact and towards the end of the impact when concrete was being fully crushed. Both were impacted with a steel striker with impact velocity of 19 m/s.

Photos (c-d) are taken at 0.00011 seconds (0.11 milliseconds, 110 microseconds) when the striker had impacted the specimen and cracks were being developed in the specimen (some of the concrete specimen's FE elements shown in Figure 3.17(c) have red colour which is an indication of plastic strain/cracking in the concrete). At this point of contact, stress pulses were generated within the specimen, however the stress pulses did not yet reach the strain gauge which was located a meter away from the bar face at this time.

Photo (e-f) is taken at 0.00021 seconds into the impact when the specimen was being crushed. The duration of impact recorded at the strain gauge for this experiment was 0.00022 seconds or 220 microseconds. The impact strain rate for test 1 using CSCM was 986 S^{-1}. The impact strain rate for K&C model for test 1 was 1340 S^{-1}.

Figure 3.18 illustrates the impact of a concrete striker against a concrete specimen attached to the HPB as well as its FE simulation illustrating concrete cracking and crushing. The difference in this test compared to the other tests was that the striker was also made of concrete and as soon as they came into contact both faces started to fracture which led to severe

crushing of both. The strain rate for K&C in test 6 was 767 S^{-1}. For the same test the strain rate of CSCM was 422 S^{-1}. The duration of impact for test 6 was 0.000276 seconds (276 microseconds). The contact duration in this test was greater than test 1 because of the plastic work being done on the contact surfaces of the concrete striker and the specimen while they were in contact. As they both were being crushed, they stayed in contact for a longer period of time compared to the test 1 when one of the impact sides was the steel HPB that remained elastic at all times and had a smooth contact surface (HPB was protected at all times to avoid damage).

Great effort was made in validating both K&C and CSC models against the behaviour observed in the experiment including correctly capturing the position of the striker and the specimen attached to it milliseconds before the impact. Once the striker was thrown by the gas gun, even though it travelled through a few bearings that helped in controlling the striker movement, it still did not manage to travel in a straight line and by the time it arrived to the specimen it was misaligned, therefore the impact was never perfect. Imperfect contact is a common event that occurs in impact of structures. When two bodies have a perfect impact meaning the two surfaces come into full contact, the stress magnitudes are higher. However, if the impact is misaligned, a part of a specimen's edge comes into contact with the other surface and this speed up the crushing process and as a result the specimen breaks quicker and the stress magnitudes decrease.

The other important factor that influenced the shape of the stress pulses travelling through the bar was the microscopic irregularities on the concrete surface. Apart from the irregularities, even the slightest spalling of concrete on the surface or the existence of one or two small aggregates in the surface can influence the results.

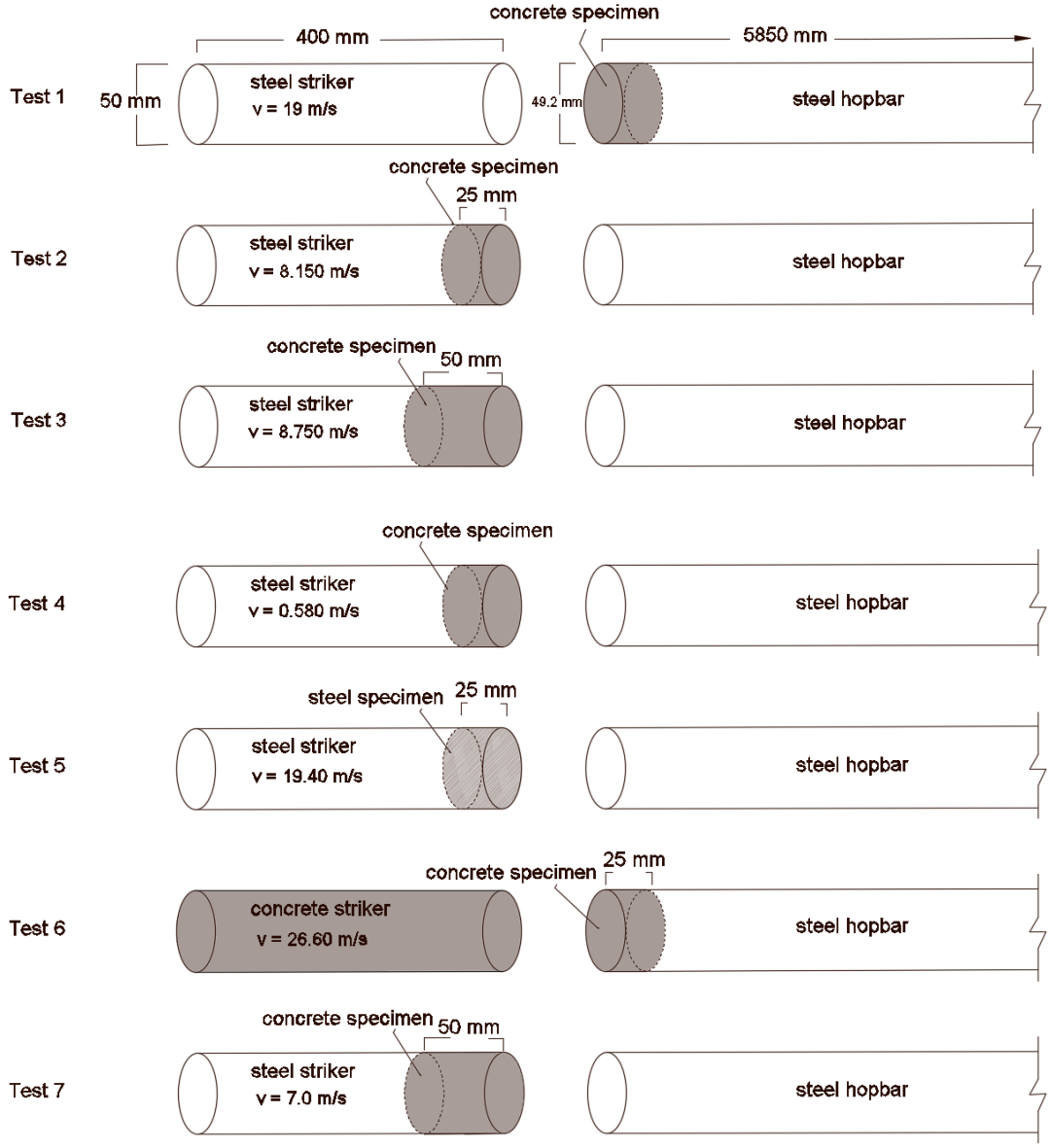

Figure 3.16 direct HPB test arrangements of bar, specimen and the striker for all 7 tests

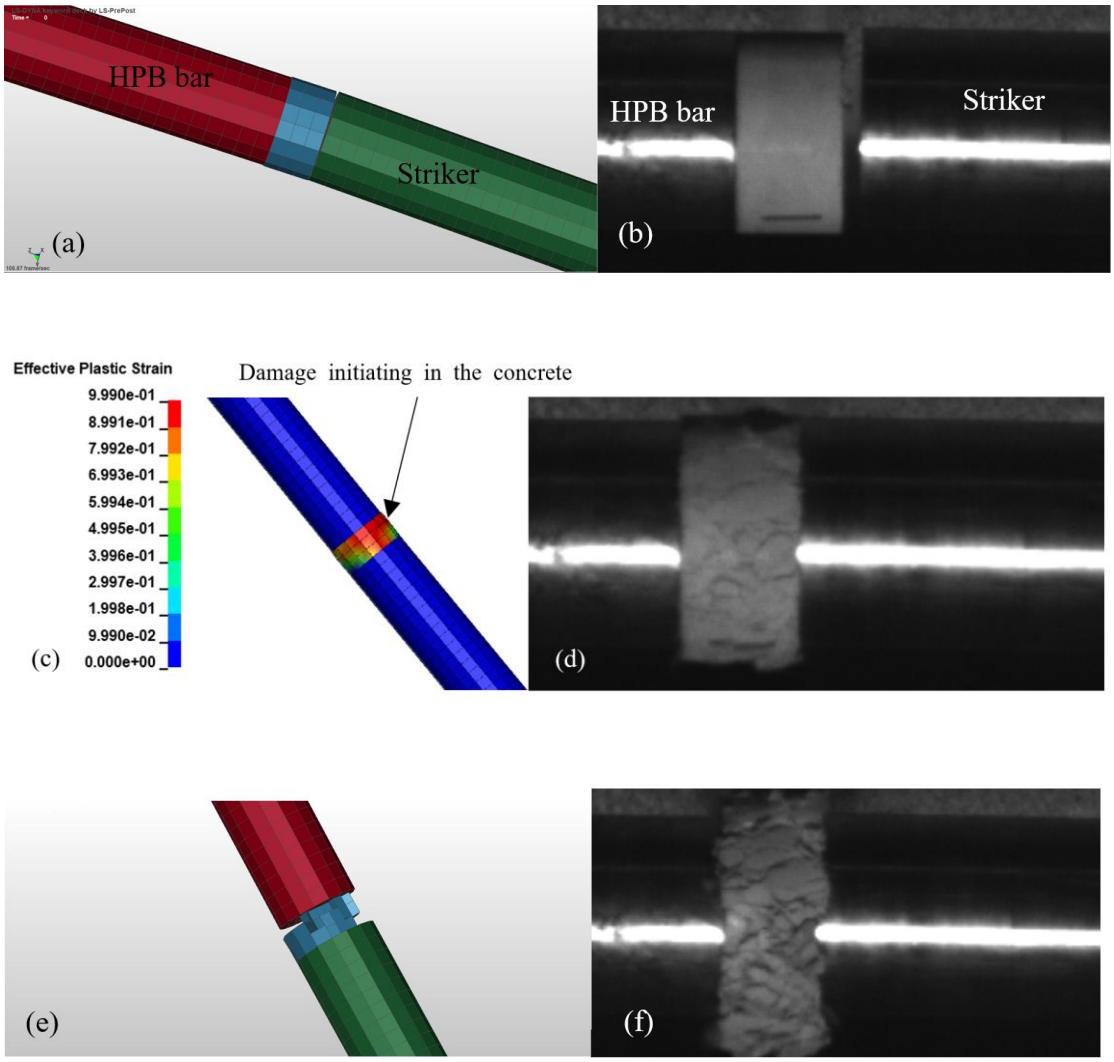

Figure 3.17 Comparison of FE simulation versus direct HPB experiment 1 using CSCM

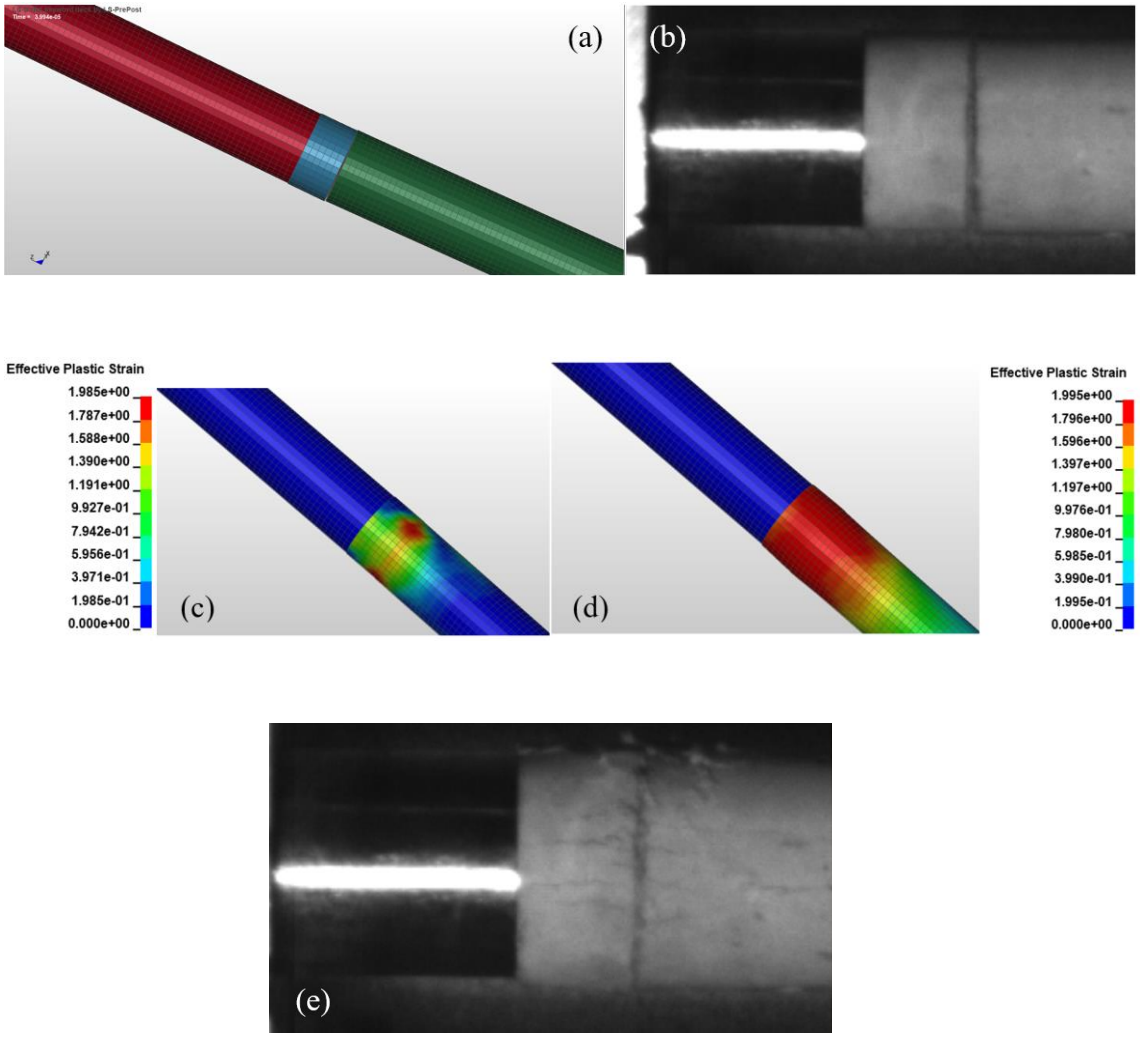

Figure 3.18 Comparison of FE simulation versus direct HPB experiment 6 using K&C model

3.8 Impact generated pulse

Before moving onto the discussion of direct HPB impacts results using K&C and CSC models, it is important to provide a brief introduction on how impact stress pulses are generated.

As soon as two bodies come into contact, as a result of the external applied stress, every microscopic particle inside the object starts to move with a certain velocity. As it moves, it collides with its neighbouring particles and transfers its momentum onto them and that is how stress waves are generated and start to propagate through the body of the colliding objects. Contact/impact stresses are obtained using the below equation:

$$\sigma = 0.5\rho AC\ (v_1\text{-}v_2) \qquad 3.12$$

These elastic stress waves move at a certain speed in different materials, and it is shown by:

$$C = \sqrt{\frac{E}{\rho}} \qquad 3.13$$

Where C is the wave velocity, ρ is the density, A is the cross-sectional area. v_1 and v_2 are the colliding masses' velocities, and E is the young modulus.

The ideal stress wave is a perfect rectangular shape expressed in Figure 3.19. However, in reality, the stress waves generating from impacts of objects have many oscillations with an initial long rise time and long down fall and variable impact time duration. The rise time and the impact duration depend on the axial alignment between the projectile and the impacted bar as well as their initial velocities and their material type.

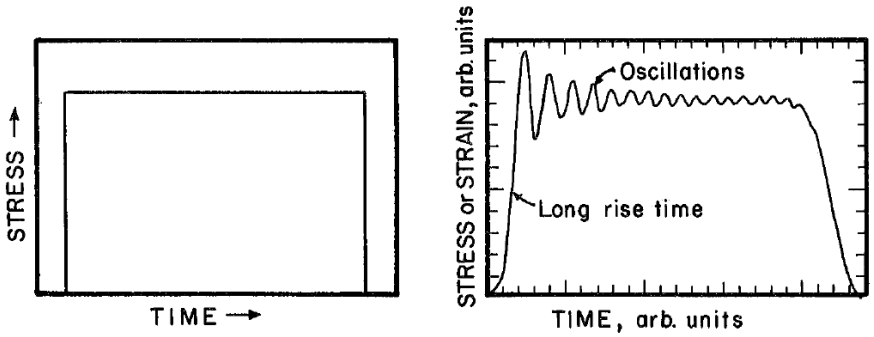

Figure 3.19 Stress pulses; (1) ideal pulse on the left, (2) real pulse with oscillations on the right (Meyers, 1994)

As shown in previous section, stress waves are responsible for the damages caused to the specimen. In the next sections, stress-time histories obtained from the FE simulation of direct HPB are compared against the recorded stress-time histories of direct HPB tests.

3.8.1 Results comparison of direct HPB simulations against the experiments

Stress-time histories obtained from the numerical simulations using both K&C and the CSC models is compared against the experimental data as shown in Figure 3.20 and it is observed that the FE simulation results agree quite well with the experimental data. Some of the differences between the FE simulations' results and the experiments are attributed to the unevenness of the concrete samples' surfaces that occurred during casting and drying process as well as surface roughness, and the presence of small aggregates very close to the surfaces

of the striker and the specimens that was not possible to capture using the FE model. Usually, the smoother the surfaces, the easier it is to capture stress pulses using the numerical simulations, however smooth surface is hard to achieve when casting cylindrical concrete samples using firm plastic tubes as shown in Figure 3.2. Another challenging task in validating the numerical simulations against the direct HPB tests particularly for higher impact velocities was replicating the misalignment between the colliding bars. Measurements of the misalignment between the contacting specimens were obtained from movies recorded by a high speed camera.

3.8.1.1 Discussion on impact stress pulses in direct HPB tests

In impacts of flat surfaces with higher velocities, the stress pulse magnitudes are higher compared to the lower impact velocity cases. Sometimes in high velocity impact cases, the stress pulses duration is longer, and this is due to the crushing of the samples which extends the loading duration. Great difficulty in validating direct HPB simulations arises when a lot of plastic deformation/damage occurs such as tests 1, 7 and particularly test 6 that has the highest impact velocity of 26.6 m/s out of all. Once impact with high velocity occurs, stress waves travel fast through the striker and the specimen that is attached to it; this is for the cases where the specimen is attached to the striker such as tests 2,3,4,5 and 7. The stress waves in the specimen quickly travel to the striker, hit the back of the striker and return to the front. At the same time, stress pulses are generated in the HPB and they are travelling from the front of the bar to its end. At this moment, the specimen and the bar are still in contact and the waves in the striker are now skipping from the striker and are transferring onto the bar. It continues to travel through the bar, and they are measured at about 1m away from the face of the bar. Passing that recording data point (strain gauges), it continues to travel through the 5.85m length of the HPB, hits the free end and comes back as a tensile stress wave. If the end of the HPB is restrained, it comes back as a compressive wave. However, in this work the end of HPB is free therefore the reflected stress waves are tensile.

The generated stress pulses are travelling from the point of contact (face of the bar) towards the end of the bar; these are the first generation of the stress pulses. However, while there are still in contact, more stress pulses are being generated. The first generation of pulses reach the end of the bar and return. At the same time as these pulses are returning, there are more stress pulses travelling opposite to them towards the end of the bar. In the design of the test set-up one has to make sure to use a bar that is long enough for the ongoing and outgoing stress pulses to be captured correctly in the tests, so they don't interact while moving opposite to each other. If they interact, the stress pulses moving in the opposite directions merge and

become a large stress pulse with an extensive time duration and inaccurate peak stress. In most high velocity impacts, particularly the ones that occur between two different types of materials, once the impact is completed the striker does not fully stop, therefore, there is still small amount of velocity stuck in the striker which results in residual velocity that is observed as a tail in the stress pulses (can be seen clearly in tests 1, 3 and 7).

From tests 1, 2, and 6, it is observed that stress is higher in shorter specimens. This is due to the plastic work being extended over the whole length of the shorter specimen resulting in a stiffer impact which strains the specimen more and as a result drives the stress pulses further up. Opposite to the impact of shorter specimens, for longer specimens the plastic work is mostly being extended over the front side of the specimen which results in slowing down the transfer of the energy waves through the specimen, therefore it takes longer for the full event to be over.

In this Chapter, comparison of the concrete simulations gave an insight into the concrete models' performances. In terms of displaying damage and crushing shown as element erosion in the models, both material models performed well providing the ERODE value (based on maximum principal strain) for K&C is set to 0.07 and for CSCM is 1.09.

It was observed that impact was stiffer in the simulation that included K&C material model, whereas the model with CSCM experienced a softer impact due to the existence of larger mesh elements in the model as well as CSCM formulation which is based on fracture energies.

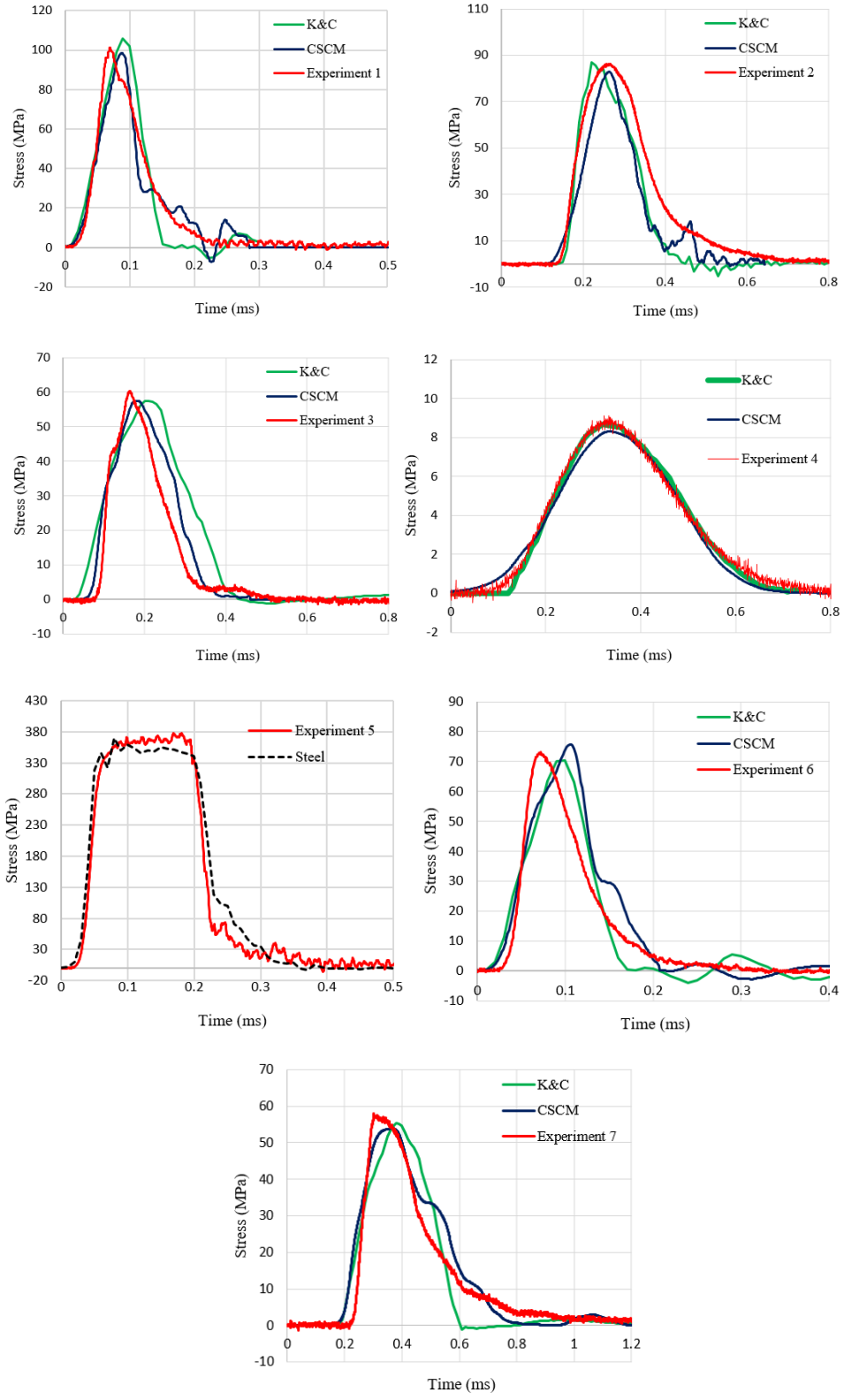

Figure 3.20 Comparison of stress-time histories obtained from the numerical simulations using CSCM and K&C against direct HPB tests

3.9 Summary

To simulate structural pounding with confidence in the accuracy of the results, a methodology has been adopted to first validate direct HPB simulations against impact tests, thereafter, developing the methodology to validate shaking table simulations against the tests, and finally combining both methodologies into a reliable simulation to be used for modelling of structural pounding. Chapter 3 presented the results of the direct HPB impact experiments at material level and the validation process of direct HPB simulations against the tests. Experimental stress-time histories were used to demonstrate the accuracy of the FE numerical simulations. The direct HPB tests conducted assisted in understanding the contact behaviour of concrete and the importance of factors influencing the contact response of materials. However, the main purpose of conducting such an experiment was to validate the numerical simulation of the direct HPB. The main goal was to lay a foundation for investigating concrete pounding/impact response at material level and to find a set of concrete parameters to accurately resemble impact response of concrete. It is concluded that the original parameters of both concrete models projected a realistic behaviour of concrete under different impact velocities in direct HPB simulations. As part of this study, it is confirmed that both concrete material models parameters in their automated original forms can simulate realistic concrete behaviour in wide ranges of strain rates.

Both material models, particularly CSCM were outstandingly in great agreement with the test data, with peak stresses differing no more than 10%. Element erosion replicating concrete crushing observed in the tests was depicted by both material models based on the maximum principal strain values; CSCM with erode value of 1.09, and K&C with the aid of *MAT_ADD_EROSION with erosion of 0.07. The established set of parameters will be used in the validation of shaking table simulation in the next chapter.

With this background established, the resulting question is: “which one of the material models perform better at structural level and will the established parameters work for the shaking table simulation too?”

Chapter 4

4. FE Simulations for Building Shaking Table Tests

As described in the previous chapters, there is the lack of controlled large scale experimental work on structural pounding in the current literature. Therefore, in this work, a reliable strategy is developed by combining, (1) the knowledge obtained from the results of direct HPB simulations on the impact of building materials, with (2) the knowledge obtained from the simulation of dynamic behaviour of buildings subject to variable seismic motions against shaking table tests.

This chapter depicts the process of constructing Finite Element simulation of a two-storey building and its validation against shaking table tests conducted by Garcia et al. (2010) under variable seismic motion intensities. The knowledge attained from this chapter on the seismic response of the building along with the findings of the previous chapter on the impact response of materials is then combined into one methodology that can simulate structural pounding.

In Chapter 3, the results of direct HPB tests and numerical validations were presented and the material models' capabilities in simulating impact was investigated and the performances of K&C and CSC material models for concrete have been compared. The next step is to investigate the capability of the Finite Element Method together with these material models in portraying the dynamic behaviour of an actual building that includes reinforcements and to observe the capability of these models in capturing erosion/damage caused in the building by the earthquake.

The FE models of the two-storey concrete building is validated (1) once with Continuous Surface Cap Model (CSCM or MAT_159) (Murray, 2007a), and (2) with Karagozian and Case

(K&C or MAT_72R3) Model (Crawford and Malver, 1997) under earthquake motions with variable PGAs from 0.05g to 0.4g. The influence of erosion values in both CSCM and K&C performances have been investigated. For the K&C model, the application of the dynamic increase factor (DIF) was also studied in the validation process. The performances of the material models are then compared and the capability of these models in simulating the dynamic behaviour of buildings in earthquake events is established.

The previous Chapter was focused on impacts and high strain rate dynamic behaviour of materials; in this chapter we are dealing with structural dynamic problems subject to earthquake motions. One of the intentions of this thesis work is to find a robust material model that work for broad ranges of strain rates, i.e from high strain rate to low strain rate.

Whilst it appears that modification of K&C parameters by several researchers (e.g Xu and Lu, 2016; Hong et al., 2017; Kong et al., 2018) is successful in offering good calibration between simulations and experiments, in this thesis it is found that pounding simulation of buildings does not actually require major modifications of the material models. It is found that the automated generated parameters of the models provide equally accurate results without the associated modifications as long as the parameters are within the ranges suggested by the material models developers. Malvar et al. (1997) is the developer of Karagozian and Case Model, and Murray et al. (2007a, b) is the developer of Continuous Surface Cap Model.

4.1 Experimental study of shaking table simulation

An under-designed reinforced concrete building with one bay and two stories, regular in plan and elevation, was tested on a shaking table as part the European research project called ECOLEADER by Garcia et al. (2010). The building was designed based on an old earthquake resistance provision that was practiced in the 1960s. The frame tested was a square of 4.26 x 4.26 m^2 in plan with storey height of 3.3m. Figure 4.1 depicts a general view of the building along with the sizes of the sections and the reinforcement bars.

The concrete strength was f_c = 20 MPa with maximum aggregate size of 19 mm and modulus of elasticity of E_c = 25.545 GPa along with steel reinforcement bars with yield strength of 551 MPa and ultimate strength of 656 MPa. Masses of 9 tonnes were added as steel plates to each slab as an additional load to simulate real building loading conditions. Displacement and acceleration transducers were used to monitor the building responses during the seismic tests. However, only the displacement response of the building was studied as the acceleration readings were unreliable and noisy.

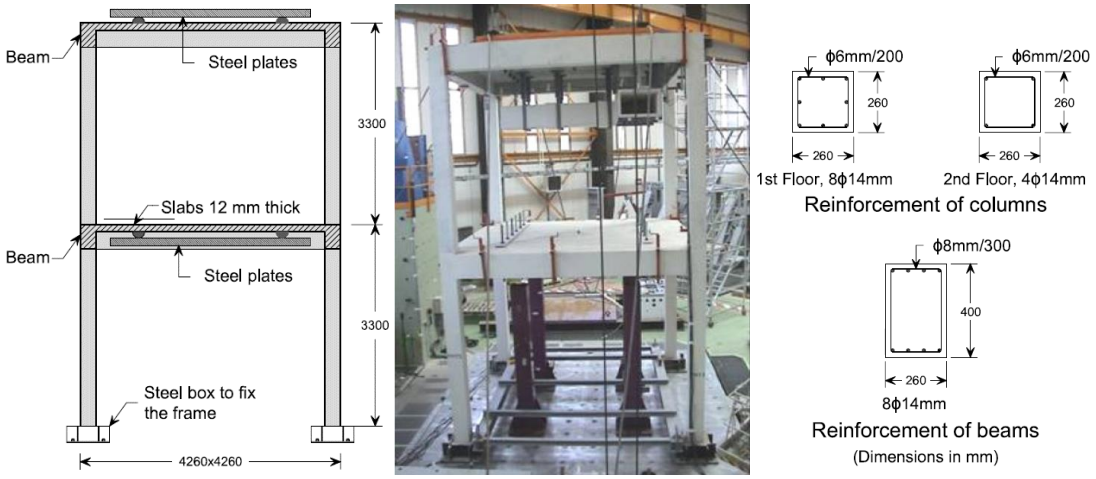

Figure 4.1 Sketch drawing of the building along with section sizes and reinforcement arrangements (Garcia et al., 2010)

4.2 FE Modelling of ECOLEADER building

FE simulations of the concrete building were developed in LS-DYNA and due to its symmetrical shape in plan, half of the model was constructed in 2D plan with 3D solid elements. The building total weight was 40 tonnes. In the simulation, half of that mass (20 tonnes) was modelled, and the masses of the steel plates were distributed equally as nodal masses between the floors. Beam and truss elements were both tested to model the reinforcement bars of the building, both produced similar behaviour during seismic motion, however, beam elements were chosen to model reinforcement bars. Reinforcement detailing at the connections from Garcia et al. (2010) is shown in Figure 4.2. The model in LS-DYNA was constructed based on the detailing given by Garcia et al. (2010).

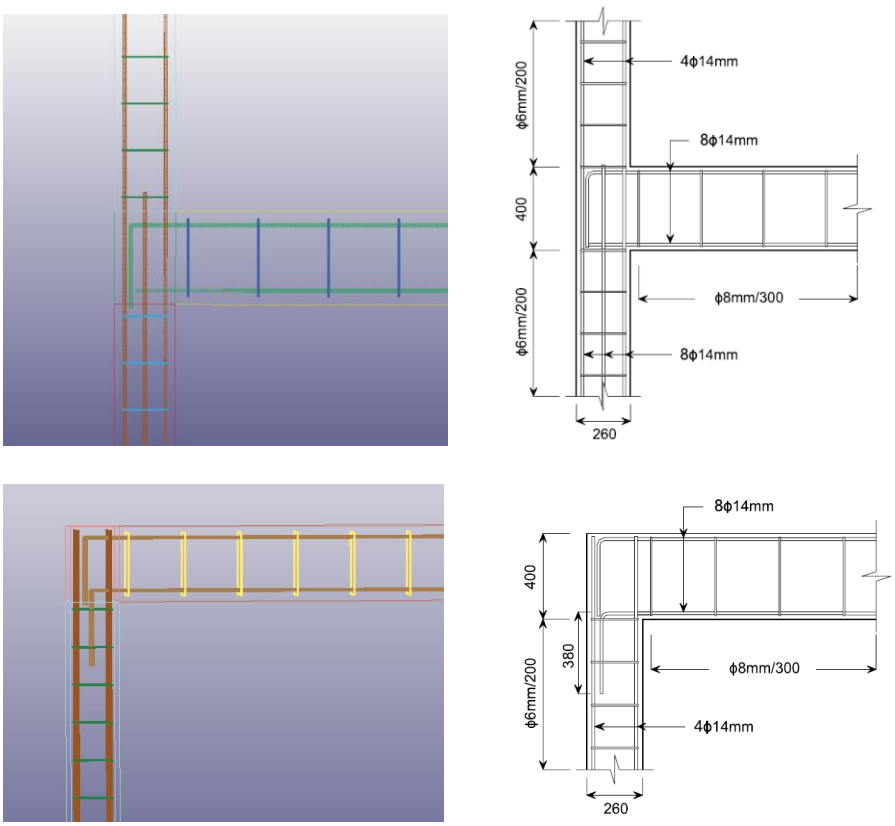

Figure 4.2 Reinforcement detail in first floor joints in LS-DYNA (on the left), and reinforcement detailing in ECOLEADER experiment by Garcia et al. (2010) is given on the right side of the illustration

4.2.1 Constrained beam in solid

Bonding between steel reinforcement and concrete is defined using the keyword *CONSTRAINED_BEAM_IN_SOLID in LS-DYNA. The concrete serves as the master component and the embedded reinforcement bars move with the Lagrangian mesh of the solid elements and are serving as slave components in the algorithm. Bond-slip behaviour for the shaking table simulations have not been considered. If included, it greatly increases the computational time of the analysis. It can be considered through setting the variable AXFOR to -10 in the *CONSTRAINED_BEAM_IN_SOLID_PENALTY card in LS-DYNA.

Global hourglass control was also added to the model to control mesh tangling and unrealistic deformation of the crushed/impacted parts. It should be noted that hourglass energy should be less than 10% of the internal energy at all time.

4.2.2 Frame boundary condition and earthquake motion

As mentioned, the model of the building was a 2D model with 3D elements and the mass of the building was applied at nodal masses onto the first floor and second floor beams representing the extra mass of the steel plates in the test. *BOUNDARY_SPC_SET was set to let the building move in X, Y and Z-rotation and *BOUNDARY_PRESCRIBED_MOTION_SET was used to apply earthquake histories to the base of the building in X-direction.

4.2.3 Material models

An elastic-plastic material model available in LS-DYNA called *MAT_PLASTIC_KINEMATIC is used to model steel reinforcements with the parameters expressed in Table 4.1 based on the reinforcement's properties used in the experiments. Due to the simulation low strain rate, strain rate effects is ignored.

The numerical model of the shaking table was validated against the experiments using CSCM (MAT_159) and K&C (MAT_72R3) model for concrete strength of 20 MPa with the input parameters shown in Table 4.2 and Table 4.3. These are the same parameters used to validate direct HPB numerical models in Chapter 3, except they are generated for a concrete of 20 MPa in this set of validation. The same parameters were used for the shaking table simulations cross referenced with the input data of direct HPB simulations meaning that all the parameters were consistent for both FE models and the specific parameters were changed for both of them (e.g erosion is set to 1.09 for CSCM and 0.07 for K&C).

Table 4.1 Plastic kinematic material model parameters for steel

Density (kg/m^3)	**Young Modulus (GPa)**	**Poisson's ratio**	**Yield strength (MPa)**
7850	212	0.29	551

Table 4.2 CSCM long input parameters for concrete of 20 MPa

(* Units are Newton, metre, kilograms, and seconds)

Section 1: Control parameters

MID	159
NPLOT	1
INCRE	1.1638E-05
IRATE	1
ERODE	1.09
RECOV	10
IRETRC	1

Section 2: Stiffness parameters

G_0	1.0010E+10 (Pascal)
K_0	1.0960E+10 (Pascal)

Section 3: Shear surface hardening parameters

N_H	1
C_H	0

Section 4: Yield surface parameters

α	1.2840E+07 (Pascal)
θ	0.26640
λ	1.0510E+07 (Pascal)
β	1.9290E-08 (Pascal^{-1} or 1 m s^2/kg)
α_1	0.7473
θ_1	1.3720E-09 (Pascal^{-1} or 1 m s^2/kg)
λ_1	0.17
β_1	7.8290E-08 (Pascal^{-1} or 1 m s^2/kg)
α_2	0.66
θ_2	1.6500E-09 (Pascal^{-1} or 1 m s^2/kg)
λ_2	0.16
β_2	7.8290E-08 (Pascal^{-1} or 1 m s^2/kg)

Section 5: Cap parameters

R	5.0
X_0	8.6890E+07 (Pascal)
W	0.05
D_1	2.5000E-10 (Pascal^{-1})
D_2	3.492E-19 (Pascal^{-2})

Section 6: Damage parameters

b	100
d	0.1
G_{fc}	5148 Pascal-meter
G_{ft}	51.48 Pascal-meter
G_{fs}	51.48 Pascal-meter
pwrc	5
pwrt	1
pmod	0

Section 7: Rate effects parameters

η_{co}	1.1990E-04
N_c	0.78
η_{to}	5.4700E-05
N_t	0.480
overc	1.8830E+07 (Pascal)
overt	1.8830E+07 (Pascal)
S_{rate}	1.0
repow	1.0

Table 4.3 K&C long input parameters for concrete 20 MPa

(* Units are Newton, meter, kilogram, and seconds, and Pascal)

MID	72
A_0	5.912E+06 (Pascal)
A_1	4.463E-01
A_2	4.040E-09 (Pascal^{-1} or 1 m s^2/kg)
A_{1F}	4.417E-01
A_{2F}	5.91500E-9 (Pascal^{-1} or 1 m s^2/kg)
A_{0Y}	4.464E+06 (Pascal)
A_{1Y}	6.250E-01
A_{2Y}	1.288E-8 (Pascal^{-1} or 1 m s^2/kg)
LOC_{WIDTH}	0.0254 (m)
RSIZE	39.37 (in/m)
UCF	0.000145 (psi/Pascal)

ρ	2400 (kg/m^3)
PR (Poisson's ratio)	0.2
F_t	2.216E+06 (Pascal)
b_1	1.6
b_2	1.35
b_3	1.15
ω	0.5
S_λ (stretch factor)	100
NOUT (output selector for plastic strain)	2.0
EDROP	1.0
NPTS (Npoints)	13

4.3 Eigenvalue analysis- structural period

To validate the FE model of the two-storey building natural frequencies as well as mode shapes of the building were determined in the absence of damping using eigenvalue analysis. The frequencies that the building naturally vibrates at, when disturbed, are called natural frequencies. Mode of vibration of the building is the deformed shape of that building at one particular natural frequency of vibration, therefore, each mode shape is linked to an exact natural frequency. The mode shapes and the natural frequencies are the results of the properties and boundary conditions of the building.

The fundamental periods of the building for the first two vibration modes which were determined by running an implicit eigenvalue analysis in LS-DYNA are depicted in Table 4.4. The difference between the periods of the actual building and the simulation is mainly due to the stiffness of concrete. In the shaking table tests, the frame was subjected to many pre-experiment vibrations for setting up process that caused cracking in the frame and reduced concrete stiffness to begin with.

Table 4.4 Comparison of structural period obtained from experiments against the numerical analysis of LS-DYNA

Structural period	Experiment	LS-DYNA analysis
First mode	0.53	0.433
Second mode	0.18	0.164

4.3.1 Dynamic Relaxation (DR)

Dynamic Relaxation (DR) is used to preload the FE model of the structure with gravity before the start of the analysis. If the gravity load is suddenly applied without dynamic relaxation in advance, dynamic oscillation will be excited in the structure. During the DR phase, the model reaches a steady state pre-loaded condition nearly free from dynamic oscillation. During the DR phase, the load is ramped and then held constant until the solution converges, and along with that, 5% damping was applied to the building.

4.4 Validation of the FE building model

Dynamic analysis of the FE model of the building was performed under earthquake motions at variable PGA levels of 0.05g, 0.1g, 0.2g, 0.3g and 0.4g. The performances of the same two material models, CSCM, and K&C for modelling concrete were compared together with the shaking table test results of Garcia et al. (2010) along with their capabilities in capturing cracks and spalling of concrete. Displacement-time histories of the experiment were compared to the simulation's displacement-time histories for both CSCM (MAT_159) and K&C (MAT_72R3) material models. It was observed that both material models were capable of simulating the displacement response of the building, in particular CSCM performance was very good in capturing the peak displacements. CSCM was also more reasonable in capturing concrete cracks, spalling and crushing.

4.4.1 Mesh size effect

From the previously conducted mesh convergence analysis on the FE simulations with CSCM and K&C, it is known that the size of the mesh element should be at least, at minimum a similar size to the aggregate in the concrete mix. So, when concrete fractures, the fracture zone (FPZ) must be large enough to at least include the size of the largest aggregate in the mix, otherwise incorrect results are obtained. Bazant and Oh (1983), and Denarie et al. (2001) determined the optimum size of the fracture zone to be three times of the maximum aggregate size used in the concrete mixture. Experiment performed by Kang et al. (2018) on the response of concrete to dynamic loading also showed the fracture zone to be about three times larger than the size of the aggregate in the concrete mixture. Dai et al. (2019) carried out three-point bending test to investigate the characteristics of fracture process zone in concrete including digital imaging. Their investigation confirmed that the fracture zone is about three times larger than the maximum aggregate size used in the concrete mixture.

As discussed in Chapter 3, mesh elements in a FE model using smear crack material models such as CSCM must be large enough to include fracture process zone (FPZ). The element also has to be large enough to include the reinforcement bar diameter. For the FE simulation to properly model concrete behaviour, the element must be large enough to include the fracture zone (also dependent on the aggregate size) and to be able to dissipate the right amount of fracture energy. It is learnt in the previous chapter that small mesh elements trap fracture energy within them and it only take small amount of energy for that element to quickly fail. As a result, fracture energies are dissipated from every small element, and it results in excessive erosion of elements in the numerical FE simulation.

Mesh analyses were carried out with four variable mesh sizes of 40, 50, 60, and 80 mm for the FE model of the concrete building. From the comparison shown in Figure 4.3 for the CSCM model and Figure 4.4 for the K&C model, the 50mm mesh size was found to be the most suitable mesh size to continue with the analyses as it best predicts the experimental results. Based on the explanation above, for a concrete mix with aggregate size of 19mm, a mesh size of 50mm provides enough area for the fracture energy to dissipate for both FE simulations using CSCM and K&C material models. The mesh area is larger than the maximum aggregate size and it provides a fracture zone about nearly 3 times of the aggregate size. At the same time, it is time effective and keeps computational effort at minimum. Also, as the models are mesh dependent, the 50mm mesh best resembled concrete cracking and spalling.

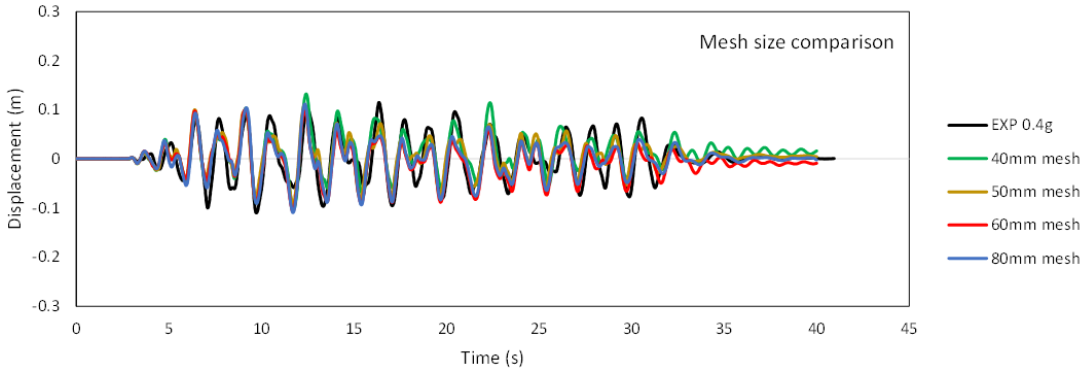

Figure 4.3 Comparison of variable mesh sizes for CSC Model

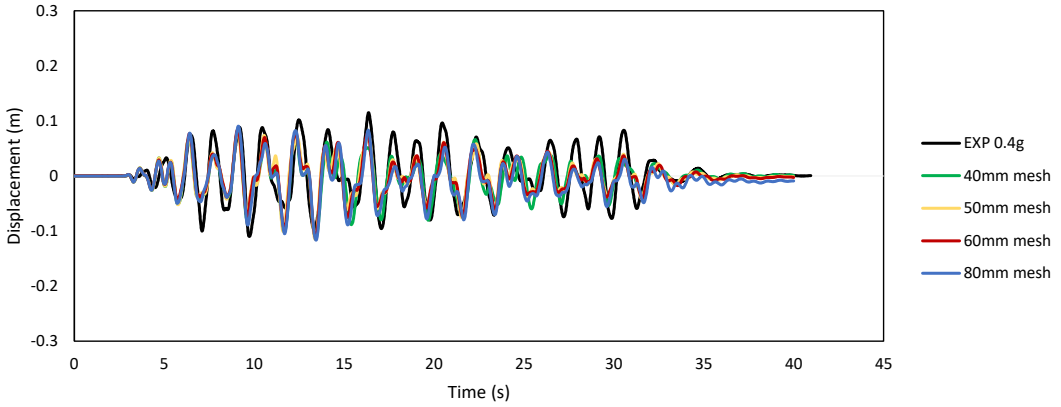

Figure 4.4 Comparison of variable mesh sizes for K&C Model

4.4.2 CSCM Performance in Modelling Concrete

Experimental displacement-time histories of ECOLEADER building obtained for variable PGA levels of 0.05g-0.4g have been compared against the performances of CSCM and K&C models for all earthquake motions in LS-DYNA. To avoid repetitive figures, the results of 0.05g, 0.2g and 0.4g are illustrated for CSCM and K&C models. The erosion values for CSCM is kept as 1.09 and for K&C model is 0.07 throughout this thesis. Figure 4.5 to Figure 4.10 depict comparison of experimental and numerical displacement-time histories of CSCM against the experiments. Cracking and spalling of concrete observed in the tests for 0.4g and the capability of the numerical simulation with CSCM in capturing these cracks have been compared and illustrated in Figure 4.11 to Figure 4.14. The element deletion is representative of cracks and spalling of concrete. Results show CSCM is more capable of capturing these

spalling/cracking of concrete compared to the K&C model. CSCM performance was very good as it was able to capture the peak displacements observed in the experiments by a difference of approximately 5- 10%.

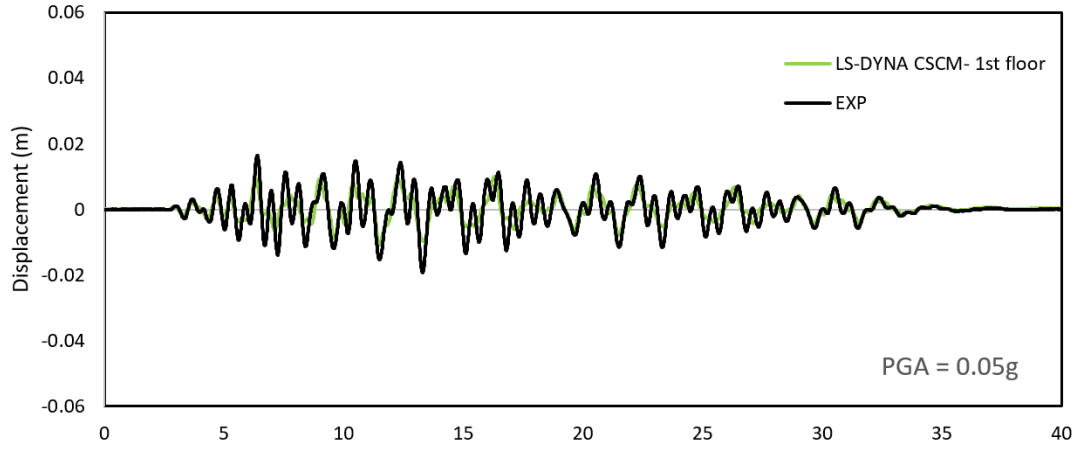

Figure 4.5 First floor displacement-time history using CSCM (MAT_159) at PGA level of 0.05g

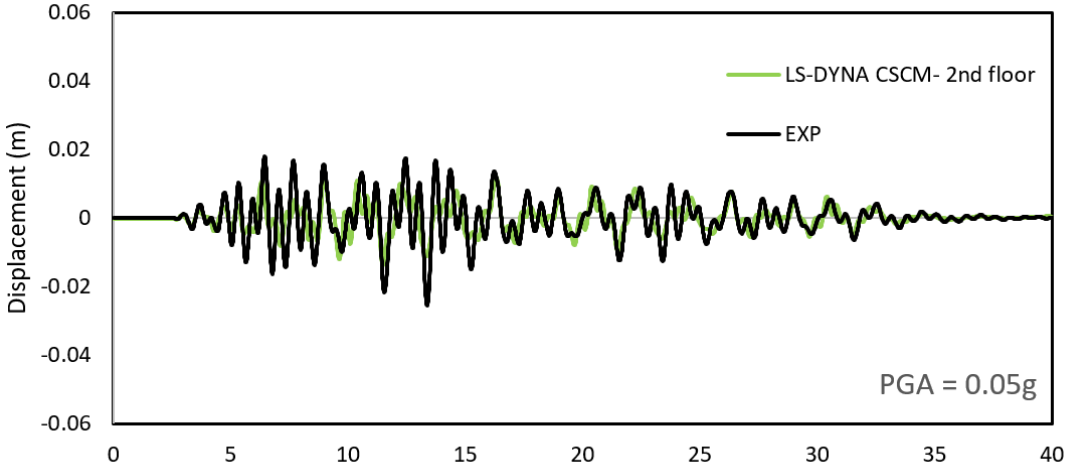

Figure 4.6 Second floor displacement-time history using CSCM (MAT_159) at PGA level of 0.05g

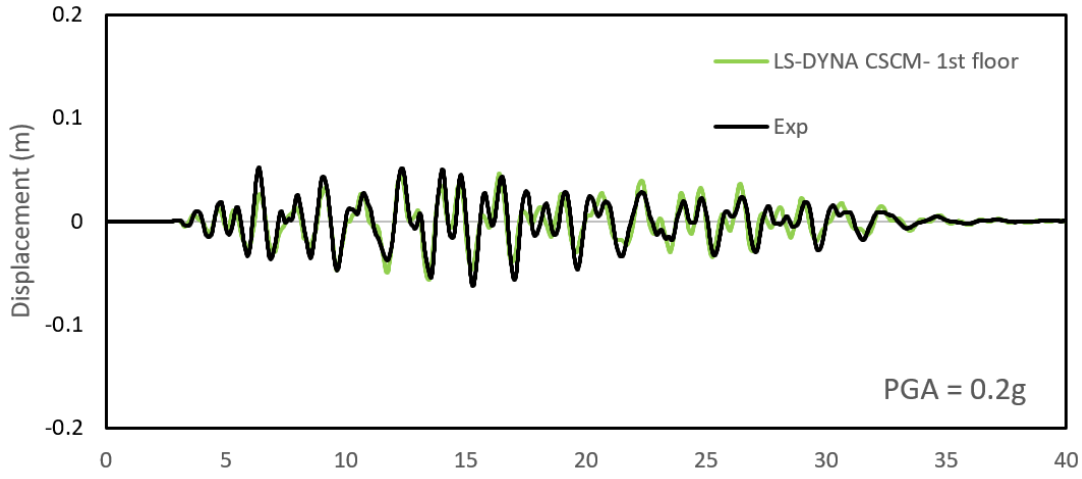

Figure 4.7 First floor displacement-time history using CSCM (MAT_159) at PGA level of 0.2g

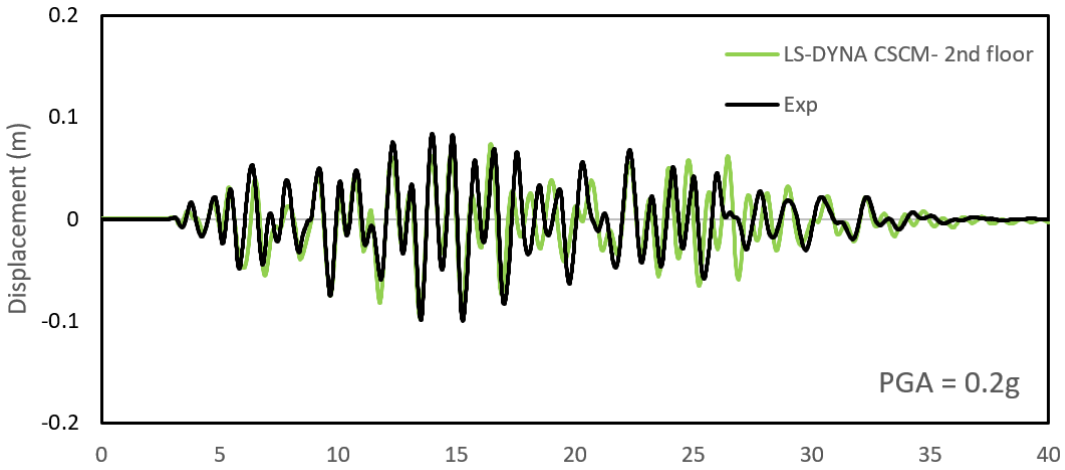

Figure 4.8 Second floor displacement-time history using CSCM (MAT_159) at PGA level of 0.2g

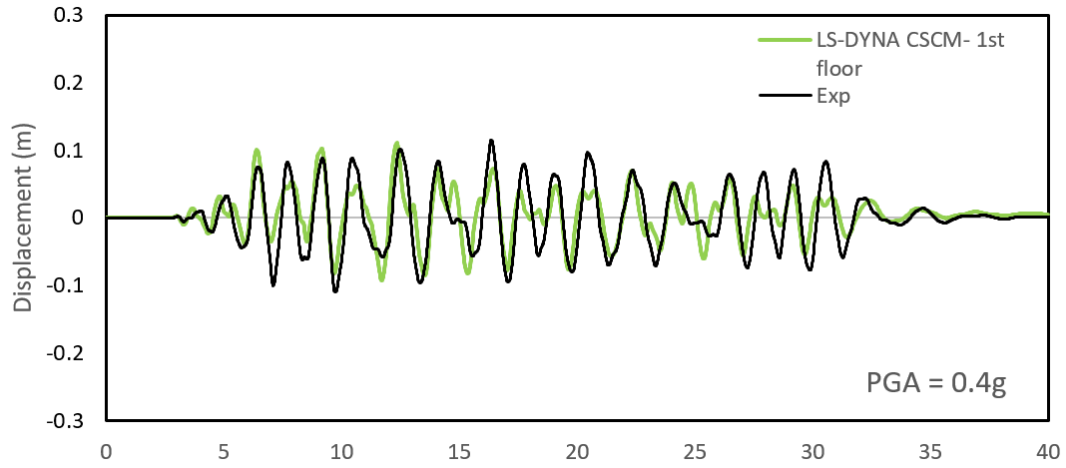

Figure 4.9 First floor displacement-time history using CSCM (MAT_159) at PGA level of 0.4g

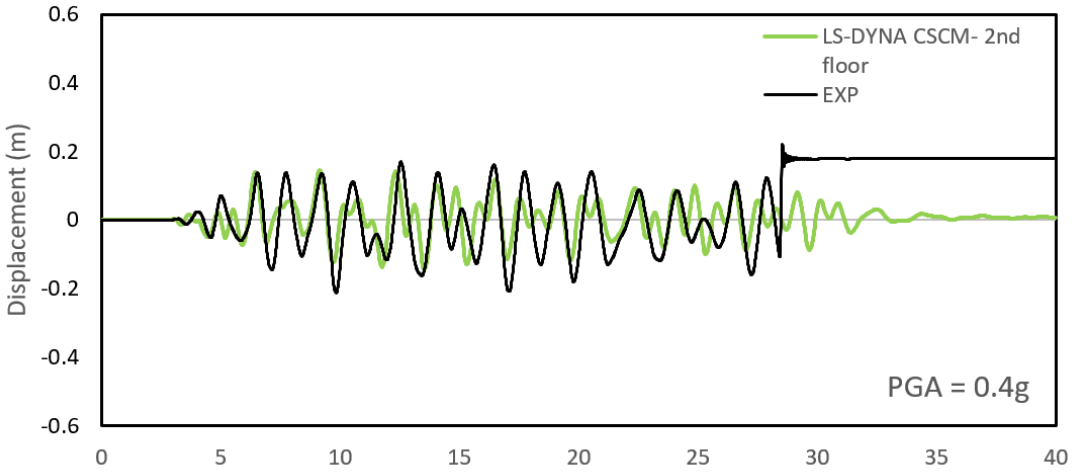

Figure 4.10 Second floor displacement-time history using CSCM (MAT_159) at PGA level of 0.4g

It should be noted that the transducer on the second floor broke in the middle of the experiment and did not record the rest of the experiment and that is the reason it shows as a constant straight line after about 28 seconds in Figure 4.10.

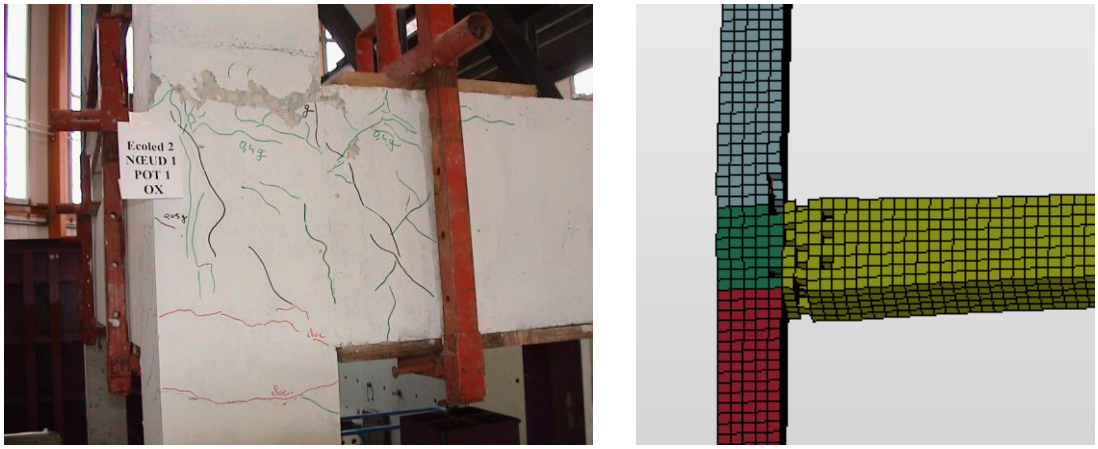

Figure 4.11 (photo on the left) cracks and spalling of concrete in the first floor's right-side beam-column connection at PGA level of 0.4g observed in the experiment, (photo on the right) resembling concrete spalling and cracking observed in the experiment using CSCM in LS-DYNA

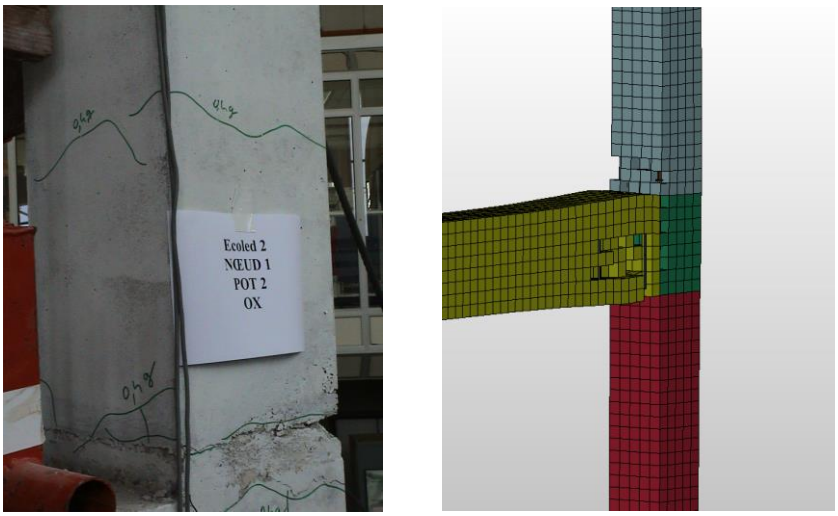

Figure 4.12 (photo on the left) cracks and spalling of concrete in the first-floor left side beam-column connection at PGA level of 0.4g observed in the experiment (photo on the right) resembling similar concrete spalling and cracking in LS-DYNA using CSCM

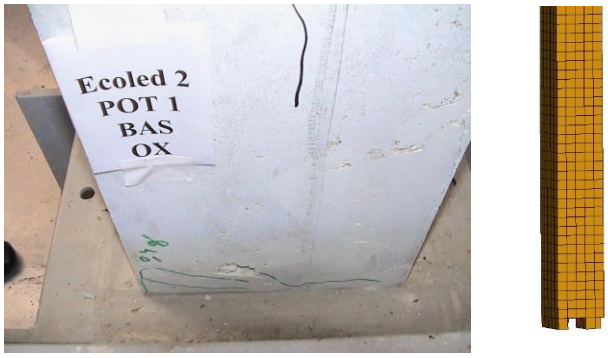

Figure 4.13 (On the left) concrete cracking and spalling in the base of the column observed in the experiment, (on the right) concrete erosion resembling cracking/spalling in LS-DYNA simulation

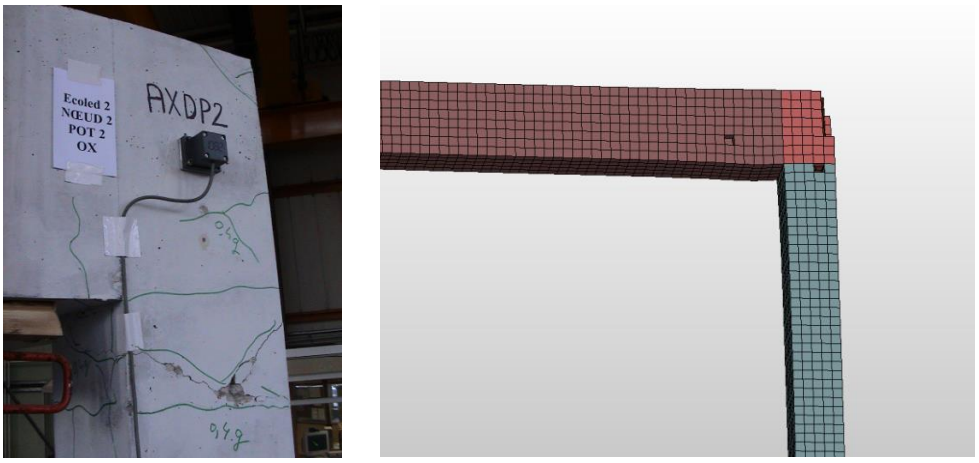

Figure 4.14 (On the left) top floor left connection cracks and spalling of concrete observed in the experiment, (on the right) cracking/spalling of concrete by means of erosion in LS-DYNA simulation

4.4.3 Performance of the K&C (MAT_72R3) model for concrete including dynamic increase factor and erosion

The performance of the Karagozian and Case model by means of displacement-time histories have been compared against the shaking table tests performed at PGA levels of 0.05g-0.4g. Comparative Figure 4.15 to Figure 4.20 showing first floor and second floor displacement histories for earthquakes with PGA levels of 0.05g, 0.2g and 0.4g. Strain rate sensitivity in the building's response has been investigated as well as the capability of K&C in capturing cracking and spalling of concrete by means of erosion. Finally, ERODE value of 0.07 (the

same value used for K&C in the direct HPB simulations) is used in the validation of K&C shaking table simulation against the experiments.

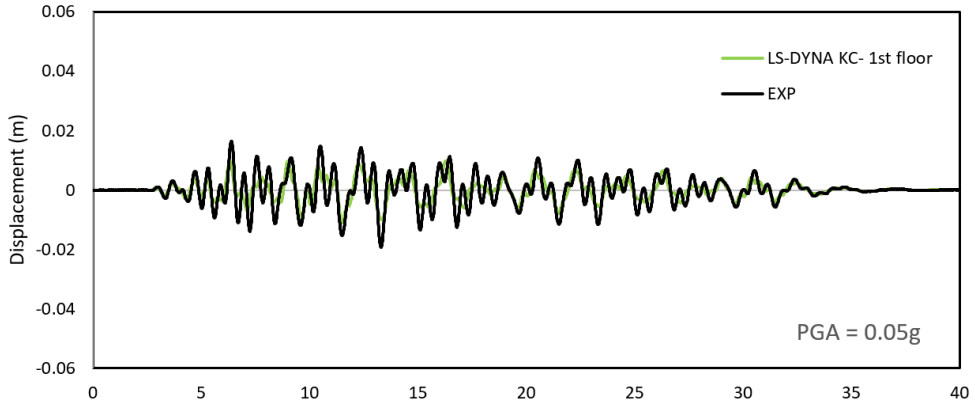

Figure 4.15 First floor displacement history using K&C model in LS-DYNA at PGA level of 0.05g

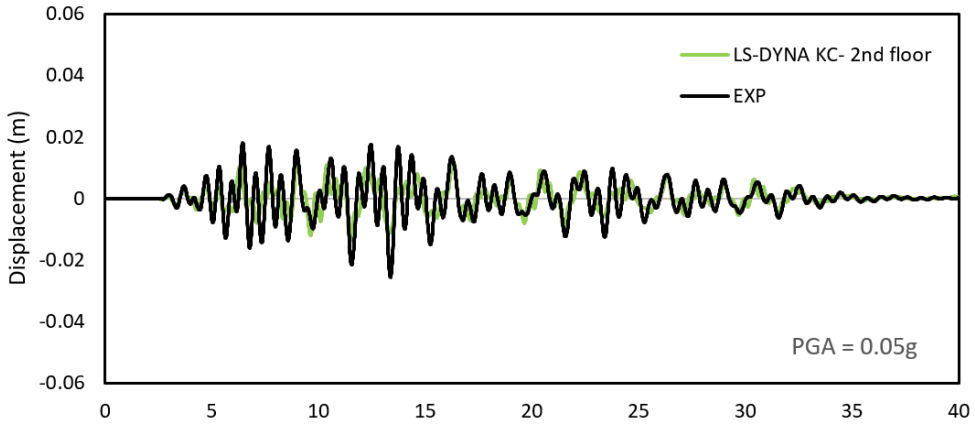

Figure 4.16 Second floor displacement history using K&C at PGA level of 0.05g

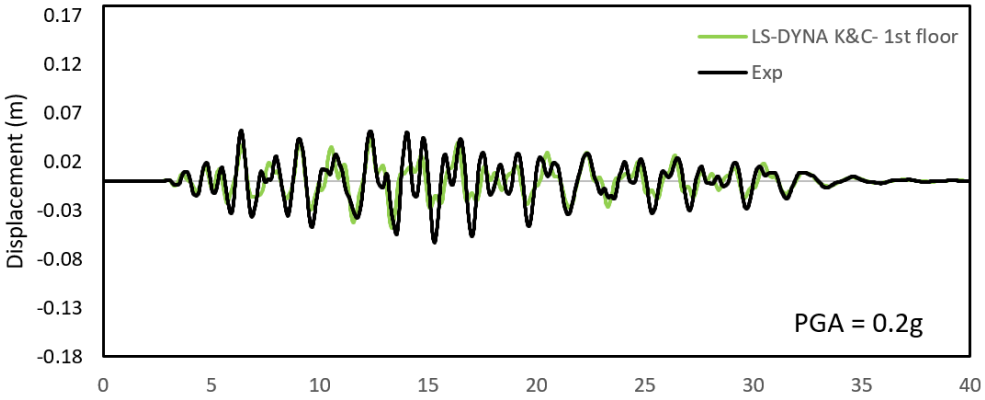

Figure 4.17 First floor displacement history using K&C at PGA level of 0.2g

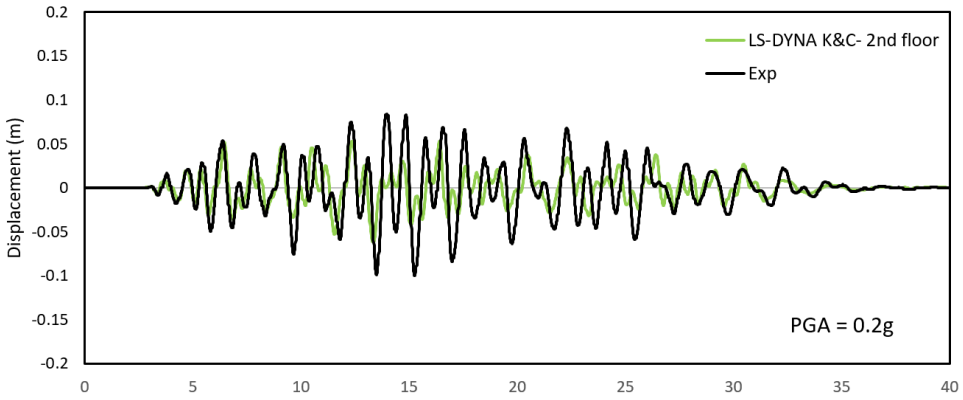

Figure 4.18 Second floor displacement history using K&C at PGA level of 0.2g

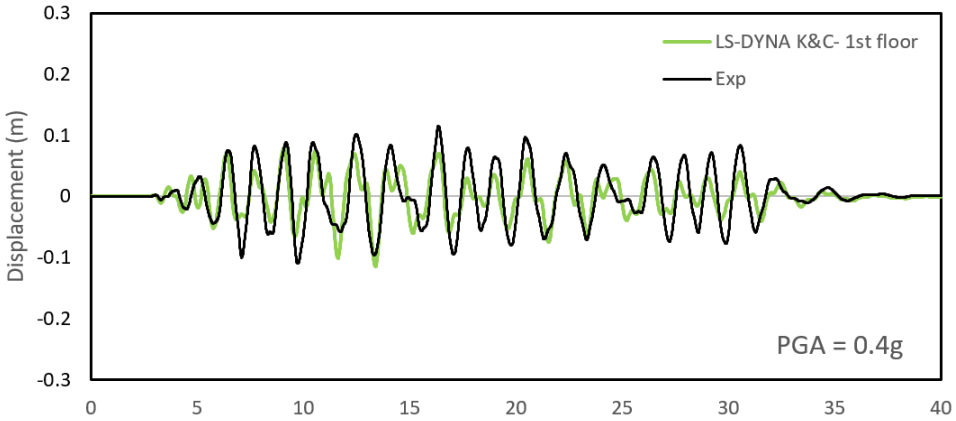

Figure 4.19 First floor displacement history using K&C at PGA level of 0.4g

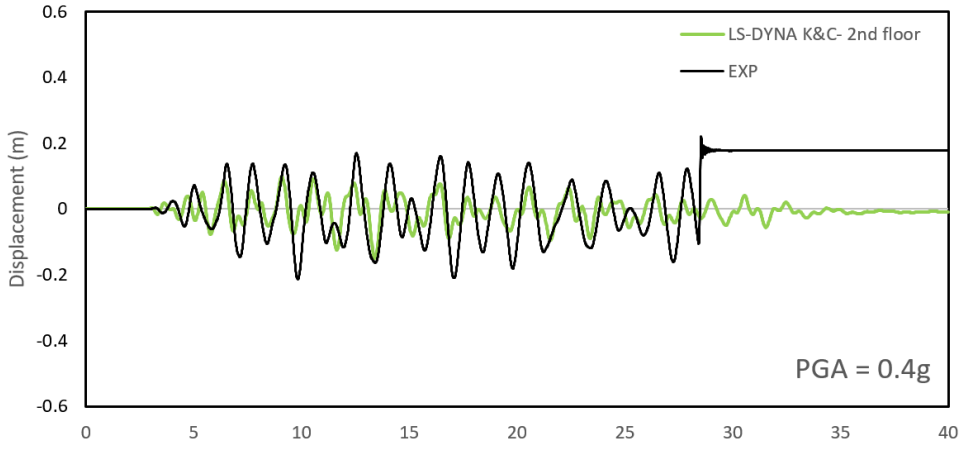

Figure 4.20 Second floor displacement history using K&C at PGA level of 0.4g- breakage of transducer at second 28

K&C has shown a good level of performance at this stage as it is capable of capturing the peak displacement of the building during seismic motions by about 10-15% difference compared

to the experiment. Reasons for the differences are for example before the shaking table test commences, the frame was transported onto the shaking table which caused small cracks in the frame. Also, after transporting the frame and before commencing the test, seismic signals were tested several times to make sure they were being sent from a device/laptop onto the shaking table clearly and as a result it caused more cracks in the building.

However, erosion study of K&C in the next section has shown that the lack of this feature can disadvantage its powerful capability in some ways as by adding an extra erosion formulation, K&C representation of concrete behaviour (e.g crushing) can get far from reality. The discussion is covered in more detail in the section 4.5 called "the numerical erosion".

4.4.4 Performance of Karagozian and Case Model including Dynamic Increase Factor (DIF)

Displacement responses of two buildings, one building with strain rate sensitivity (including dynamic increase factor- DIF), and the other one with no strain rate (denoted as LCRATE in LS-DYNA manual) included, have been compared. As examples, comparative figures for 0.1g and 0.3g have been expressed in Figure 4.21 and Figure 4.22. The results of analyses for earthquakes with PGA levels up to 0.3g have shown almost no concrete strain rate sensitivity, however for earthquakes with higher PGA levels than 0.3g the application of DIF was beneficial as it increased the concrete strength to comply with the experimental results. This finding does not fully agree with the conclusion drawn in Chapter 3 (validation of direct HPB simulation) dismissing the application of DIF in simulation of concrete impact.

In the direct HPB simulations due to impacts (some with higher velocities), inertial confinement contributed to the enhancement of concrete strength. However, in the case of shaking table simulations with low velocities, the application of DIF was influential particularly when concrete was in tension due to its low tensile strength. If users require to include this feature (only available in the more recent versions of LS-DYNA- version R10.1.0) LCRATE parameter in K&C model can be set to -1 and the program automatically includes strain rate as per discussion given in Chapter 3. DIF has been included in the validation of shaking table simulations using K&C model in this chapter.

In CSCM simulations, the strain rates for earthquakes with PGA levels of 0.05g, 0.1g and 0.2g range from 0.00038 (for the lowest PGA level of 0.05g) to 0.2 s^{-1} (for PGA level of 0.2g), and for earthquakes with PGA levels of 0.3g and 0.4g the range is within 0.356- 0.48 s^{-1}. In K&C simulations with DIF included, up to PGA level of 0.3g, the strain rate range is similar to the strain rates obtained in CSCM simulations, however, for earthquakes with PGA levels of 0.3g

and 0.4g, the strain rate increases to 0.114-0.135 s^{-1}. This also confirms that DIF is not influential in seismic motions with lower PGA levels, but it is effective for earthquakes at PGA levels of 0.3g and 0.4g.

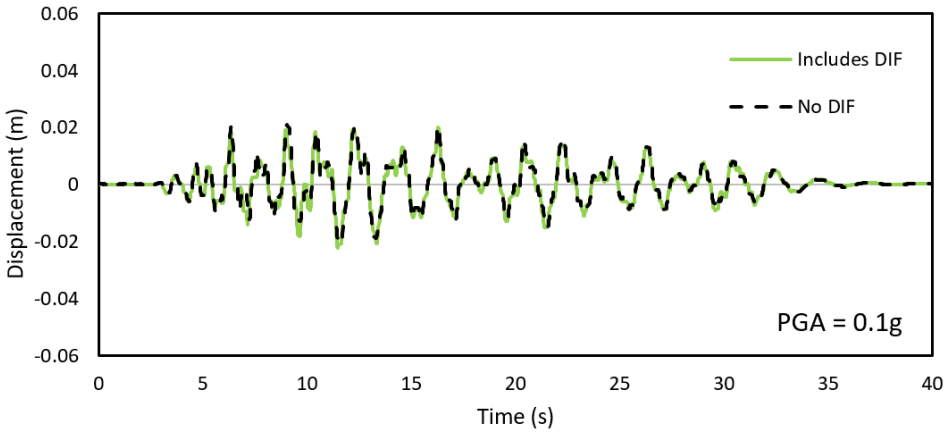

Figure 4.21 The effect of strain rate enhancement in the case of K&C has been compared to when strain rate is not included for earthquake at PGA level of 0.1g

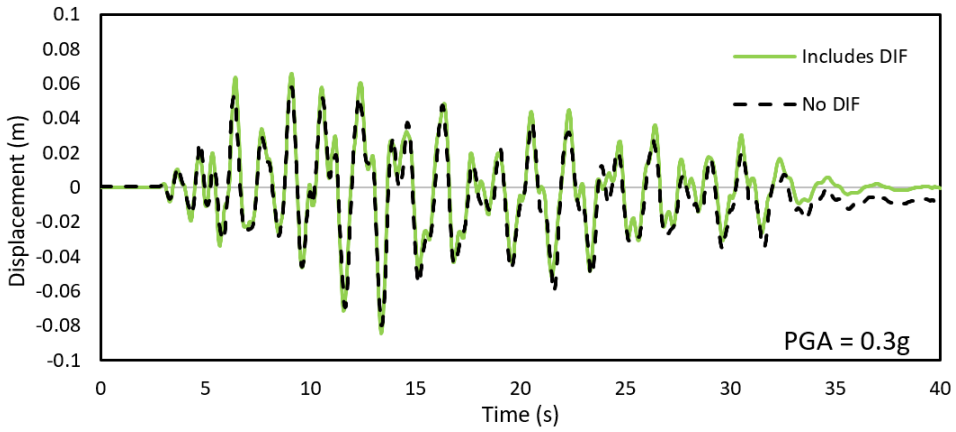

Figure 4.22 The effect of strain rate enhancement in the case of K&C has been compared to the same case only when strain rate was not included for earthquake at PGA level of 0.3g

4.4.5 Comparison of the performances of the K&C and CSC Models

The performances of CSC and K&C models have been compared with the experimental data and they are depicted in Figure 4.23 and Figure 4.24 for earthquakes at PGA level of 0.3g and 0.4g. The performances of both material models have also been compared and shown in Figure 4.25 and Figure 4.26. The comparison shows that the displacement-time histories simulated by both material models are very close. Their element deletion capability is what sets them apart and make them suitable/or unsuitable for pounding simulation of buildings.

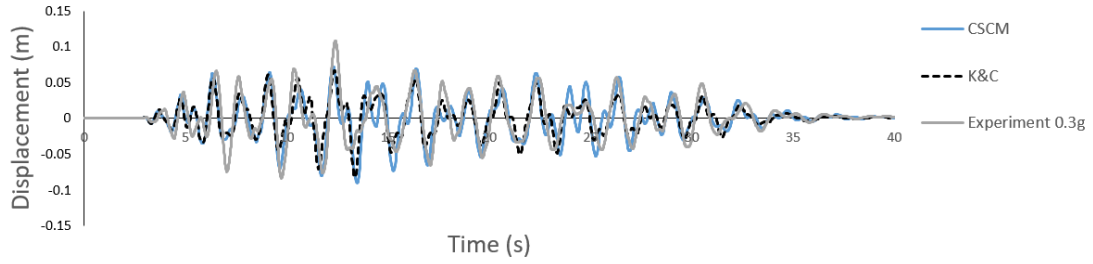

Figure 4.23 Performances of shaking table experiment with CSCM versus K&C model at PGA level of 0.3g

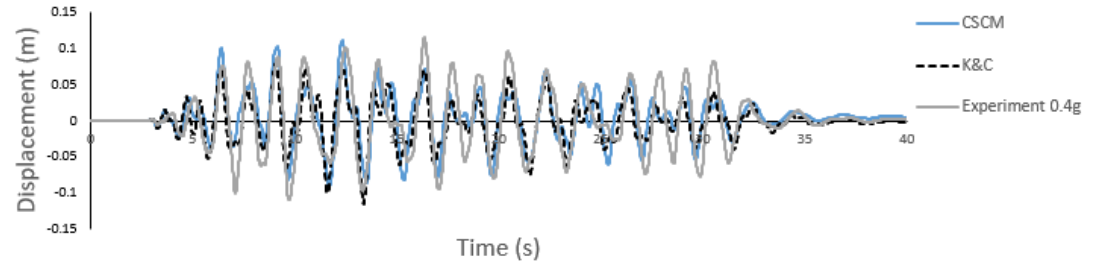

Figure 4.24 Performances of shaking table experiment with CSCM versus K&C model at PGA level of 0.4g

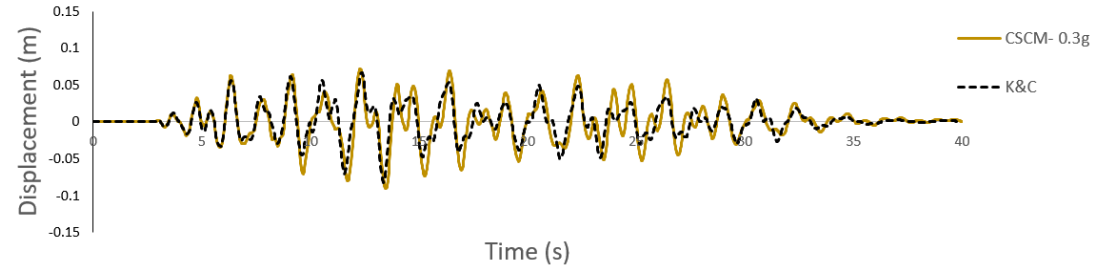

Figure 4.25 comparison of CSCM performance against K&C at PGA level of 0.3g

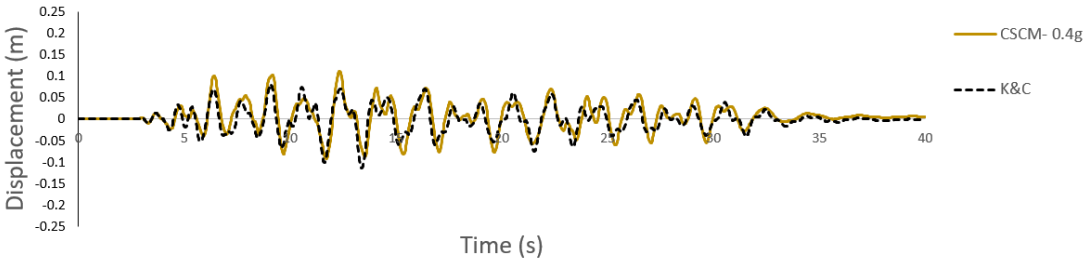

Figure 4.26 comparison of CSCM performance against K&C at PGA level of 0.4g

4.5 The numerical erosion

The function of element deletion (separation of eroded elements and their elimination from the rest of the simulation) despite having material's physical appearances, is not a material property neither a physical phenomenon. It is rather mimicking material's behaviour and is purely a numerical trick which provides a graphical representation of concrete spalling and crushing for the users (Wu et al., 2011). Apart from making it possible for the users to visual concrete crushing, it has an important purpose and that is in fact preventing mesh tangling. Without this technique, in Lagrangian mesh, the time step for those elements that have been crushed and have lost strength become very small resulting in numerous computational cycles with almost no improvement in computational time (Luccioni and Araoz, 2011). Besides, Lagrangian elements have the tendency to tangle up leading to severe distortion in the mesh.

Erosion enables the simulation to continue by removing the Lagrangian cells if a criterion is pre-defined, then the mass of the deleted element is distributed to the adjacent nodes. However, the internal energy as well as the compressive strength of the element material is lost. Loss of energy occurs when elements are eroded therefore the erosion criteria/limit should be determined in a way that elements are not omitted/deleted until these elements are heavily deformed, and the overall results are not influenced by the elements mass and compressive strength (ANSYS, 2009). It is recommended that the effect of erosion is evaluated by comparing simulations with variable erosion values and to set the criteria for erosion values in a way that are high and practicable (Luccioni and Araoz, 2011).

It has been one of the intentions of this thesis to understand the influence of erosion values on the numerical simulations of concrete using K&C and CSCM. A set of erosion values based on previous research on concrete simulation under blast/impact load have been chosen and the patterns of eroding elements (using different erosion criteria) in the models are observed to understand the influence of erosion in the simulations' final results.

Concrete models are two types: (1) with an in-built erosion formulation, and (2) without the formulation. It has been described previously that *MAT_ADD_EROSION is used along with K&C model to delete elements and prevent excessive distortion of the mesh. A desirable erosion value for a numerical model that includes *MAT_ADD_EROSION is an ad hoc number based on trial and error and there is not a value that can be used for every simulation. For example, a study by Chung et al. (2015) on missile impact on concrete plates found the criteria for element deletion based on maximum principal strain to be 0.10 using *MAT_ADD_EROSION for K&C model as well as Winfrith model (MAT_84) which also does not include an in-built erosion algorithm. Tang and Hao, (2010) also found 0.10 to be a reasonable value for erosion in their simulation of cable-stayed bridge against blast load using K&C model. However, Shi et al. (2010) found principal strain of 0.15 to be a reasonable limit for eroding elements in RC frames modelled with K&C under blast loading. They found that by increasing this value, larger distortion occurs in the model and reducing it resulted in premature deletion of elements in the simulation. Suitable erosion value used in the simulation of reinforced concrete plates under blast loading by Xu K and Lu Y (2006) was found to be 0.01. All the erosion values for different studies mentioned in this section are based on maximum principal strain. Maximum principal strain is also used as a criterion in this thesis. Several research (Weng et al. (2020), Yu et al. (2018), Pham et al. (2017a), Yu et al. (2019), Pham et al. (2017b)) also found that maximum principal strain provides reasonable failure in concrete particularly in structural dynamic simulations.

Apart from its suitability, as mentioned previously, CSCM in-built failure system is based on maximum principal strain meaning as soon as the maximum principal strain exceeds the limiting strain, erosion occurs by means of deleting elements. For this reason, in the K&C models, *MAT_ADD_EROSION, is also set based on maximum principal strain to make the concrete crushing/failure pattern comparison between the two material models more reasonable.

4.5.1 Erosion study of CSCM for concrete

In CSCM, elements are deleted when the maximum principal strain surpasses (ERODE-1.0). If ERODE is set to any value less than 1.0, erosion does not happen at all. If erosion is required and the value is set larger than 1, for example if an erosion value of 1.09 is chosen for a particular simulation, considering the relationship (ERODE-1.0), the erosion value becomes 0.09 and it is said that erosion is 9% maximum principal strain.

Chung et al. (2015) found an erode parameter of 1.4 to be suitable for CSC Model of concrete plates against missile impact. Pham et al. (2017a) found an erode value of 1.1 to be suitable for modelling concrete beam under progressive collapse. In a numerical study of flat concrete slab subject to progressive loading by Weng et al. (2020), erosion value of 1.10 was found to be the most suitable to represent concrete crushing. Bermejo et al. (2017) found 1.05 best resemble crushing of concrete structures under blast loading. Jaime (2011) used an erode value of 1.05 which provided very good correlation with the rock fragmentation process observed in the laboratory. Murray et al. (2007), the developer of CSCM, have suggested the erosion coefficient to be 5 to 10% maximum principal strain (ERODE = 1.05-1.10).

The result of erosion study in this thesis shows that erode parameter is not causing much problem in impact cases of direct HPB with high strain rate in the previous chapter, however it became significant when dealing with low strain rate cases. In the direct HPB simulations, erosion values ranging from 1.0 to 1.10 did not influence the deletion pattern of the elements as much as it did for the dynamic simulations of buildings, because in the impact cases, concrete crushed immediately. Basically, it took much smaller amount of energy to cause the element to reach a critical state and fail in the direct HPB simulations. However, this does not apply to the shaking table simulations as shown in Figure 4.27 to Figure 4.33, particularly that in this case the elements are much larger. When ERODE is set to a number larger than 1.1, concrete is exposed to a greater deformation before it cracks/spalls and eliminates from the analysis, meaning it takes more energy for that element to reach a critical state to fail/ or get deleted. Any other value between 1.01-1.10 can be examined to observe its suitability. Figure 4.27 illustrates erosion occurrence replicating concrete failure in the shaking table simulation using erode values of 1.05, 1.07 and 1.09 in CSCM, followed by Figure 4.28 illustrating a comparison between their associating displacement- time histories.

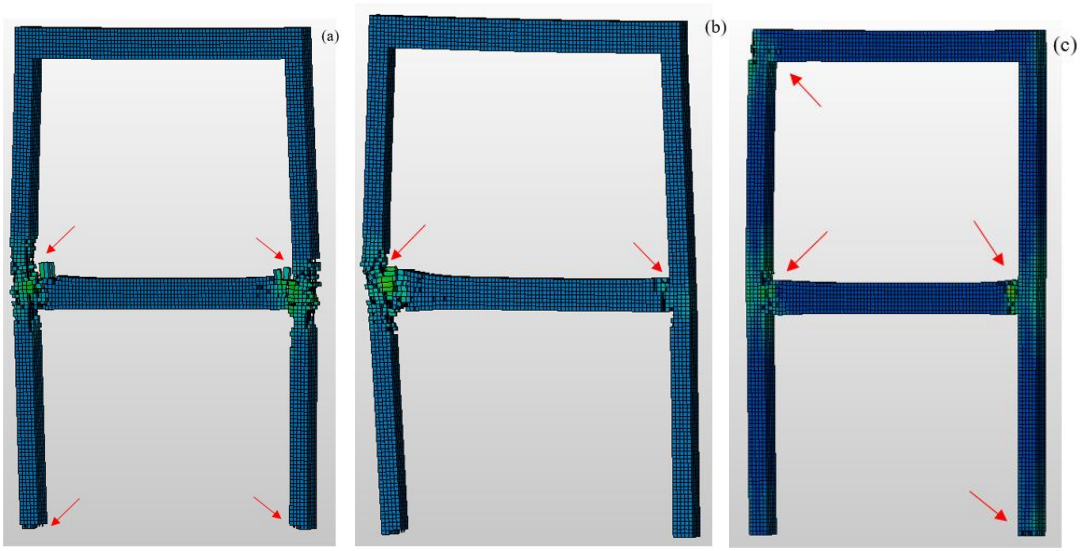

Figure 4.27 Examples of element removal in CSC Model with (a) erode 1.05, (b) erode 1.07, and (c) erode 1.09

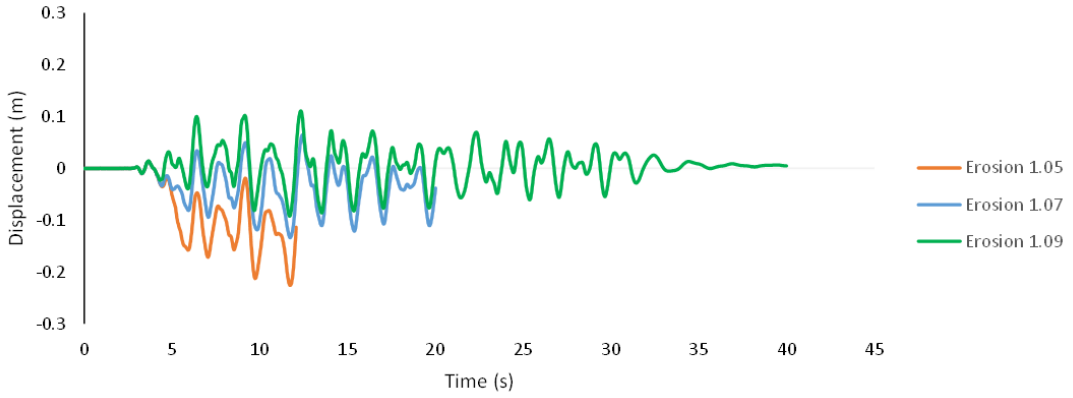

Figure 4.28 Comparison of displacement- time histories of the building with erosion values of 1.05, 1.07, and 1.09 using CSCM

In simulations with CSC Model, premature failure did not occur for values from 1.05 to 1.10. However, for values of 1.05-1.08 too many elements were eroded (compared to the concrete cracking/spalling in the experiment) that could have caused instability in the building. In general, erosion pattern in CSCM is much more sensible compared to the damage pattern seen in K&C models. The model that included erosion of 1.09 best predicted the damage pattern observed in the experiments (it is shown in section 4.4.2, Figure 4.11 to Figure 4.14). The

erode value of 1.09 is used in all the FE simulations that include CSC model throughout this thesis.

4.5.2 Erosion in K&C model

Erosion study of K&C model is conducted using variable erosion values from 0.01 to 1 based on maximum principal strain for earthquake motions at all PGA levels, however the result of earthquake at PGA level of 0.4g is presented in this section as the most concrete damage was observed at this PGA level. For impact cases with principal strain values of 0.03 and below, erosion occurred too early and the erosion pattern and the location where erosion initiated was different in each case. The cracking/spalling behaviour of concrete for erosion values of 0.01, 0.02 and 0.03 are shown in Figure 4.29 to Figure 4.31. Jaime (2011) numerical simulation of rock cutting using K&C model also showed that erosion values at 0.03 and below produced very quick failure of the mesh elements. Any value below 0.03 was found to cause irrational erosion patterns with large deformations. This is also true for the shaking table simulation herein.

A desirable erosion value for a numerical simulation that includes *MAT_ADD_EROSION to replicate true concrete failure is best to be compared against experimental work. However, as mentioned previously there are researchers who use erosion values reported by the other researchers as reference values in similar simulations. For example, in simulation of pounding of bridge segments, He et al. (2017) used an erode value of 0.15 based on maximum principal strain value that was reported by Bi and Hao (2013).

Figure 4.29 depicts the behaviour of the concrete building when an erosion value of 0.01 is used. In this model with such a low erode value, concrete elements had an early pre-mature failure before the analysis termination time. This was also the case for the other two erode values of 0.02 and 0.03. Figure 4.32 illustrates the associating displacement- time histories of the frame with erosion values of 0.01, 0.02, 0.03, and 0.07 (erosion values between 0.05 to 0.07 resulted in similar behaviour).

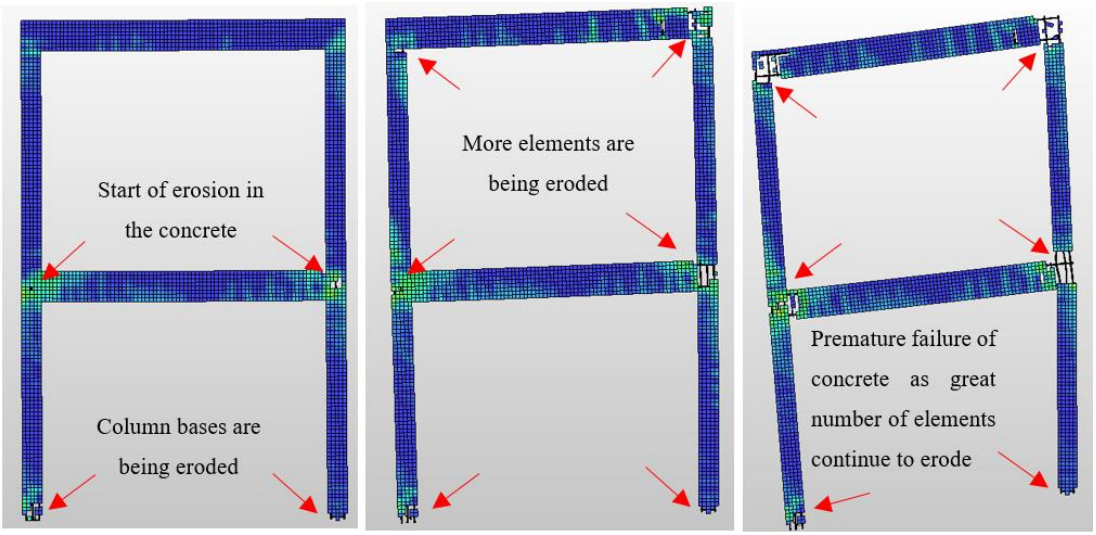

Figure 4.29 Erosion occurring in the concrete building during seismic motions at 7.15 and 7.30 and 7.45 seconds- erosion value is 0.01 based on maximum principal strain

In the case of strain-based erosion value of 0.02 compared to erosion value of 0.01, erosion did not initiate until at 11:66 seconds and the frame lost stability at 16 seconds into the analysis.

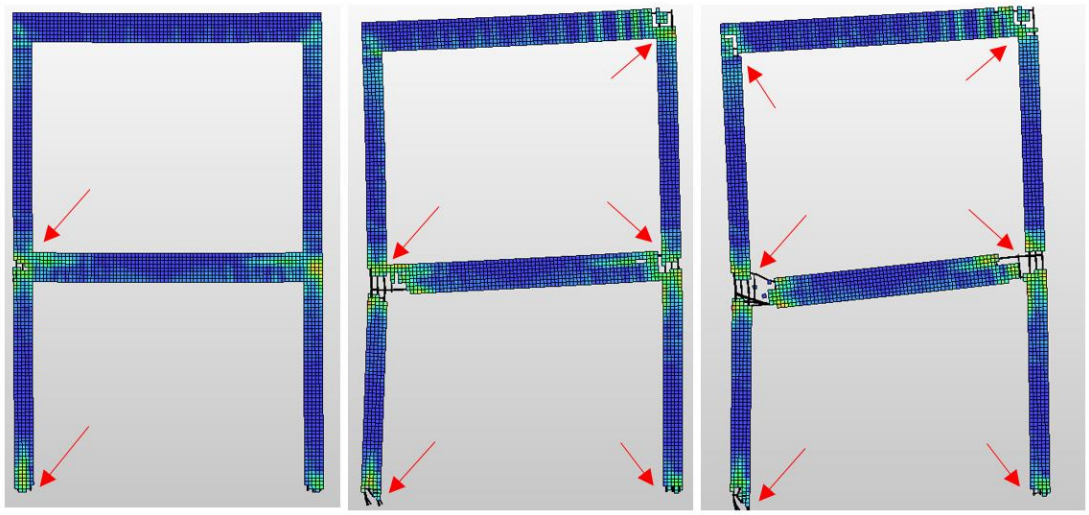

Figure 4.30 Erosion occurring in the concrete building during seismic motions- erosion value is 0.02 based on maximum principal strain; start of erosion in the first frame at 11:66 seconds, second frame shows continuous erosion occurring at 12:18 seconds, and at last the building fails at 16 seconds

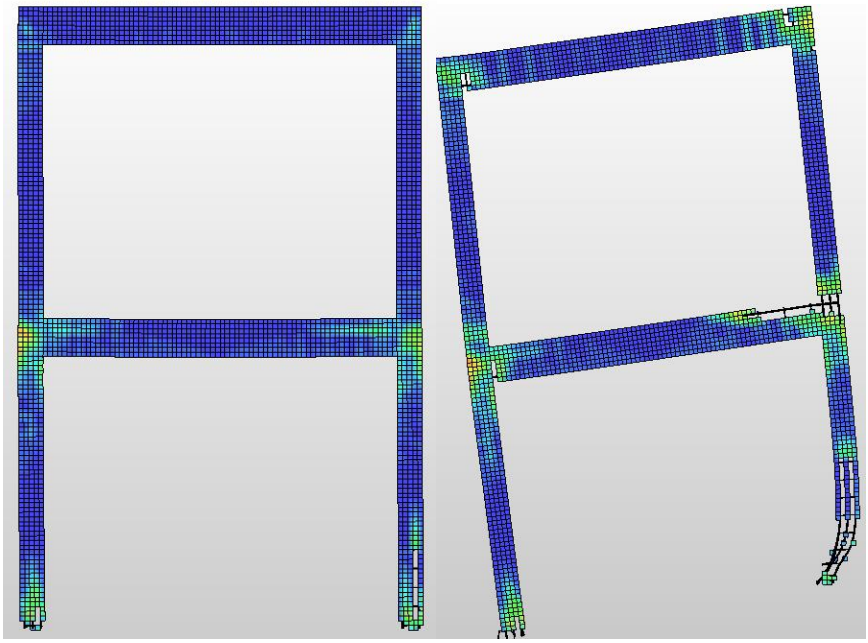

Figure 4.31 Erosion occurring in the building during seismic motions- erosion value is 0.03 based on maximum principal strain; start of erosion in the first frame at 12:18 seconds, second frame shows building's total collapse at 14:98 seconds

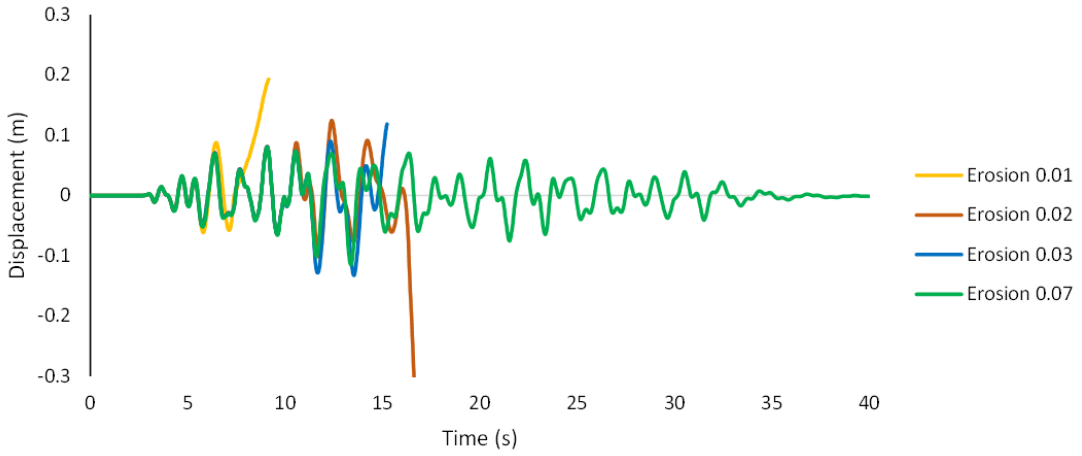

Figure 4.32 Comparison of displacement- time histories of the building with erosion values of 0.01, 0.02, 0.03, and 0.07 using K&C

It has been found that at maximum principal strain value of 0.04 and above, cracking and crushing are not captured by K&C except in the bases of the columns as shown in Figure 4.33. None of the erosion values in the range of 0.01-0.04 were suitable to correctly capture the experiment crushing pattern. The erode value based on maximum principal strain should be high enough to prevent pre-mature failure of concrete. However, on the other hand, erosion

might not occur all together if a very high value is used. Similar to the pattern observed with erode value of 0.04, erosion values in the range of 0.04- 0.07 reproduced a similar pattern to 0.04. Erosion was not captured for values larger than this range.

The removal of too many elements in the bases of the columns can lead to instability and building failure without the building reaching its full capacity. The columns of such a building in a pounding scenario fail after a few mild impacts/contacts with the other structures. Therefore, an erode value of 0.07 is recognised as suitably high enough to not cause early failure and also does not remove many elements (as shown in Figure 4.33) in the columns' bases, consequently, it is chosen to carry out K&C simulations. Erode value of 0.07 at least shows a small erosion of elements in the building (similar to the experiment) but it is not overly high to cause pre-mature or excessive failure in the building.

As shown in the previous comparative figures of K&C performance against the experiments, K&C is also perfectly capable of capturing the displacement-time history of the shaking table test as it is a powerful concrete model. However, the application of *MAT_ADD_EROSION somewhat disadvantages the K&C model as it is unable to capture spalling of concrete correctly were expected without failing the building compared to the capability of CSCM model in capturing these cracks/spalling.

In general, *MAT_ADD_EROSION should be used carefully by examining the performance of a particular simulation against experiments. For as long as it does not cause problem or lead to the total collapse of the building, in low-strain rate dynamic cases, either a higher value of erosion should be used, or erosion should be omitted altogether meaning no observation of concrete spalling as long as it does not influence the final results. This makes the application of K&C in the pounding simulation of buildings unsuitable as in this type of simulations, element erosion is necessary to prevent large deformations and mesh tangling. On the other hand, if mesh erosion occurs in wrong places, it can lead to a false collapse of the buildings which no longer represent real pounding effect. The erosion behaviour of K&C and CSCM have been put into another test in Chapter 5 using push-over analysis. Even though, this feature effectively does not have a physical meaning, it still plays a significant role in the destiny of numerical simulations of concrete buildings.

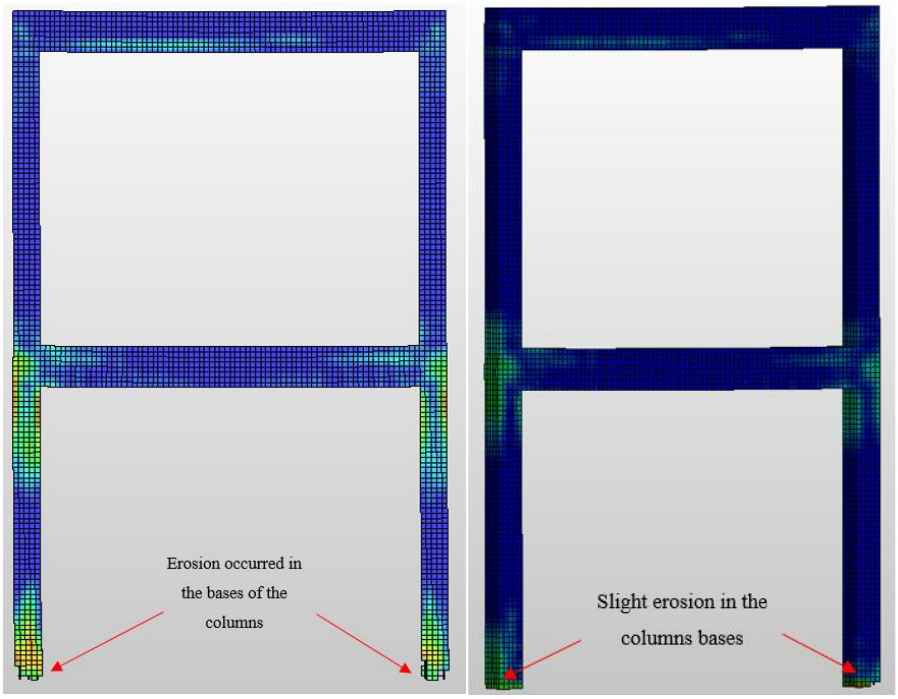

Figure 4.33 Erosion occurred in the bases of the columns; (left frame) too many elements eroded in the bases when erode value of 0.04 is used, (Right frame) slight erosion occurred in the columns' bases when erosion is 0.07

4.6 Summary

So far, studies on impact behaviour of building materials and dynamic response of reinforced concrete buildings under earthquake motions have been combined into a set of simulations that is ready to be applied onto the pounding simulations of buildings. As part of these calibrations, shaking table simulations under variable seismic intensities (at PGA levels of 0.05g-0.4g) using K&C model (MAT_72R3) as well as CSCM (MAT_159) have been compared and validated against shaking table tests. It is shown that the two-storey building simulation particularly using CSCM is in very good agreement with the experimental data and that the results match the periods of the experimental traces. This is an indication of the numerical simulations having a similar evolution of damage to that experienced by the frame. The small differences between the numerical simulation and experimental data are attributed to the fact that the structure experienced cracking prior to commencing the tests. Causes of these cracks are shrinkage of concrete, transporting the structure onto the shaking table, conducting white noise tests, and many pre-experiments testing of earthquake signals from a device/laptop onto the shaking table.

Both material models with their original parameters, the same as the parameter applied in the direct HPB simulations, were used and demonstrated that both material models are capable of simulating the displacement-time histories of the concrete building under all motion intensities. However, an important part of concrete simulation is element deletion pattern in the simulations. If such solution is not used, it can lead to very large deformation and abnormal concrete behaviour and mesh tangling particularly in CSCM due to its development based on fracture energy. Consequently, it must be used with care, so it does not cause pre-mature concrete failure.

CSCM has its own in-built erosion formulation where users have the choice of implementing values between 1.01-1.10 based on maximum principal strain. K&C does not have such an advantage and therefore is used along with a command called *MAT_ADD_EROSION. This extra command has the capability of eroding elements once they reach a certain value based on a defined criterion. The criteria chosen for K&C is also based on the maximum principal strain. This is to enable comparison between the two material models' erosion behaviour as CSC Model erosion formulation is also strain based.

In the K&C model, when erosion value of 0.03 or less is used, as soon as any element reaches this value, the model experiences total collapse because of excessive erosion of elements. Values at 0.04 provide element removals in the bases of the columns which often lead to building failure. The column's erosion pattern re-occurs for models with values of 0.05 and above. It was observed that 0.07 provided more reasonable erosion in the bases of the columns so it did not make the building vulnerable to pre-mature failure and at least was able to capture crushing of concrete in columns' bases which was seen in the experiments. That is the only erosion pattern that K&C was able to capture that represented the crushing seen in the experiments.

Erosion pattern observed in simulations with CSC Model was more consistent for different values. Consistency by means of erosion occurrences in the same locations in all FE simulations, only elements removal was decreased for higher values of erosion. This model was able to demonstrate cracking and crushing of concrete in the joints, column bases as well as the top floor joint which is also seen in the experiments.

On the other hand, for K&C model, erosion is an ad hoc solution to elements removal, and it is best to be compared against experiments. The disadvantage of such an external erosion formulation is that erosion solution to a problem might work for that particular case but not for a similar problem. Therefore, it is not advisable for the same value to be used in even similar simulations.

Despite all complexity associated with erosion and its behaviour, the application of erosion is necessary in numerical simulations as it prevents excessive mesh distortion as a result of large deformations. In the validation of shaking table simulations, best erosion patterns were observed with the material model that has an implemented in-built algorithm (CSCM). It should be noted that no comparison should be made between the erosion values of 0.07 and 1.09 as both values are ad hoc values and it was found that there is no correlation between them.

Erosion in CSCM has a different mechanism to the K&C model. The formulation of CSCM model is developed based on fracture energy that represents strain softening. Fracture energy in such a model is mesh element dependent. On the other hand, erosion is also mesh size dependent. Therefore, if a very large erosion value is used in the CSCM simulation, a lot of deformation is allowed before an element fails. However, in K&C simulation, a large erosion value simply does not let erosion to occur.

In calibrating of shaking table simulations, K&C might be still applicable and acceptable to be used in the validation process when for example capturing the displacement-time histories is of matter and not concrete crushing. However, this material model is not suitable for pounding simulations of buildings describe in Chapter 6 due to its inconsistency in capturing erosion. To confirm such findings even further, ability of both material models in resembling cracking and crushing of concrete is put into further examination using push-over analysis in Chapter 5.

Chapter 5

5. Push-over analysis on a two-storey building

A monotonic push-over analysis is carried out on the same two-storey ECOLEADER building from Chapter 4 using the K&C model, and CSC Model. The purpose of this chapter is to examine the seismic performances of both material models in capturing crushing and ultimate failure of the concrete building to find out if both/or any one of the material models can be used for pounding simulation of buildings. The push-over analysis is carried out to find out if the erosion behaviour in the concrete building using the two concrete material models make sense when subject to earthquake loading, and if the concrete models can capture a sensible behaviour. This chapter gives an insight into the concrete models' suitability to be used in the next chapter on pounding simulation of buildings.

So far, a promising approach is made towards the buildings pounding simulation by extracting reliable data on the failure of specimens starting from direct HPB tests and transferring the findings onto the shaking table simulations. With this promising approach established to get the model ready for simulating pounding between two buildings, the question is: "are both material models capable of representing sensible failure mechanism, if not which one is?". This chapter will answer this question.

5.1 Erosion in CSCM (MAT_159) and K&C (MAT_72R3) during push-over analysis

It has been described previously that erosion is an artificial numerical trick to prevent mesh tangling in finite element analysis. However, it is an important part of concrete modelling when resembling damage such as crushing/spalling of concrete. The ability of the material models to represent damage sets them apart.

In K&C (MAT_72R3) material model, there is no erosion feature included in the original form of the model which in impact simulations, in the absence of erosion, when concrete specimen was crushed, it expanded and behaved like a soft dough until mesh tangling happened and the analysis could-not converge to a solution. Even in the simulation of shaking tables, despite sensibly apprehending the peak displacement responses of the buildings, K&C (MAT_72R3) was technically unable to capture concrete spalling, until erosion was included in the simulation. The application of such a command apart from serving its main purpose which is to stop mesh tangling is also to resemble the real behaviour of concrete.

On the other hand, the added erosion may dilute the accuracy of a material model by causing too many element failures or too few. The observed erosion patterns using variable values were not very much consistent for the models compared to the tests. Substantial element erosion occurred in the middle of the columns and in their bases for K&C model, which made the building instable and vulnerable to pre-mature failure. Erosion feature can-not be disregarded, and it is necessary to be included as part of pounding/impact simulations.

CSCM has shown more capability in resembling concrete crushing in the previous chapters. Before moving onto the pounding simulation of actual buildings, to make sure the material model is resembling real concrete cracking and spalling behaviour, its performance is put onto a test once more by carrying out push-over analysis.

5.1.1 Monotonic push-over analysis using incremental load

Fully fixed boundary conditions were considered for the bases of the building. An increasing triangular lateral load starting from 0 to 1000 kN was applied onto one side of the building (2F at the top slab and 1F at the bottom slab) using *LOAD_NODE_SET as well as *BOUNDARY_PRESCRIBED_MOTION_SET and pushed the building until ultimate failure was achieved. As part of *LOAD_NODE_SET, two sets of tabulated curves were defined for the first floor and the second floor separately. Two simulations were carried out with CSC, and K&C models with the exact same parameters used in the validations of direct

HPB and the shaking table simulations provided in the previous chapters. Similar to the simulations in previous chapters, erosion parameters used for the CSCM and K&C in the push-over analysis were also 1.09 and 0.07. The push-over analysis in this chapter confirmed the findings of the previous simulations, direct HPB and the shaking table simulations. In the previous chapters, particularly in the shaking table simulations, it was observed that K&C performed very brittle and was unable to capture the building's deformations correctly as erosion occurred at the mid-height of the column which was not expected neither was representative of real concrete structural behaviour.

5.1.2 Performance of K&C model in push-over analysis

Building with K&C model was subjected to monotonic lateral loads. Figure 5.1 and Figure 5.2 depict the stages that the concrete building was being pushed to one side i.e started to tilt until it was brought to a critical deformed condition. As soon as the analysis started, erosion occured in the bases followed by unnecessary elements deletion in the middle of the columns.

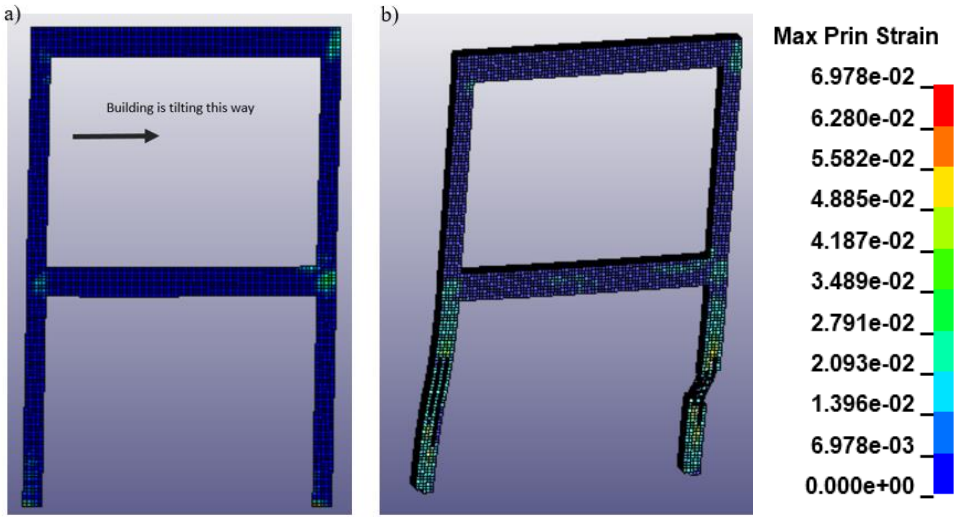

Figure 5.1 Frame (a) is captured at about 4 seconds, and frame (b) at 5 seconds

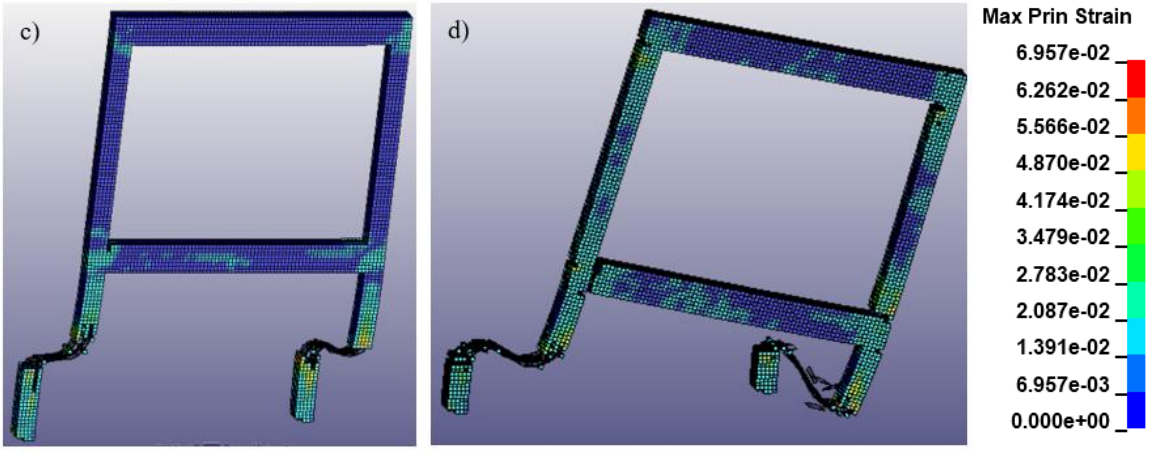

Figure 5.2 Failure of the building as a result of excessive element erosion in the columns; frame (c) at 5.9 seconds and frame (d) at 6.22 seconds

The behaviour of K&C model reflected similar erosion behaviour seen in the shaking table simulations. Push-over analysis is another method to prove that K&C with the "added" extra erosion is not very much suitable to simulate pounding.

5.1.3 Performance of CSC Model in push-over analysis

The same simulation was carried out using CSCM. Frame behaviour was very reasonable and close to the behaviour observed in the shaking table experiment. Figure 5.3 (a) and (b) demonstrate that the elements in the bases and in the connections are strained. Compared to the K&C model, at about the same time that frame (b) using CSCM (~ 6.7 seconds) was experiencing mild plastic deformation in the joints, the K&C frame had already experienced concentration of plasticity at the middle of the columns followed by excessive removal of elements. Damage distribution in the building with CSCM was much more reasonable. Base shear force against top floor displacement curves for both concrete models have been plotted and compared against the result of Garcia et al. (2010) simulation in DRAIN-3DX software (Campbell et al., 1994) and is illustrated in Figure 5.7. It is shown that the building with K&C model failed much quicker than the CSC building.

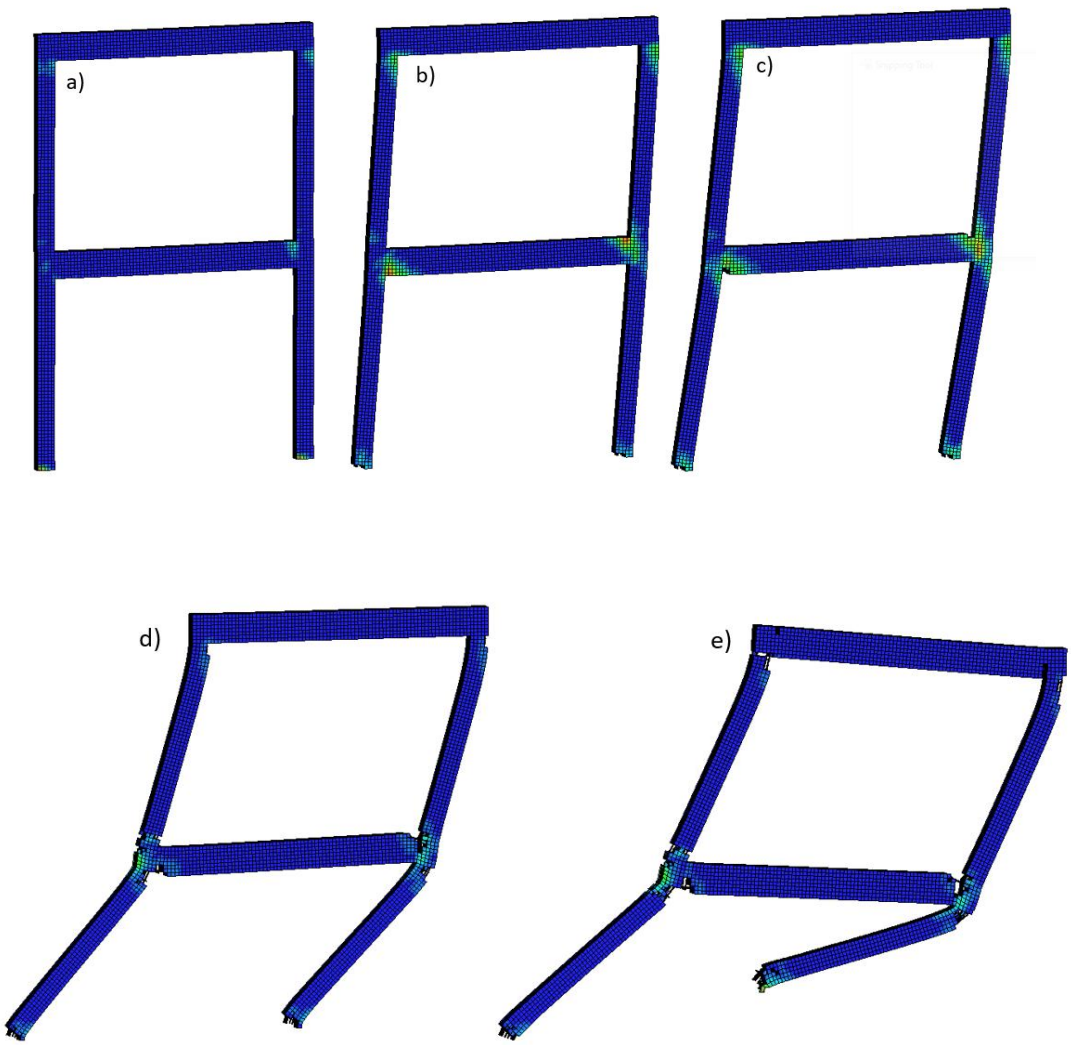

Figure 5.3 Frame (a) starts to experience plastic deformations in the connections and in the column bases at about 5.9 seconds but no element erosion at this point; frame (b) shows element erosion in the bases of the column at about 6.7 seconds and gradualy element erosion is observed in frame (c) in the connections; Frame (d) showing building collapse at 7.9 seconds, and frame (e) is captured at 8.1 seconds

The behaviour of the frame with CSC model is considered realistic because as soon as the push-over analysis started, the bases of the columns started to erode where there was maximum bending occuring. Also erosion occurred from the side of the column that was being pushed and was in tension as shown in Figure 5.4. The is the behaviour that is expected to occur in real concrete building when subject to lateral load.

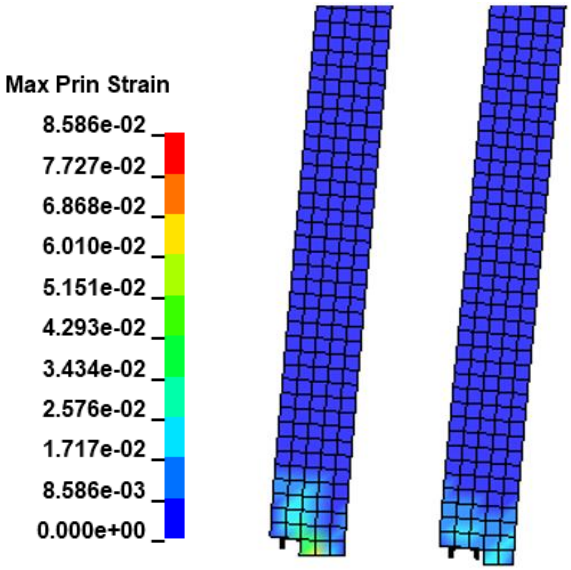

Figure 5.4 Erosion in the bases of the left and right columns

As the analysis progressed, erosion started to occur from the inner angle of the left connection and the opposite outer angle of the right connection where there was great bending moment occuring in both locations as depicted in Figure 5.5. This behaviour is reasonable and it is expected to occur in reality. Elements started to erode from the inside of the top left connection and the outside of the right connection of the second floor which is reasonable to occur in such a situation as shown in Figure 5.6.

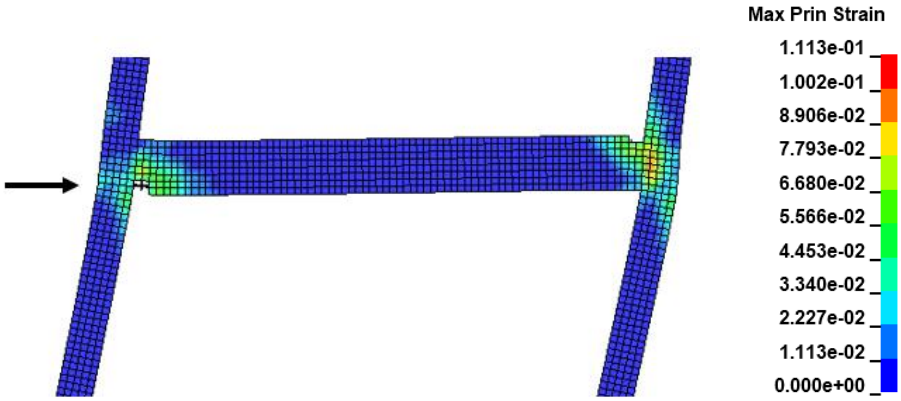

Figure 5.5 Erosion occurring inside of the left connection and outside of the right connection

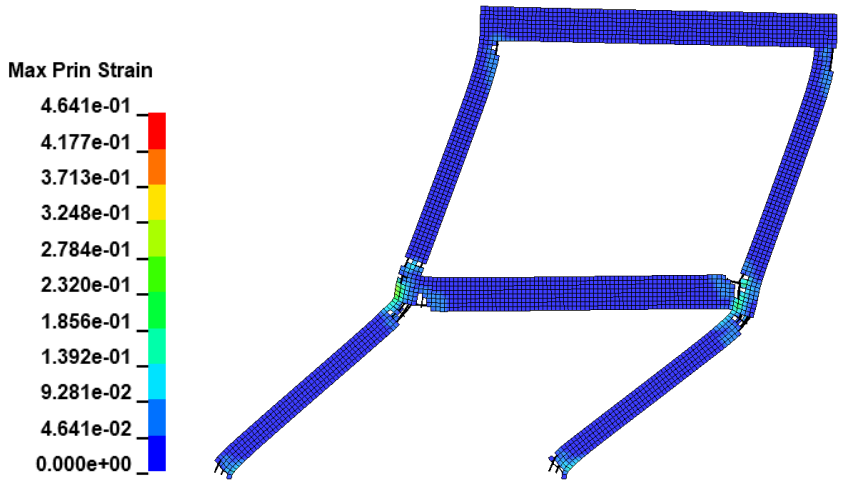

Figure 5.6 Erosion occurred in the top floor connections

Push-over results obtained from Garcia et al. (2010) experiment on the ECOLEADER building has been compared against the performances of both material models using shear force against top floor displacement as illustrated in Figure 5.7. The model with K&C behaved brittle and failed much quicker than expected compared to Garcia et al. (2010) push-over analysis results, as well as the CSC model. The shear force-displacement presented by CSCM is the behaviour expected to obtain from the push-over analysis. There is a very good correlation between CSCM results and the results of the DRAIN-3DX analysis by Garcia et al. (2010). This is another confirmation that CSCM is much more suitable to be applied in the pounding simulations of buildings.

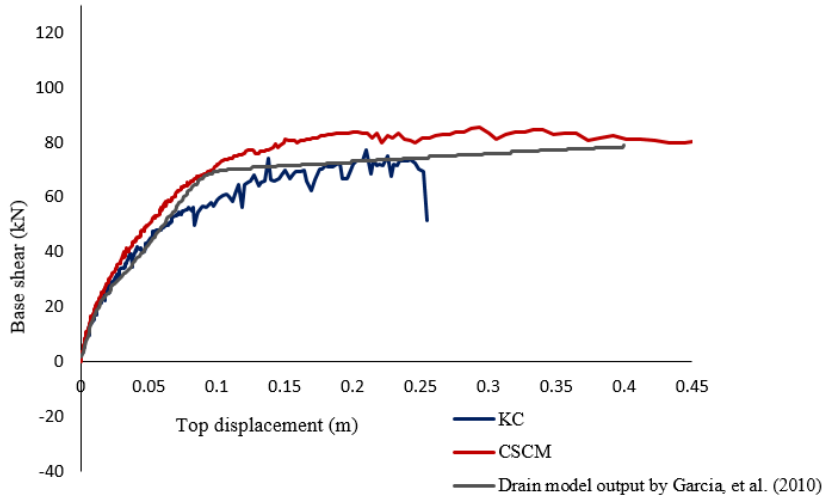

Figure 5.7 Base shear force against top floor displacement for K&C and CSC models

5.2 Summary

It has been demonstrated that erosion can overrule the capability of a concrete material model in simulating dynamic problems. In the shaking table simulation, by a large difference, K&C was unable to capture concrete spalling and crushing compared to the CSC model. Unusual erosion/excessive element removal was observed in the concrete, particularly, in the bases of the columns. Erosion pattern was not consitent and in some cases it caused the removal of too many elements. Therefore, its suitability had to be checked before including it in the pounding simulation of buildings.

Monotonic push-over analysis was conducted to specifically observe if the concrete models were capable of modeling concrete crushing/spalling by means of element erosion and if it was behaving reasonable at all. Resembling a logical concrete failure by the material models is very important in the application of pounding simulation and in general in simulating any concrete structure.

Erosion occurance in K&C model was excessive and unreasonable and led to pre-mature failure in the budiling with K&C model compared to the CSCM simulation. Performances of both material models were compared against Garcia et al. (2010) push-over analysis results that was conducted in DRAIN-3DX software (Campbell et al. 1994). It was established that CSCM demonstrated a reasonable concrete failure when subjected to lateral load. Therefore, due to the erosion uncertainties associated with K&C model and its unreasonbale performance, it is deemed unsuitable for carrying out pounding simulation of buildings in the Chapter 6 of this thesis, and it is no longer included in any further pounding analysis conducted. The numerical simulations carried out on the pounding of buildings in the next chapter are performed using only CSCM.

Chapter 6

6. FE pounding simulation of buildings

In this chapter, the outcome of the conducted experiments as well as the numerical simulations validated against these experiments in the previous chapters are incorporated into a final pounding model of buildings against each other. Two pounding scenarios are studied, (1) pounding of two equal height buildings, and (2) pounding of a shorter building's roof against the column of the same two-storey building (ECOLEADER) that was studied in Chapter 4.

Contrasting the existing contact models which idealise buildings as lumped masses, a wide range of data with small details can be extracted from anywhere on the incorporated FE model such as force-time histories, displacement/velocity/acceleration histories, measurement of contact areas on the buildings, the location of the first and subsequent contacts/impacts, the time of the contacts and their durations, as well as concrete crushing/spalling, etc. Effectively there is the lack of experimental data available on the pounding of concrete buildings, neither there is a reliable existing contact model. The existing contact models whether implemented as a link/gap element in a software or performed analytically require contact parameters such as impact stiffness, coefficient of restitution, and damping ratio to be inputted onto the model. It has been described earlier that these are subjective values with no proper reliable existing formulas to calculate them for impact of flat surfaces. The performance of the existing contact models is greatly influenced by these parameters, they can be tuned for a specific problem to match an experimental test or so, however a lot of times fail to accurately model pounding (Khatiwada and Chouw, 2014).

The incorporated FE model is intended to simulate pounding with more accuracy and it proposes the outcome of the chosen pounding scenarios to be as illustrated in the following sections. It should be noted that the purpose of this chapter is not only to observe what happens to the buildings in these scenarios but also to show that the approach developed here allows better insights into the mechanisms of structural and material responses during pounding events.

The two pounding scenarios including their geometries and reinforcement detailing studied are slab to slab pounding (see section 6.1.1) and mid-column pounding presented in section 6.1.2. In these scenarios, two heavy and light one-storey buildings were placed next to each other and the pounding responses of them were investigated. In the second scenario, the same one-storey light building was placed against a two-storey building and their impact responses were studied. The buildings in the pounding scenarios were then compared to when they are not in a pounding state and it was observed whether pounding is beneficial to these structures or more detrimental. As part of the investigation, how the frames came into contact, concrete cracking, spalling and crushing, the magnitude of their contact forces, and their contact duration along with displacement, velocity, and acceleration responses were studied and are presented in the further sections.

6.1 Pounding of buildings case studies

Two building pounding scenarios have been studied; (1) pounding of the same one-storey building against another one-storey building of the same height, (2) mid-column pounding which is the pounding of a shorter building's roof against the column of the two-storey concrete building under an earthquake at PGA level of 0.4g.

6.1.1 Slab to slab pounding case

In the slab to slab pounding case, a one-storey building was placed next to another building of the same height with a separation distance of 25 mm as shown in Figure 6.1. The height of both buildings was 3.8m to make their floors aligned and pound during seismic motion.

The reinforcement detailing of both buildings were the same as illustrated in Figure 6.1. In order for the buildings to have out of phase responses, buildings were modelled with different masses. The total weight of the building (frame 1) is 15.2 tonnes which includes an additional mass of a steel plate which weighs 6.4 tonnes added to its floor. Half of the building was modelled making the frame 7.7 tonnes in total including the mass of the plates.

The second one-storey building had a mass of 21.4 tonnes including an additional mass of 6.2 tonnes added to its floor. Half of its weight which is 10.7 tonnes in total including the weight of the steel plate is modelled in LS-DYNA. From this point onwards the lighter building (7.7 tonnes) is referred to frame 1, and the heavier building (10.7 tonnes) is referred to frame 2.

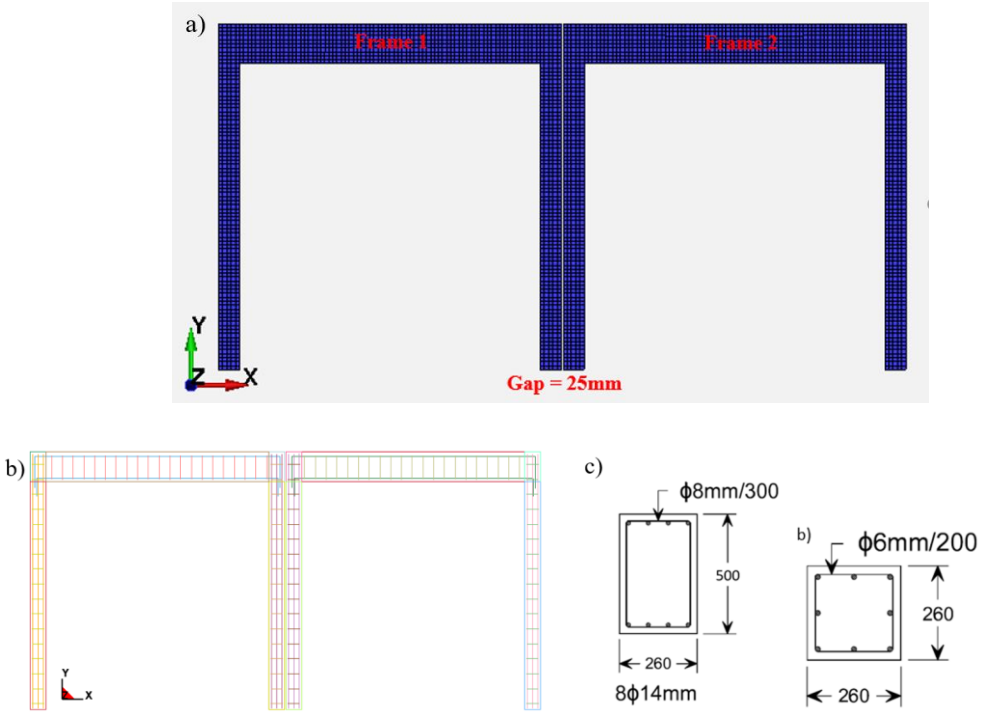

Figure 6.1 (a) geometry of two adjacent one-storey buildings with 25mm gap in between, (b) frame reinforcement constructed in LS-DYNA, (c) drawings of the reinforcement detailing (Garcia et al. 2010)

6.1.2 Mid-column pounding case

The model of the two-storey concrete building with the exact same dimensions described in Chapter 4 was placed next to the lighter one-storey concrete frame (frame 1) with a separation distance of 25mm. The one-storey concrete frame consisted of one bay and had a symmetrical shape with square area of 4.26 × 4.26 m^2 in plan with a storey height of 3.8m with a beam size of 0.26 × 0.50 m^2. Reinforcement detailing of the building is illustrated in Figure 6.2.

The model was constructed in 2D with 3D solid elements. The compressive strength of both buildings was f_c = 20 MPa with maximum aggregate size of 19mm and Young modulus E_c of 25.545 GPa as well as steel reinforcement bars with yield and ultimate strengths of 551 MPa and 656 MPa. The total mass of the two-storey building was 20 tonnes including two 9 tonnes

of steel plates that was added to each floor (mentioned previously in Chapter 4) and the mass of the one-storey building was 7.7 tonnes (frame 1).

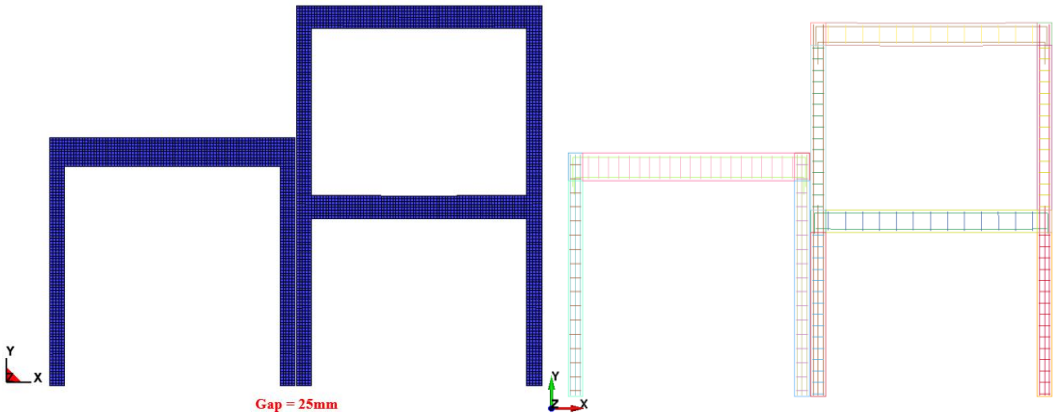

Figure 6.2 General view of the mid-column pounding case with 25mm gap in between

6.2 Material models and boundary condition

CSCM has been used to model concrete in both pounding cases studied. CSCM parameters were defined previously. Erosion value used in the pounding cases is 1.09.

6.3 Fundamental periods of the buildings

The fundamental periods of all three buildings for their first vibration modes were obtained by eigenvalue analysis in LS-DYNA and are given in Table 6.1.

Table 6.1 Periods of buildings used in the pounding case studies

Building type	Mass (Tonnes)	Structural period (s)
Weight of One-storey building (frame 1) in both pounding cases	7.7	0.26
Weight of one-storey building (frame 2) in slab to slab pounding case	10.7	0.32
Two-storey ECOLEADER building in mid-column pounding case	20	0.43

6.4 Slab to slab pounding results and discussion

The effect of pounding on the same storey height buildings was investigated and the results showed that the pounding effect for the buildings with the same height is severely damaging for both heavy and the lighter building as described further in more detail. Contact/impact between the two buildings was investigated at the location where it is marked in red circle as shown in Figure 6.3.

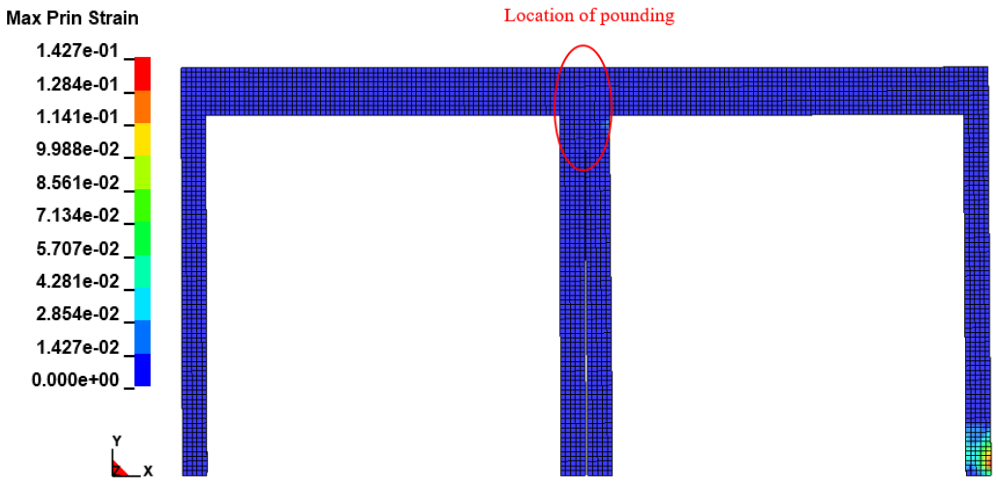

Figure 6.3 Contact/impact at slab level where it is indicated in red circle

The movements of the frames were tracked through the indicated location. Data histories provided further correspond to the face of impact at the location marked in red circle. By looking at X-coordinates of both buildings during pounding, it was observed that a total of 4 impacts occurred during 10 seconds of seismic motion between frame 1 and 2 as shown in Figure 6.4. Where two lines have crossed is an indication of impact between the slabs which is shown in black circles with pointing arrows. In Figure 6.4, the difference between the two lines on the X-axis is the initial gap between the frames which was 25 mm.

It was observed that at times the slabs came very close and barely touched the other slab but did not cause any damage in the frames, however subsequent impacts were the reason that led to progression of plastic deformation in concrete further in the frames. Concrete spalling occurred in the bases of the columns as well as the point of contact and at the far end of the slabs. Reinforcement yielding also occurred close to the point of impact. Contact force-time histories obtained are provided in Figure 6.5. The duration of the impacts on average were about 20 milliseconds.

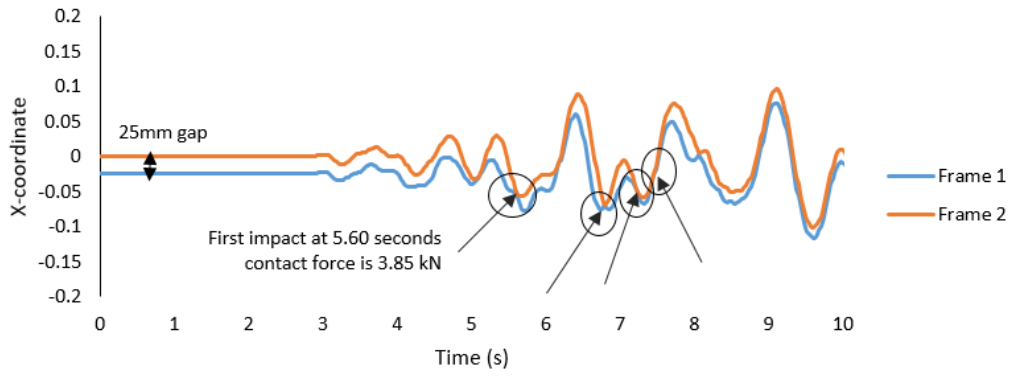

Figure 6.4 Multiple impacts between frames 1 and 2 shown on the X-coordinate-time history between the two frames

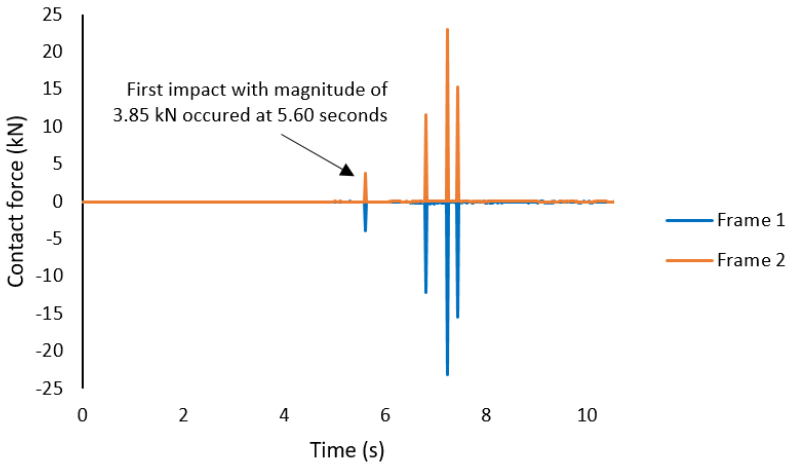

Figure 6.5 Pounding force-time history of slab-to-slab impact

The first time the frames came together occurred at 5.08 seconds which was a soft impact where the two frames only touched. At 5.60 second, an impact occurred over a contact surface area of 650mm between the buildings which led to concrete cracking in the base of the column of the second frame. Impacts occurred at 6.8, 7.22 and 7.42 seconds resulted in developing more plastic deformations in the frames and the slabs of both frames experienced severe damage as shown in Figure 6.6. The largest contact force at that location had a magnitude of 23 kN and occurred at 7.22 seconds as shown in Figure 6.5.

A great advantage of the detailed FE modelling developed in this thesis compared to the existing pounding simulation methods is that number of impacts and their intensities anywhere on the model can be identified and there is no need to pre-locate gap contact elements and

study the building behaviour only through those contact elements. These advantages over the existing pounding models provide researchers with greater insight onto modelling impact between different types of buildings in different scenarios. It also assists in investigating pounding mechanism and understanding the phenomena better including where concrete spalling/crushing and reinforcement yielding initiate in the buildings and how it propagates through the buildings and cause more damage elsewhere.

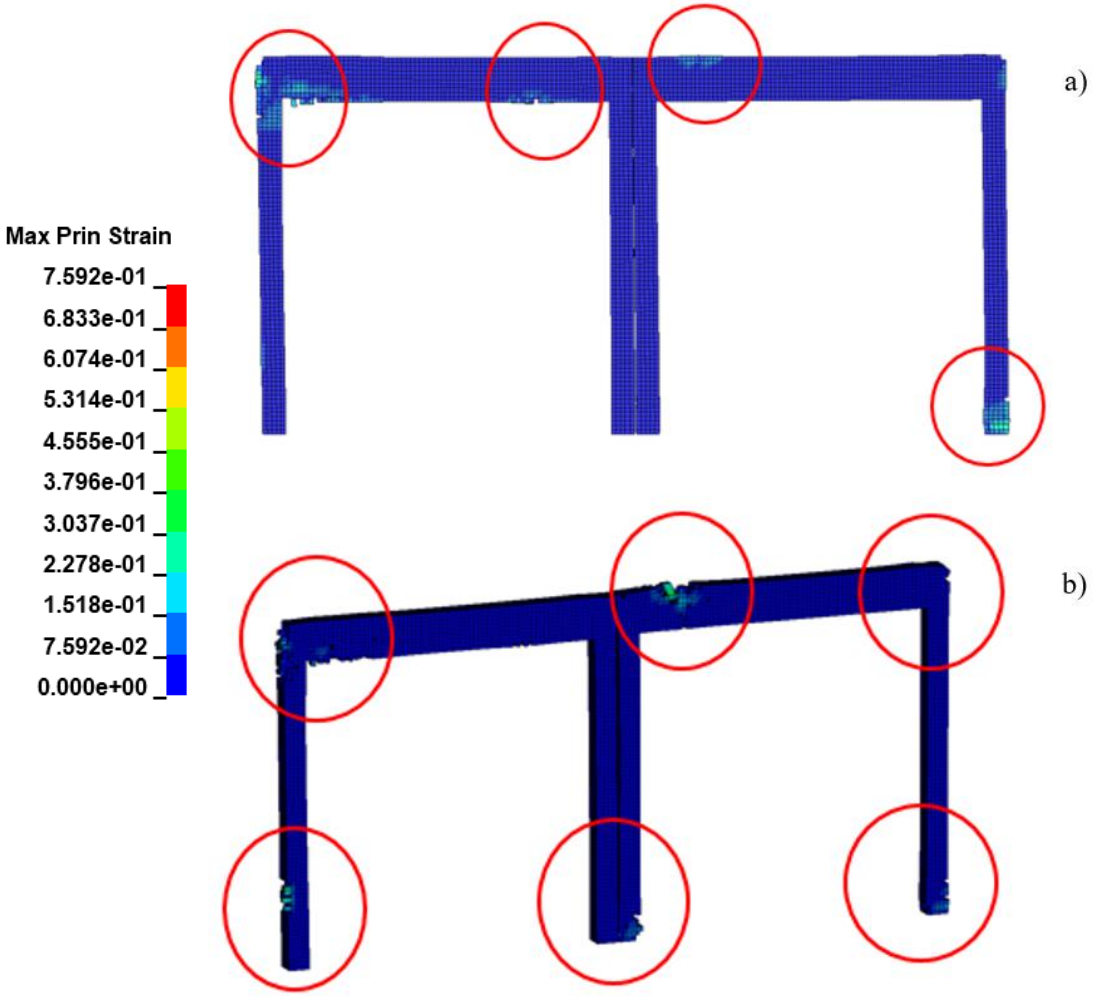

Figure 6.6 (a) Impact of buildings at 7.22 seconds, (b) progressive plastic deformation as a result of second impact at 7.42 seconds and the subsequent impact

6.4.1 No-pounding state of frame 1 and frame 2

Each one of the frames 1 and 2 were subjected to earthquake individually in a no-pounding situation to observe where damage occurs when they shake alone and to find out if the pounding was detrimental to the frames or in fact the building benefited from pounding by restricting its movement. Frame 1 in no-pounding case experienced cracking in the bases and

upper parts of its columns as shown in Figure 6.7 at 7.22 seconds. The time at 7.22 seconds is the time where both frames experienced concrete crushing during pounding which was also shown in Figure 6.5 and Figure 6.6. Individual frames did not experience concrete crushing during the 10 seconds of earthquake. However, when the frames were put against each other to pound, none of them experienced concrete cracking that is shown in Figure 6.7 until the first impact at 5.60 seconds where minor cracked appeared in the right column of the heavier building (frame 2). Pounding of frame 1 against frame 2 restricted both of their movements and stopped concrete cracking for a few seconds, however after the second impact (6.8 seconds), concrete spalling started to develop in the frames. Red mesh elements in Figure 6.7 are indicators of plastic changes in concrete (cracking mainly).

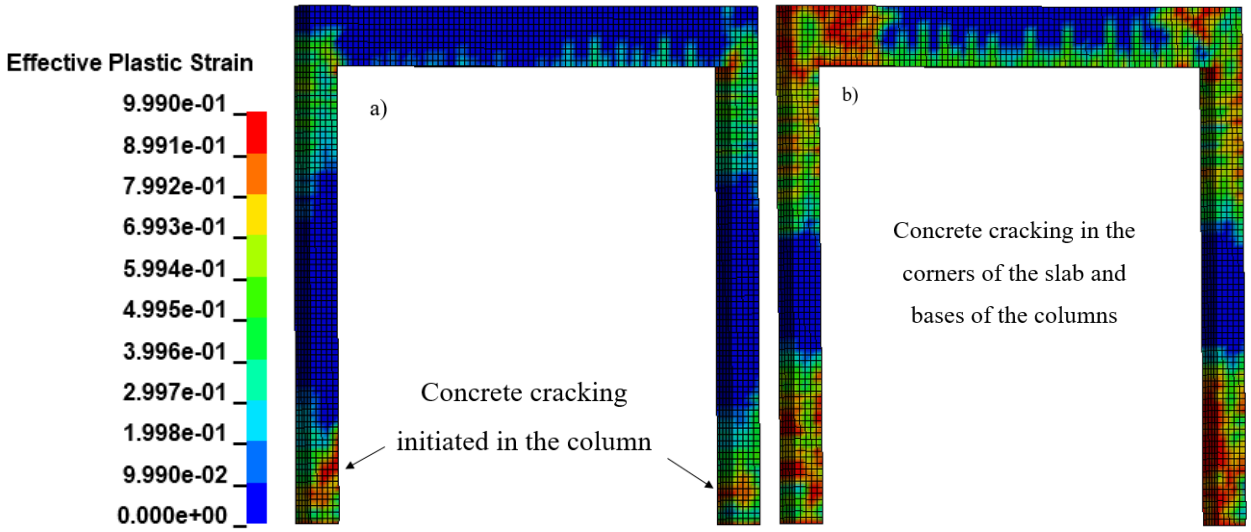

Figure 6.7 (a) Frame 1 (lighter frame) concrete cracking in the columns at 7.22 seconds shown in red colour, (b) frame 2 (heavier frame) concrete cracking in the corners and the bases of the frame at 7.22 seconds in a no-pounding case

6.4.2 The effect of pounding on the displacement response of the buildings

Displacement-time histories of both heavy and the lighter frames are illustrated in Figure 6.8 and Figure 6.9. The peak displacement history of the heavier frame (frame 2) in the pounding case was 0.132 m. However, it is 0.140m for the no-pounding case indicating pounding restricted the movement of the frame 2 and benefited the frame by stopping the development of concrete cracking that occurred in the frame in the no-pounding case.

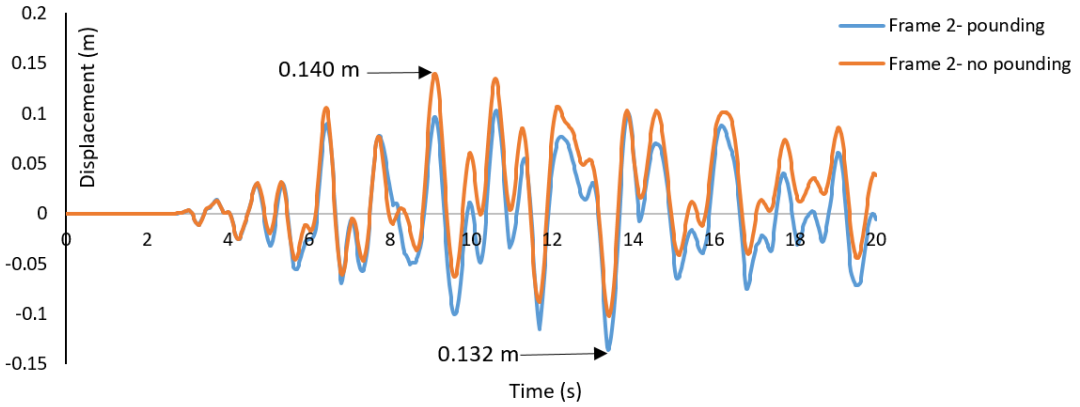

Figure 6.8 Displacement-time response of frame 2 (heavy frame) with and without pounding

On the other hand, for the lighter frame, pounding amplified the displacement response of the frame. Comparing the pounding case with the no-pounding case, the displacement response was increased by 0.044m (4.4cm).

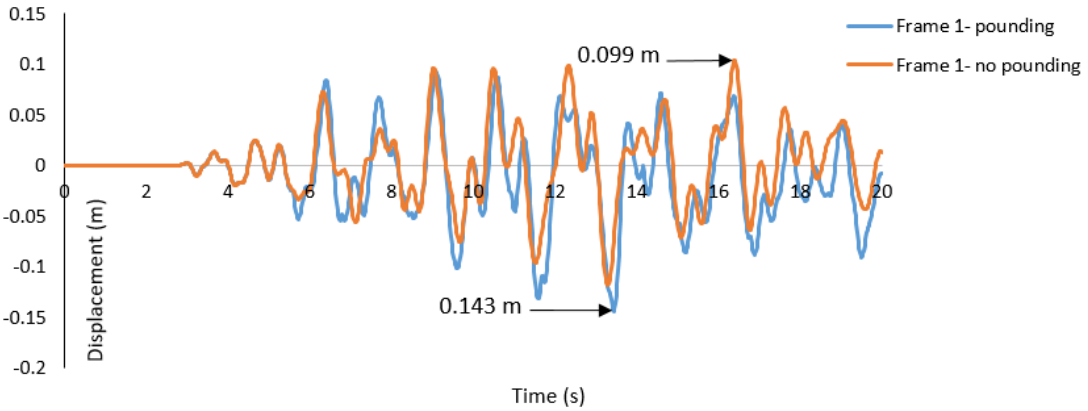

Figure 6.9 Displacement-time response of frame 1 (lighter frame) with and without pounding

6.4.3 Impact velocity

The impact velocities for the times of contacts between the frames are provided in Table 6.2 (for a short period of time every time the frames came into contact, their velocities became very similar as they were stuck together moving in the same direction). The table shows that the impact velocities are small. In a no-pounding situation, the maximum velocity of the frame 1 (lighter frame) is about 0.66 m/s and the frame 2 velocity is about 0.75 m/s. In the pounding case (not necessarily while the buildings came into contact as the impact velocities were

variant throughout the earthquake), the maximum velocity of frame 1 was about 0.93 m/s and frame 2 was 0.84 m/s which are still very low.

Table 6.2 Impact velocities of pounding frames

Number of impacts	Time of impact (s)	Impact velocity (m/s)
First impact	5.60	0.23
Second impact	6.80	0.22
Third impact	7.22	0.33
Fourth impact	7.42	0.38

6.4.4 The effect of pounding on the acceleration response of the buildings

Longitudinal acceleration-time histories of frames 1 and 2 in pounding and no pounding conditions have been compared and illustrated in Figure 6.10 and Figure 6.11. Peak acceleration in the pounding case for frame 1 which is the lighter frame is 2440 m/s^2 and frame 2 is 2150 m/s^2. Acceleration of frame 1 is significantly amplified as a result of pounding compared to the no-pounding situation. In a no-pounding state, the maximum acceleration is 747 m/s^2 as seen in Figure 6.10.

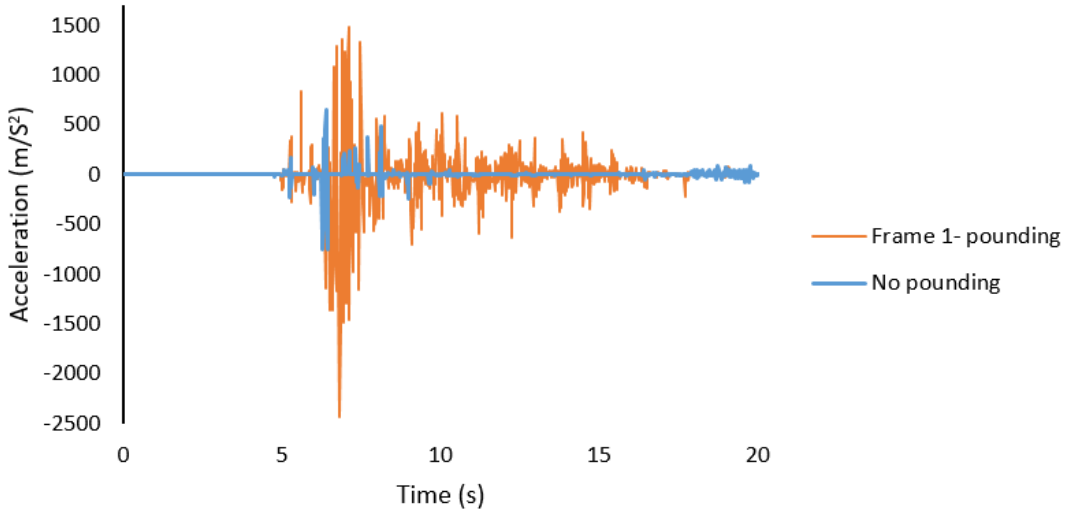

Figure 6.10 Comparison of acceleration-time histories of frame 1 in pounding and no pounding conditions

In frame 2, the maximum acceleration is 337 m/s^2 in a no-pounding state, however it goes up to 2150 m/s^2 during pounding. From the comparison of frames' responses, it is anticipated that

pounding has induced the acceleration response of the lighter building (frame 1) as shown in Figure 6.11. Figure 6.12 illustrates a comparison between accelerations of both buildings during pounding indicating frame 1 to be more influenced for a longer period of time by pounding.

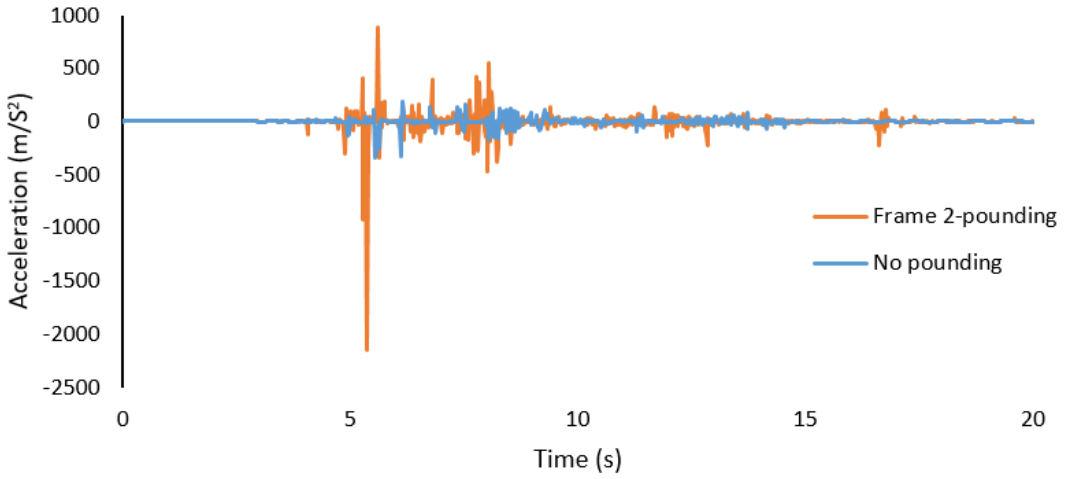

Figure 6.11 Comparison of acceleration-time histories of frame 2 in pounding and no pounding conditions

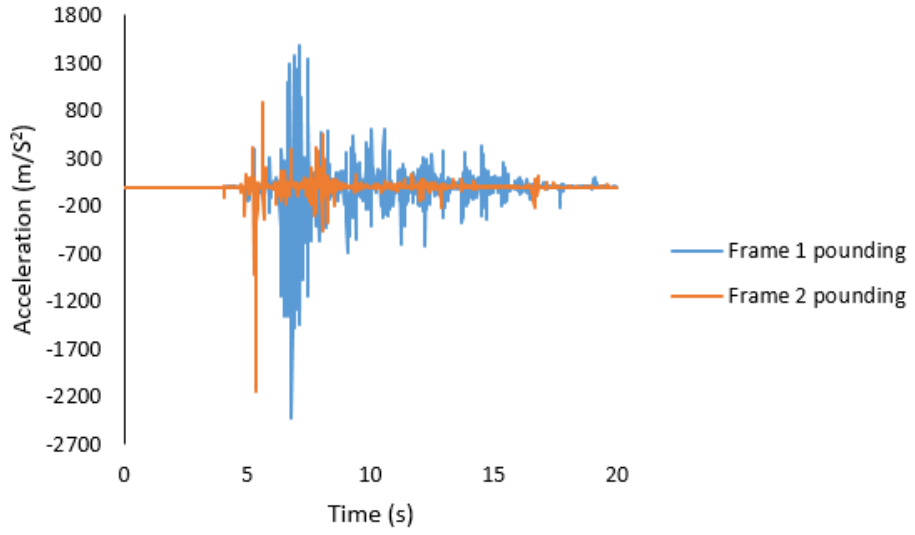

Figure 6.12 Comparison of acceleration-time histories of frame 1 and 2

6.5 Mid-column pounding results and discussion

The influence of pounding on two buildings with different heights was studied and the results demonstrated that pounding was catastrophic for the taller building. In this situation, the slab of the one-storey building (frame 1 from the slab to slab pounding case) collided against the column of the two-storey building (ECOLEADER building from Chapter 4) which is commonly referred to as mid-column pounding as shown in Figure 6.13.

Impact occurs at 4.77 seconds, between the two-storey building's second floor column and – column-beam connection, and the beam-column connection of the one-storey building as shown in Figure 6.13. Contact area is measured as 1.3m between the buildings. In the case of slab-to-slab pounding, the contact area was smaller (0.65m) because the slabs were at the same height and were aligned. However, in mid-column pounding, more area on the adjacent parts of the buildings can come in to contact.

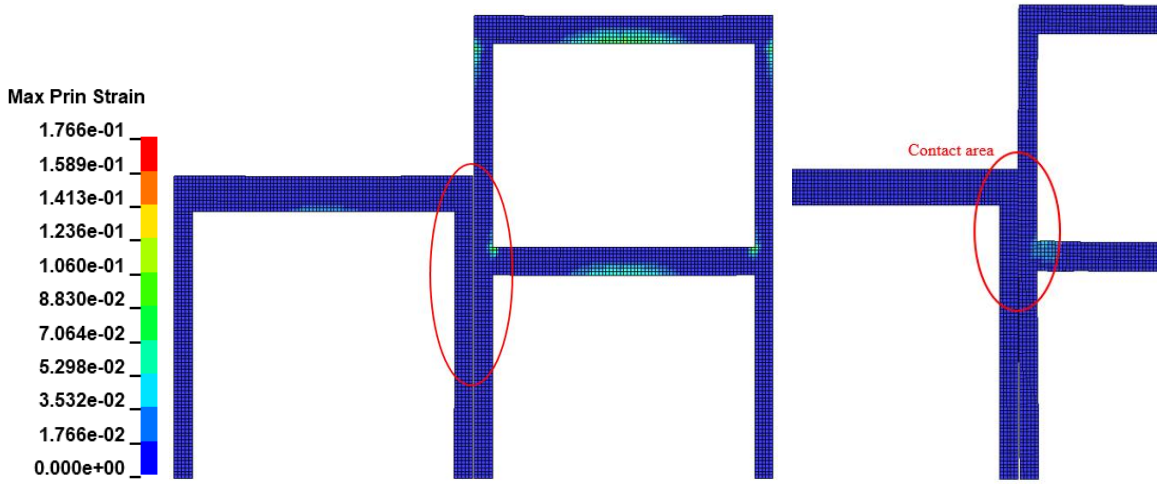

Figure 6.13 The first contact occurred at 4.46 seconds covering a large area between the connections of both buildings

Contrary to slab-to-slab pounding case where the impact duration between the two buildings was short because after the impact they quickly bounced back, in the mid-column pounding case, the buildings stay in contact for a longer period and continue to push each other. Mainly the one-storey building continued to push the two-storey building and caused crushing in the connections. The duration of the first contact that caused plastic deformation between the buildings was 1.28 seconds. It is observed that the more the buildings stay in contact the more plastic deformation develops locally within the contact area. However, in the slab-to-slab pounding, plastic deformation rather occurred elsewhere in the buildings particularly initially

in the bases of the columns. Failure in the mid-column pounding is more local whereas in the slab to slab pounding it was more global.

A critical location on both buildings have been chosen to investigate pounding further and compare the behaviour with the no-pounding case as illustrated in Figure 6.14. Data presented further are obtained through this location.

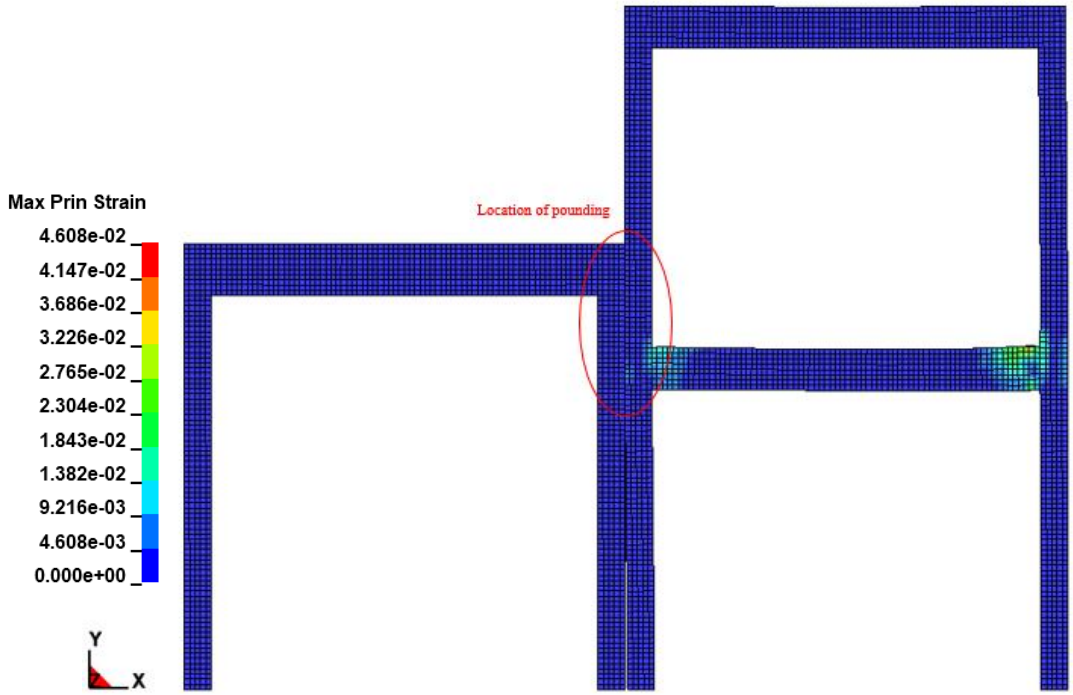

Figure 6.14 Contact between the buildings is investigated at the location marked in red circle at 4.29 seconds

Frequent impacts occurred between the buildings at the location shown in red circle, some over 10 milliseconds and some as long as 880 milliseconds. The highest impact force magnitude obtained was 50 kN at 6.82 seconds with a time duration of 140 millisecond as shown in Figure 6.15. The intensity of the contact forces are as double greater compared to the slab to slab pounding case. Figure 6.16 illustrates concrete cracking and spalling and ultimately connection failure at 6.82 seconds when pounding force was at its maximum ~ 50 kN. The strain rate for both buildings was within the range of 0.06-0.1 S^{-1}.

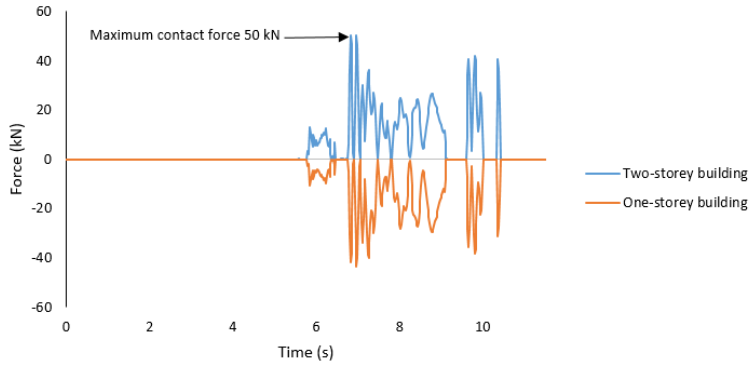

Figure 6.15 Contact force-time histories of the two-storey and one-storey buildings during collision

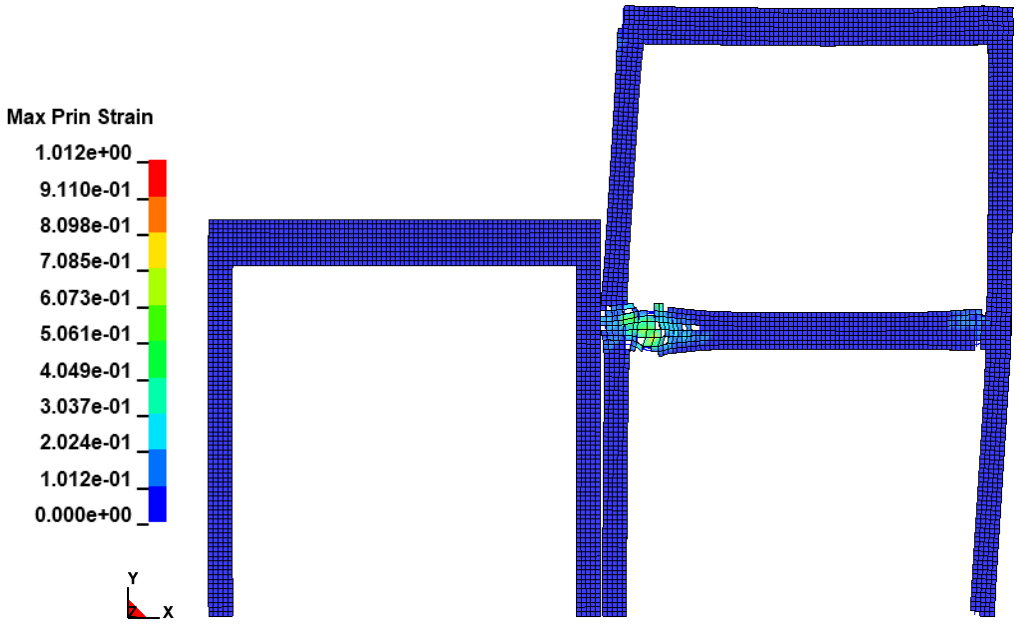

Figure 6.16 Beam-column connection failure of the two-storey building as a result of pounding force of 50 kN at 6.82 seconds

6.5.1 No-pounding condition of the buildings

As mentioned before, the one-storey building in the mid-column pounding simulation is the same as frame 1 investigated in the slab to slab pounding case. One-storey building's behaviour in no-pounding condition was described in section 6.4.1. As shown in Figure 6.17, frame 1 experienced cracking and plastic deformation when subjected to seismic motion

alone, however, pounding restricted the frame's movement that led to minimising concrete cracking greatly, therefore pounding was favourable to the one-storey building.

On the other hand, the two-storey building experienced concrete cracking/spalling in the connections as well as in the columns' bases when it was shaking alone as depicted in Figure 6.18. Pounding aggravated the response of the building and it led to connection failure and building instability indicating mid-column pounding to be very catasrophic for the taller building.

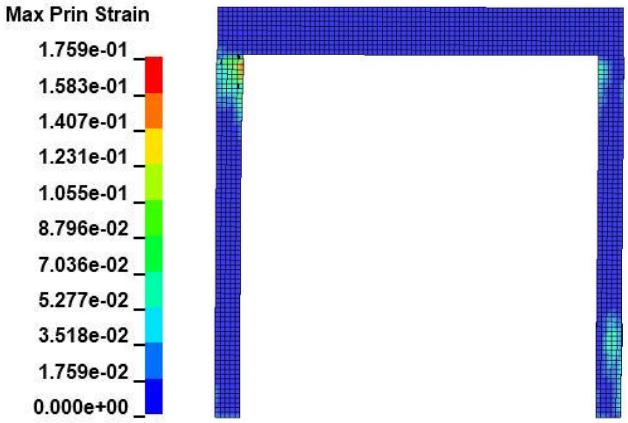

Figure 6.17 One-storey building in no-pounding state

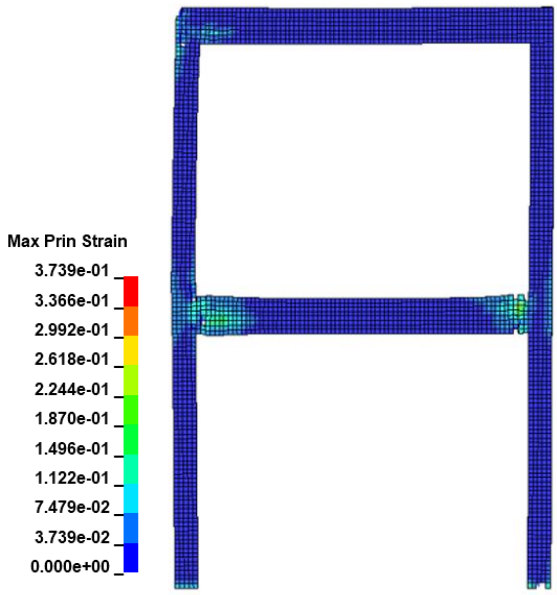

Figure 6.18 Dynamic response of the two-storey building in no-pounding state

6.5.2 The influence of pounding on the displacement response of the buildings

Displacement-time histories of the two-storey building obtained from the location of impact on the connection is depicted in Figure 6.19. As shown in the figure, the peak displacement of the building in a no-pounding position is 0.087m. However, pounding exacerbates the displacement response of the building and amplified it to 0.14m.

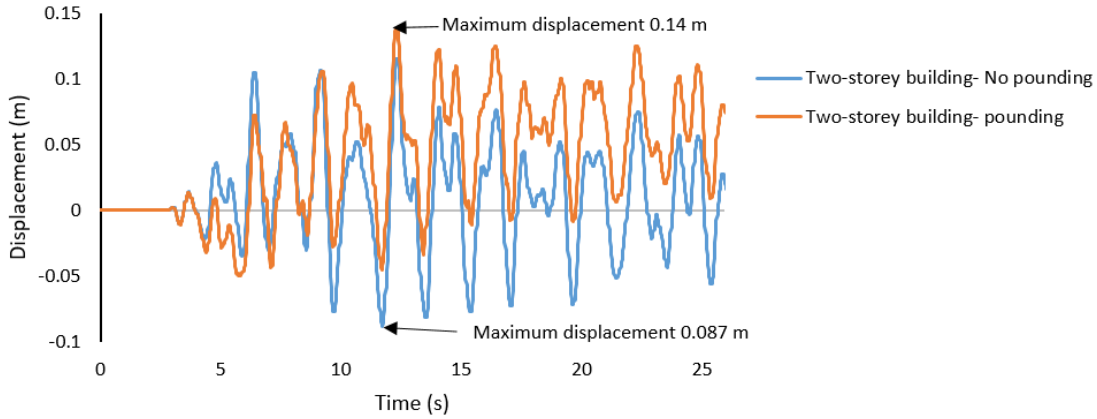

Figure 6.19 Comparison of pounding with no-pounding displacement-time histories of the two-storey building

The displacement response of the one-storey building (frame 1) in pounding compared to no-pounding state is illustrated in Figure 6.20. Maximum displacement of the building is 0.099m in no pounding state, whereas during pounding it is 0.138m.

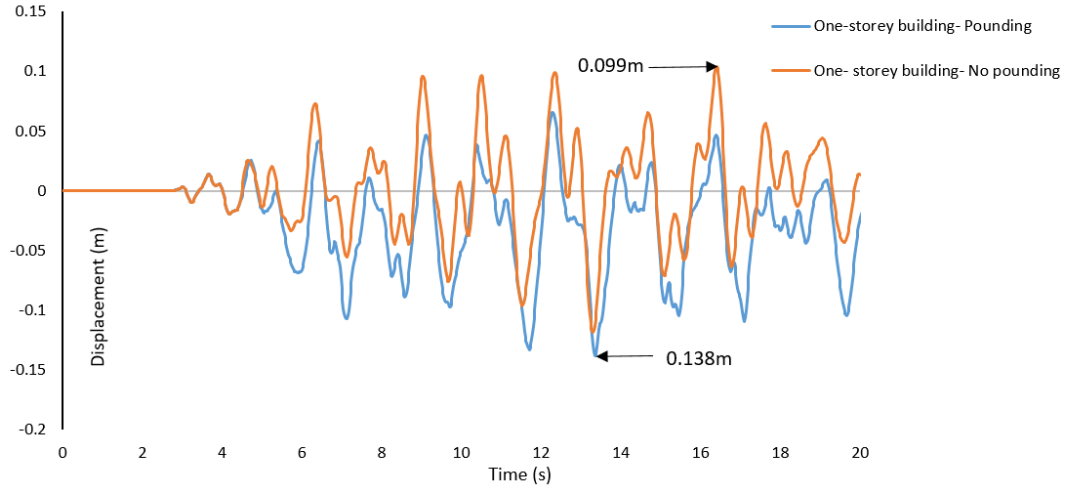

Figure 6.20 Comparison of pounding with no-pounding displacement histories of the one-storey building

Despite pounding amplifying the response of the one-storey building, it did not cause concrete crushing; albeit minor cracking was detected in the frame however it was not detrimental for the lighter building. This shows that the displacement response of the buildings is not always necessarily an indication of detrimental plastic deformations in the buildings.

Comparing Figure 6.20 with Figure 6.9 demonstrates that the one storey building was displaced similarly during both pounding case scenarios. However, in the case of slab to slab pounding, frame experienced plastic changes including concrete cracking and some crushing particulary at the beam-column connection as depicted in Figure 6.21(a), but it did not undego any major cracking in the mid-column pounding event as shown in Figure 6.21(b).

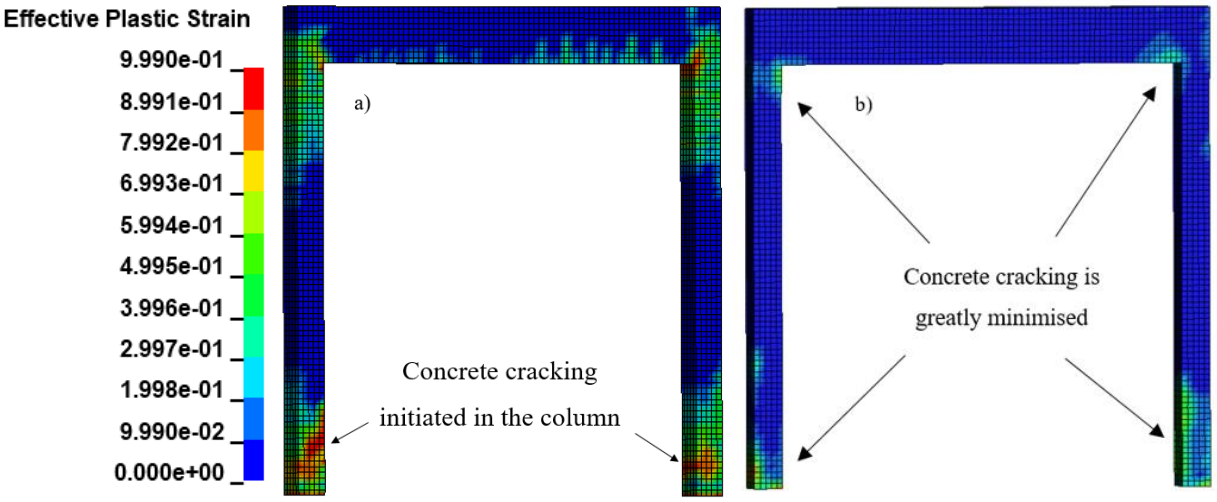

Figure 6.21 (a) one-storey building response to slab to slab pounding, compared to, (b) its response in mid-column pounding

6.5.3 Pounding velocity

Comparison of the impact velocity for both buildings is depicted in Figure 6.22. The maximum velocity of the two-storey building is 0.51 m/s during pounding and 1.11 m/s for the one-storey building during earthquakes at PGA level of 0.4g.

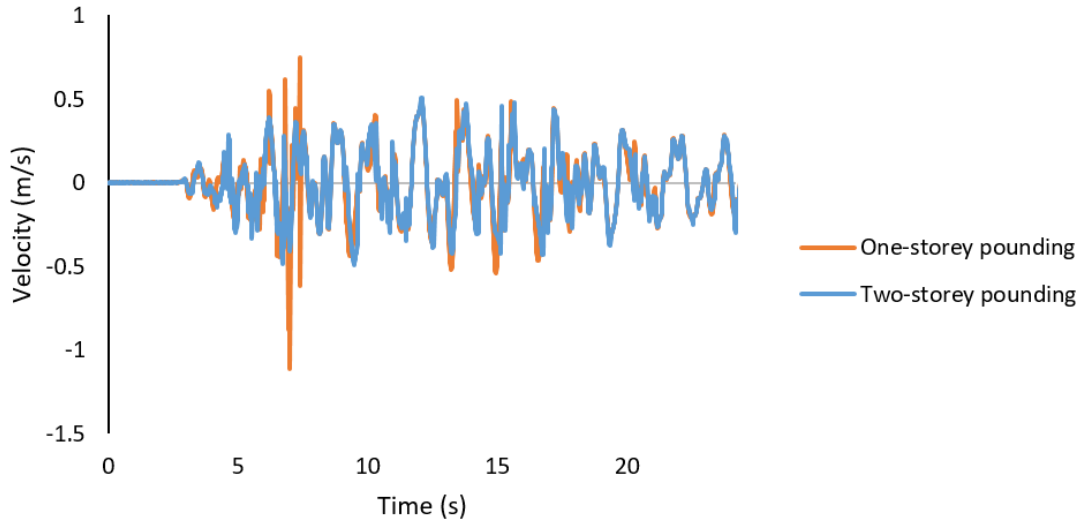

Figure 6.22 Comparison of one-storey and two-storey buildings velocities during pounding

The impact velocity of the one-storey building in the slab to slab pounding was 0.93 m/s which is not much different compared to the mid-column pounding.

The velocity of the one-storey building under seismic motion in a no pounding condition is 0.66 m/s while in pounding it increased by 41% as shown in Figure 6.23. The two-storey building before pounding had a velocity of 0.58 m/s, however velocity reduced to 0.48 m/s as a result of pounding as illustrated in Figure 6.24.

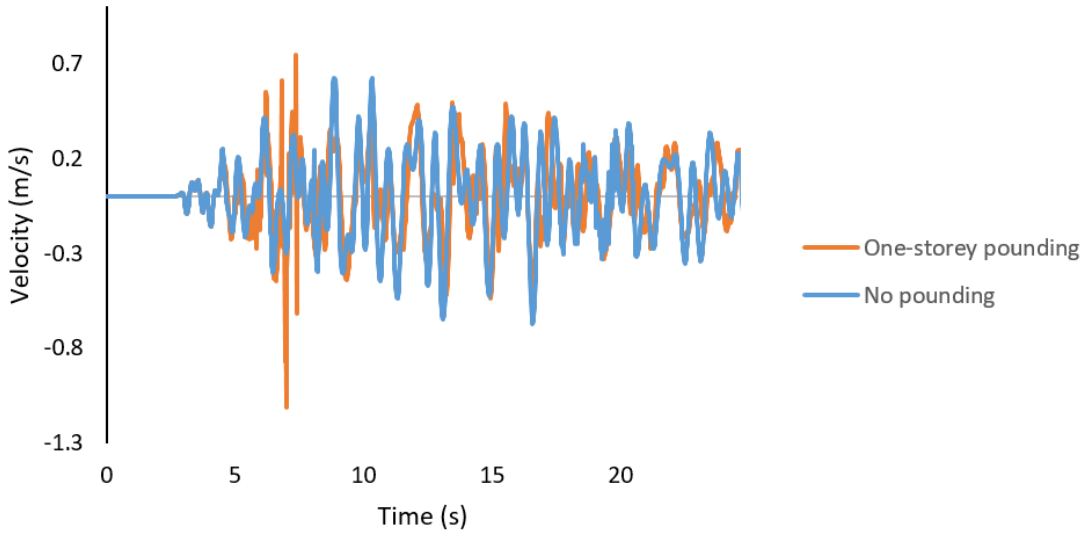

Figure 6.23 One-storey pounding velocity versus no pounding

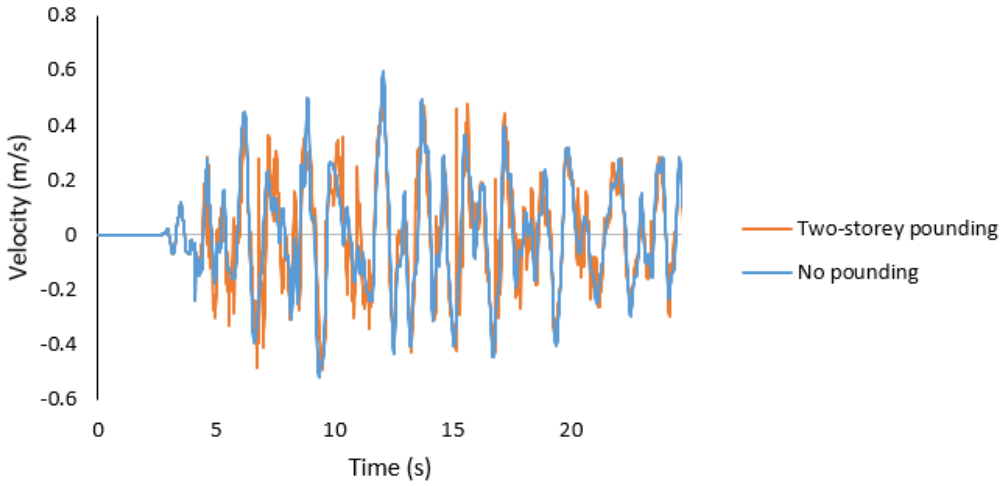

Figure 6.24 Two-storey building velocity versus no pounding

It is apparent that impact velocity range is quite low in the pounding of actual buildings under earthquake motion and one building impact velocity is not greatly influenced by the shape and type of the opposite colliding building. In pounding of buildings, impact velocity is not a representative of how much plastic deformation the building experiences; many factors are involved such as buildings masses, geometries, structural materials, etc. Building response is more dominated by the location of impact between two buildings. If it is impacted at a vulnerable or weak location, the consequences can be disastrous.

6.5.4 Acceleration responses of the buildings in the presence and in the absence of pounding

Longitudinal acceleration-time history of the one-storey building in pounding is compared against the response of the building in the absence of pounding. Acceleration of the one-storey building is 12700 m/s^2 and during pounding it increased to 129000 m/s^2 at the contact location as illustrated in Figure 6.25. In the slab to slab pounding, the acceleration of the one-storey building is 2440 m/s^2 which is much smaller than the accelertaion of 129000 m/s^2 which the building achieved in mid-column pounding event.

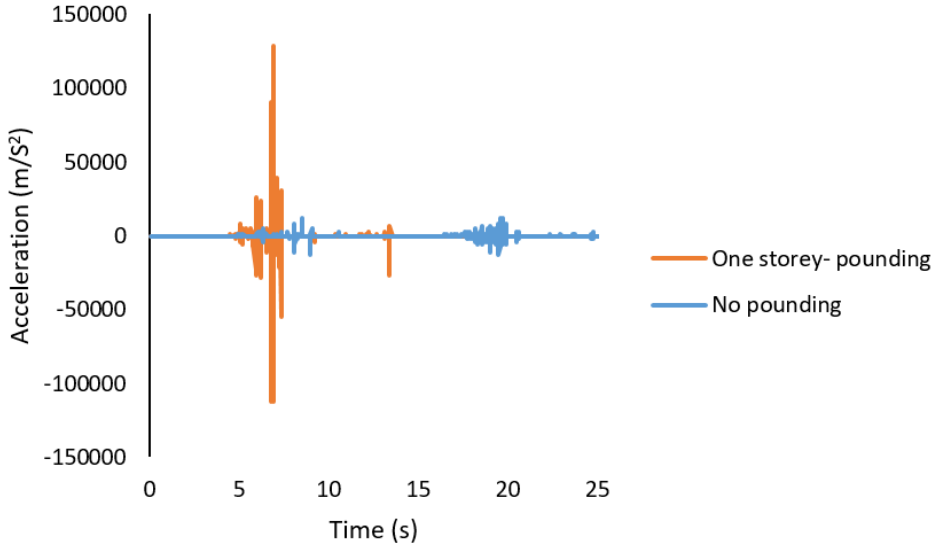

Figure 6.25 comparison of one-storey pounding against no pounding condition in mid-column pounding event

The two-storey building acceleration in no pounding scenario was 541 m/s^2 and during pounding it nearly doubled to 1100 m/s^2 as shown in Figure 6.26. Whilst pounding increased the one-storey building's acceleration by 10 times in mid-column pounding case, it only amplified its response by 3.3 times in the slab to slab pounding. Overall, comparing the acceleration-time history of the one-storey building at mid-column pounding against its response in the slab to slab pounding shows that the one-storey building's acceleration is greatly amplified in both cases. It is also significantly more influenced by pounding compared to the two-storey building's acceleration in mid-column pounding scenario as shown in Figure 6.27.

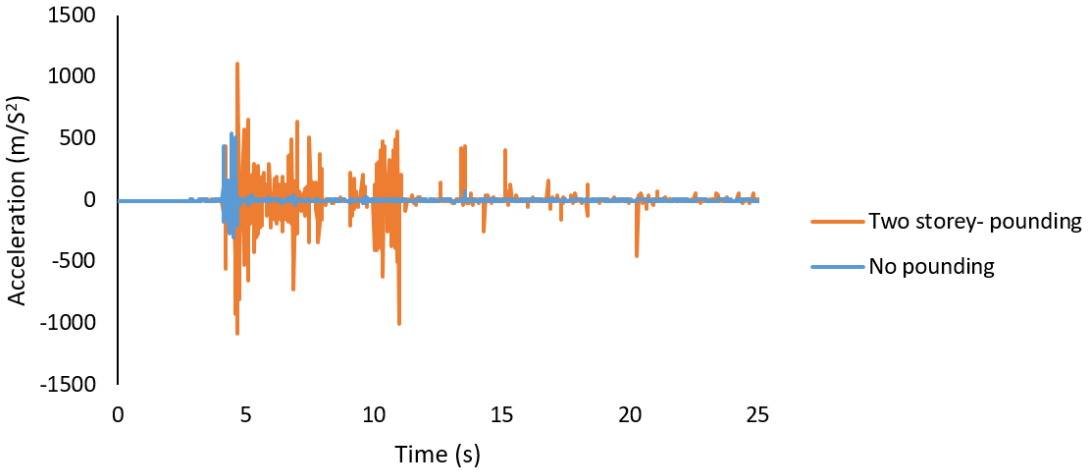

Figure 6.26 acceleration-time histories of the two-storey building in pounding against no pounding

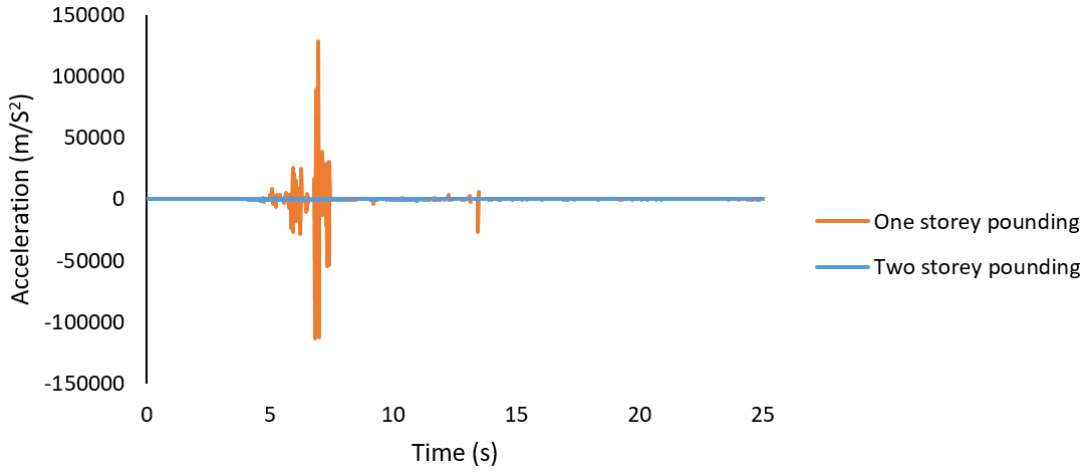

Figure 6.27 comparison of the acceleration-time responses of the one-storey and two-storey buildings in pounding

6.6 Summary

A method was developed to simulate pounding between buildings using FEM in this thesis that combined experimental work with numerical simulations that were validated against the experiments. All findings were incorporated into a final FE model that is the outcome of the new approach taken to simulate pounding with more accuracy and to overcome the uncertainties associated with the existing pounding modelling methods and their choice of contact parameters. In this method the concrete material model used has proven satisfactory in resembling reasonable concrete behaviour in pounding simulation. The new approach is capable of resembling concrete spalling and crushing and it is a tool that can be used to investigate pounding between buildings with flat surface geometries.

Contrary to lumped mass contact models, the FE model is very detail and can provide more insights onto pounding mechanisms. To demonstrate the capability of the incorporated FE model in producing small details to study pounding, two models, (1) slab to slab pounding, (2) mid-column pounding were studied. The main purpose was to show how the incorporated FE model simulates pounding. In these scenarios studied, the capability of the incorporated FE model to produce detail data is well demonstrated.

The most prominent capability is the model independency to assume contact parameters in advance. The incorporated FE model provides a way to investigate the complex phenomenon of pounding despite the geometry of the colliding buildings as it can be applied to model any type of building.

The incorporated FE model can assist in determining contact parameters such as contact stiffness and the coefficient of restitution that were the dominant reasons for diverse results obtained from the existing contact models. It can also potentially help in the development of new simplified contact models which could represent pounding between buildings without the need of using computationally expensive methods.

Chapter 7

7. Summary and conclusions

7.1 Summary

The principal aim of this work is to develop a methodology suitable for pounding simulation of buildings. The method has to simulate building pounding with more accuracy by overcoming the uncertainties associated with the existing contact models.

Chapter 2 provided a review of the current research, as well as background information on available methods of structural pounding, uncertainties and disadvantages of the current methods available in building pounding. It reported conducted experimental works as well as the application of analytical and numerical methods in modelling pounding including the available material models used in several commercial software to model building materials. It has been shown that there is currently lack of an acceptable formula to determine contact parameters and the only formula to calculate contact stiffness (K) is derived by Hertz (Goldsmith, 1960) for impact of two spherical surfaces, or a spherical and a flat surface. This is the main reason for limiting the accuracy of the analytical models making them unsuitable for the application of modelling pounding. Hence, a new method is developed and verified with experiments for application in pounding simulation of buildings that no longer suffers the uncertainties and disadvantages of the current methods.

After identifying a gap in the current literature, a methodology using the FEM is developed step by step to simulate impact between buildings starting from Chapter 3 by conducting a set of direct HPB experimental tests on the impacts of concrete to concrete, concrete to steel, and steel to steel specimens. The investigation started at basic material level and it progressed to a more complex situation at structural level. As part of chapter 3, numerical simulations

replicating the direct HPB tests were carried out in LS-DYNA and were validated against the experiments using two concrete material models of CSCM (MAT_159) and K&C (MAT_72R3). A wide range of velocities were considered in the direct HPB tests and its numerical simulations. The validated simulations at material level with variable impact velocities were then used in Chapter 4 to investigate shaking table simulations to study the dynamic response of a two-storey building in seismic motions. The FE shaking table simulations were validated against shaking table experiments conducted by Garcia et al. (2010) to observe the material models' performances at structural level. At this stage, four sets of numerical simulations had been validated against the experiments: (1) direct HPB with CSCM, (2) direct HPB with K&C, (3) shaking table with CSCM, (4) shaking table with K&C. The competency of each material model was reviewed and their capabilities in resembling concrete cracking/crushing was examined. CSCM has an implemented erosion algorithm and K&C requires an external erosion command to replicate concrete failure. K&C erosion algorithm disadvantages its powerful capability as erosion occurred at unexpected locations or in an unpredicted patterns e.g in the centre axis of a column. As a last resort to find out if both/or either of the material models is capable of resembling concrete failure in pounding simulations, push-over analysis was carried out on the same two-storey building. Similarly, K&C either did not behave reasonable at this stage because of (1) excessive erosion occurred in the mid-height of the columns which was far from reality and unexpected, and (2) pre-mature failure happened before the building reached its full capacity because of the excessive element erosion. Therefore, pounding simulations were carried out using the CSC model.

All findings in the previous chapters were gathered and incorporated into a final FE model of pounding. Simulation of pounding was carried out between (1) two buildings of the same height (one storey, one bay), as well as pounding of a one-storey building against the two-storey building validated in Chapters 4 and 5. The incorporated FE model has many advantages which the most notable one is that it no longer requires the assumption of contact parameters. The incorporated FE model developed in this thesis should be used to study the complex nature of building pounding, as well as impact between flat surfaces of buildings made of any geometry, as one of the limitations of the existing contact models is the lack of robust formula for impact of flat surfaces. The numerical simulation developed within this PhD has the potential to assist in determining contact parameters rather than assuming them. For example, it could be used as a source to calculate the contact stiffness and the coefficient of restitution. The contact parameters can then be used in the existing commercial software e.g OpenSees, Sap2000 that still use gap friction elements to model structural pounding, or it can be implemented in the existing analytical models to re-assess their performances or help in developing a new simplified contact model.

7.2 Conclusions

To this date large number of studies were conducted on the analytical force-based contact models, starting from stereomechanics model to the application of gap friction elements in commercial software. Khatiwada and Chouw (2014) published a critical review of current literature in the field of pounding and stated that the results were enormously depending on the coefficient of restitution and attempts to identify suitable contact parameters such as contact stiffness; damping and the coefficient of restitution have resulted in conflicting outcome.

The limitation of the existing models led to developing a method to model impact/pounding between buildings using FEM that employs a penalty-based method. The model no longer requires the assumption of contact parameters; however, the workability of such model lies within a choice of good material model for pounding simulation. To examine the performance of the chosen material model, understanding concrete behaviour at material level is very important in the pounding of buildings as local concrete crushing is very common in pounding events. Consequently, understanding the dynamic response of buildings at structural level is another important component of this investigation. As it is the dynamic response of the buildings that make them to have out of phase responses and collide.

Ultimately, the combination of these two have led to the development of the incorporated FE model that can simulate building pounding with more accuracy/advantages over the existing methods. The following conclusions are drawn from this research:

- Direct HPB tests was used to investigate the concrete behaviour for the validation of the concrete material model and the modelling approach, and it showed that the concrete material models are capable of resembling the behaviour seen in the tests including concrete damage
- During direct HPB tests, perfect alignment between colliding specimens was impossible to achieve. The shape of the stress pulses was also influenced by the presence of aggregates in the surfaces of the specimens.
- Stress is found to be higher in shorter specimens due to the plastic work being extended over the length of the shorter specimen resulting in a stiff impact which strained the specimen and drove the stress pulses up. Contrary to the shorter specimens' impacts, for longer specimens the plastic work was mostly being extended over the front side of the specimen which resulted in slowing down the transfer of the energy waves through the specimen, therefore it took longer for the full event to be over.

- Mesh regularisation algorithm implemented in the concrete material models for the purpose of keeping internal energies constant and independent of mesh size is not fully working in concrete models. Fracture energies found to be mesh dependent and for CSCM, the analysis converged at a larger element that had sufficient area to dissipate energy. Mesh regularisation was found to be functioning better in K&C model particularly for mesh elements larger than 25.4mm. In the direct HPB simulation, mesh elements were smaller than 25.4mm (from 1mm to 10mm), even though the implemented regularisation is for mesh elements above 25.4mm, it is still found to be working better for K&C compared to the CSCM.

- Both material models simulate crack through energy dissipation, therefore mesh element had to be large enough to accommodate fracture process zone (FPZ). Particularly the FPZ area is much larger in the shaking table simulations. Bazant and Oh (1983); Denarie et al. (2001); Dai et al. (2019) determined the optimum size of the fracture zone to be three times of the maximum aggregate size used in the concrete mixture. The model with such element size works well for the shaking table simulations.

- Erosion is a numerical trick to prevent mesh tangling in the impacting specimens. It is represented by element deletion known as “erosion”. It is a very important part of concrete modelling as choosing an unsuitable value can cause instability in the simulation. The failure pattern produced by erosion in a simulation is best to be compared against experiments. CSCM with implemented erosion algorithm is much better in resembling real concrete crushing compared to K&C that uses an external erosion algorithm.

- K&C is disadvantaged by the lack of erosion algorithm, therefore *MAT_ADD_EROSION is necessary to be used along with the material model to resemble concrete crushing. In higher impact velocity cases, concrete crushing is less challenging to replicate the failure seen in the experiments compared to the lower impact velocity cases or in the case of shaking table simulation.

- The application of DIF was found unnecessary in the validation of direct HPB simulations due to inertial effect increasing the concrete strength. However, DIF was

found to be influential in the shaking table simulations particularly for earthquakes with higher PGA levels

- In the shaking table simulation, CSCM performed much better than K&C model. The difference between the peak displacements for K&C and the experiments were about 10-15%, and for CSCM was about 5-10%. The difference was due to pre-test cracking in the frame. Concrete shrunk when drying and that caused some initial cracking. The building was then moved onto the shaking table and were examined many times to get the seismic motion input right, and these caused small cracking in the frame. This is also the reason for the differences between structural periods obtained from the tests compared to the numerical simulations.

- Erosion pattern in K&C was unreasonable overall. Values below 0.04 based on maximum principal strain caused excessive removal of elements that led to building failure. Values at 0.04 and above only captured minimal concrete spalling in the bases of the columns. K&C overall was unable to capture concrete failure properly even with the chosen erosion value of 0.07. On the other hand, CSCM was able to capture concrete cracking/crushing and spalling of concrete reasonably well when an erosion value of 1.09 based on maximum principal strain was used.

- In the push-over analysis that was carried out to observe the capability of the material models in resembling the failure response of the two-storey building, it was perceived that CSCM is better suited to demonstrate the real concrete behaviour for simulation of pounding. Erosion in K&C was excessive and damage pattern was unreasonable and led to pre-mature failure of the columns in the building. The failure was expected to occur in the column then in the connections, however it rather occurred excessively in the middle of the columns particularly in the longitudinal direction.

- Erosion must be used with care. Lack of erosion algorithm in the material model causes mesh tangling, on the other hand when used incorrectly it can cause unreasonable responses. If unreasonable value is used or its effect is not examined properly, it can cause instability and make the structure collapse.

- This FE model has laid a foundation for further research on pounding simulation by overcoming the limitations associated with the existing contact models. The explicit FE modelling method proposed here offers significant advantages over the other approaches since the contact can be modelled explicitly with penalty method rather than assuming contact element parameters or spring properties as unrealistic contact parameters are the main issue with obtaining diverse results from the existing lumped mass models.

- It has been highlighted that there is the lack of experimental work on pounding of concrete buildings. The proposed FE method have to be compared against experimental work on pounding of concrete buildings. Once tests are carried out, the numerical simulation output can be compared against the experimental work and the reliability of this method can be determined. If it is reliable enough to produce realistic results, which is expected to be in the case of the incorporated FE model as in the process of developing the method all the numerical simulations were validated against the experiments and excellent correlation was achieved, the FE model can be used as a foundation model to study the complex behaviour of building pounding. As a result, there is no need to carry out further expensive experiments and the FE model can be used as a reference base model to assess the pounding behaviour of buildings made of different geometries. Researchers do not have to go through all the steps carried out in this thesis to investigate pounding and instead they can directly implement the method in their own model and investigate pounding in detail. The FE model can be either used as it is, or it can be a tool to define more reliable contact parameters such as coefficient of restitution (post impact velocity over initial impact velocity) and contact stiffness (from force-displacement curves obtained from the FE models) and be implemented onto the existing contact models for possibly further assessment/improvements of the existing pounding models.

7.3 Recommendation for future developments

The method proposed in this PhD for simulation of pounding is a proper method that is based on experimental work as well as numerical simulations that have been validated against these tests. Therefore, it is expected that the incorporated FE model that is fundamentally based on real experiments provides results with better accuracy compared to the existing methods for simulating pounding between buildings. This PhD work has shown that FEM can be used for simulation of building pounding and the incorporated FE model is a tool that is available for researchers to study pounding simulation of buildings further. However, the areas that can be further explored are as follow:

- In the current field of pounding/impact simulation, the lack of experimental work on pounding/impact of buildings is very much evident. Many concrete impact studies have been based on very high impact velocity penetration of missiles for defence purposes that involve a different mechanism. Experimental work is required on (1) concrete with low impact velocity, (2) pounding of concrete buildings even small-scale experiment will be very beneficial. Experimental work particularly on pounding of concrete buildings will be very useful as the results of the FE simulations can be compared against the tests.

- Contact parameters such as contact stiffness for a particular pounding case can be calculated from contact force-displacement curve obtained from the incorporated FE simulation and can be implemented onto gap friction elements in FE software such as OpenSees, Sap2000, etc. Comparison can be made between the results of the incorporated FE model with the outcome of the other commercial software.

- Either experimental work or using the incorporated FE model in this PhD, contact between concrete and steel buildings can be studied. Impact of buildings with two different building materials is not explored in the current field of pounding.

- The incorporated FE model in this PhD can be used to study impact of buildings with different geometries. If irregular buildings are of interest, 3D model of that building can be modelled, and torsional effects can also be taken into account.

- Structure-soil interaction can be considered in LS-DYNA. The incorporated FE model of pounding can be used considering foundation/soil effect on pounding of buildings

during earthquake. It can further be compared against experimental tests in the field of soil-structure interaction.

- Finally, the development of a validated FEA model which includes both impact and seismic vibration would offer insights into the mechanisms affecting structural response in pounding scenarios. This would potentially lead to the development of a new generation of fast-running simplified models which could capture the important mechanisms without the need for computationally expensive FEA models. To facilitate that development, while the modelling of concrete-to-concrete impact and seismic vibration have been separately validated here against high quality experimental data, there is a need for such supporting experimental studies of entire structural pounding events.

Bibliography

Abdel Raheem, S.E., Fooly, M.Y.M., Omar, M., Mahmoud, S., 2018. Seismic pounding effects on adjacent buildings in series with different alignment configurations. *Steel and Composite Structures*, 28(3), pp. 289-308

Abdel Raheem, S.E., Fooly, M.Y., Abdel Shafy, A.G., Taha, A.M., Abbas, Y.A. and Abdel Latif, M., 2019. Numerical simulation of potential seismic pounding among adjacent buildings in series. *Bulletin of Earthquake Engineering*, *17*(1), pp.439-471.

Abu-Odeh, A., 2015. Modelling and simulation of bogie impacts on concrete bridge rails using LS-DYNA. [Online] 10th international LS-DYNA user's conference. Available at: https://www.dynalook.com/conferences/international-conf-2008/SimulationTechnology1-2.pdf [accessed 1 April 2019]

Adhikary, S.D., Li, B., Fujikake. K., 2013. Strength and behaviour in shear of reinforced concrete deep beams under dynamic loading conditions. *Nuclear Engineering and Design*. 259(1), pp.14-28

Adhikary, S.D., Li, B., Fujikake. K., 2012. Dynamic behaviour of reinforced concrete beams under varying rates of concentrated loading. *International Journal of Impact Engineering and Design. 47(1),* pp.24-38

Agardh, L., Laine, L., 1999. 3D FE-simulation of high-velocity fragment perforation of reinforced concrete slabs. *International Journal of Impact Engineering, 22 (1),* pp.911-922

Alañón, A., Cerro-Prada, E., Vázquez-Gallo, M.J. and Santos, A.P., 2018. Mesh size effect on finite-element modelling of blast-loaded reinforced concrete slab. *Engineering with Computers*, *34*(4), pp.649-658.

Anagnostopoulos, S.A., 1988. Pounding of buildings in series during earthquakes. *Earthquake Engineering and Structural Dynamics, 16(3),* pp.443-456

Anagnostopoulos, S.A., Spiliopoulos, K.V., 1992. An investigation of earthquake induced pounding between adjacent buildings. *Earthquake Engineering and Structural Dynamics, 21(4),* pp.289-302

ANSYS Century Dynamics Inc, 2009. ANSYS AUTODYN V12.0. Explicit Software for Non-linear Dynamics. Theory Manual. Houston, TX: ANSYS.

Athanassiadou, C.J., Penelis, G.G., Kappos, A.J., 1994. Seismic response of adjacent buildings with similar or different dynamic characteristics, *Earthquake Spectra, 10(2),* pp.293-317.

Auyeung, S., Alipour, A., Saini, D., 2019. Performance-based design of Bridge piers under Vehicle collision. *Engineering Structures*. *191(1),* pp.752- 765

Barros, R.C., Khatami, S.M., 2012. An estimation of damping ratio for the numerical study of impact forces between two adjacent concrete buildings subject to pounding. *15th International Conference on Experimental Mechanics*. ICEM15, Portugal

Bažant, Z.P. and Oh, B.H., 1983. Crack band theory for fracture of concrete. *Matériaux et construction*, *16*(3), pp.155-177.

Bentata, N., Bennegadi, M.L., Sereir, Z., Amziane, S., 2020. Experimental and numerical model of CFRP retrofitted concrete beams with intermediate notches subjected to drop-weight impact. *Structural Engineering International. 1,* pp.1-10

Bermejo, M., Santos, A.P. and Goicolea, J.M., 2017. Development of practical finite element models for collapse of reinforced concrete structures and experimental validation. *Shock and Vibration, 2017*.

Bi, K., Hao, H., 2013. Numerical simulation of pounding damage to bridge structures under spatially varying ground motions. *Engineering Structures. 46,* pp.62-76

Bothara, J. K., Jury, R. D., Wheeler, K., Stevens, C., 2008. Seismic Assessment of Buildings in Wellington: Experiences and Challenges. The 14th World Conference on Earthquake Engineering, Beijing, China, October 12-17

Børvik, T., Hopperstad, O.S., Berstad, T., Langseth, M., 2001. A computational model of viscoplasticity and ductile damage for impact and penetration. *European Journal of Mechanics and Solids. 20 (1),* pp.685-712

Brown, T. and Elshaer, A., 2022. Pounding of structures at proximity: A state-of-the-art review. *Journal of Building Engineering. 48(1),* pp.1-32

Bruneau, M., 1998. Performance of steel bridges during the 1995 Hyogoken-Nanbu (Kobe, Japan) earthquake - a North American perspective. *Engineering Structures, 20,* pp.1063–1078

Bruneau, M., Buckle, I., Chang, S., Flores, P., O'Rourke, T., Shinozuka, M., et al, 2000. The Chi-Chi, Taiwan earthquake of September 21, 1999. Reconnaissance report

Bruneau, M., Wilson, J.C. and Tremblay, R., 1996. Performance of steel bridges during the 1995 Hyogo-ken Nanbu (Kobe, Japan) earthquake. *Canadian Journal of Civil Engineering, 23(3),* pp.678-713.

Campbell, S., Powell, G.H. and Prakash, V., 1994. DRAIN-3DX Base program description and user guide. In *Report No. UCB/SEMM-94/07* (p. 1994). University of California Berkley.

CEB-FIP Model Code 90, Comite Europeen du Beton- Federation Internationale de la Precontrainte., 1990 (CEB-FIP Model Code 1990: Design Code, American Society of Civil Engineers, ISBN: 0727716964, August 1993).

Chau, K.T., Wei, X.X., Guo, X., Shen, C.Y., 2003. Experimental and theoretical simulations of seismic poundings between two adjacent structures, *Earthquake Engineering and Structural Dynamics, 1,* pp.1-18

Chaudat, T., Garnier, C., Cvejic, S., Poupin, S., LeCorre, M. and Mahe, M., 2005. Seismic Tests on a Reinforced Concrete Bare Frame with FRP retrofitting" Tests Report. *Ecoleader project*, (2).

Chen, W., Hao, H., Chen, SH., 2015. Numerical analysis of pre-stressed reinforced concrete beam subjected to blast loading. *Materials and Design. 65(1),* pp.662-674

Chenna, R. and Ramancharla, P.K., 2018. Damage assessment due to pounding between adjacent structures with equal and unequal heights. *Journal of Civil Structural Health Monitoring*, *8*(4), pp.635-648.

Chung, C., Lee, J., Jung, R., 2015. Numerical simulations of missile impacts on reinforced concrete plates: IRIS-2010/2012 benchmark project. *Nuclear Engineering and Design.* 295 *(1),* pp.747- 758

Chouw, N., 2002. Influence of soil-structure interaction on pounding response of adjacent buildings due to near-source earthquakes, *JSCE Journal of Applied Mechanics,* pp.543-553

Chouw, N., Hao, H., 2012. Pounding damage to buildings and bridges in the 22 February 2011 Christchurch earthquake. *Int J Prot Struct 3,* pp.123–139.

Chung, C., Lee, J. and Jung, R., 2015. Numerical simulations of missile impacts on reinforced concrete plates: IRIS-2010/2012 benchmark project. *Nuclear Engineering and Design*, *295*, pp.747-758.

Cotsovos, D.M. and Pavlović, M.N., 2008. Numerical investigation of concrete subjected to high rates of uniaxial tensile loading. *International journal of impact engineering*, *35*(5), pp.319-335.

Coughlin, A.M., Musselman, E.S., Schokker, A.J., Linzell, D.G., 2010. Behaviour of portable fibre reinforced concrete vehicle barriers subject to blasts from contact charges. *International Journal of Impact Engineering. 37(1),* pp.521- 529

Crawford, J.E., Malver, L.J., 1997. User's and Theoretical Manual for K&C Concrete Model, Technical report TR-97-53.1, Karagozian & Case, Glendale, CA.

Crawford, J.E., Wu, Y., Choi, H.J., Magallanes, J.M., and Lan, S., 2011. User's manual and documentation for release III of the K&C concrete material model in LS-DYNA, Technical report TR-11-36.6, Karagozian & Case, Glendale, CA

Crozet, V., Politopoulos, I., Chaudat, T., 2019. Shake table tests of structures subject to pounding, *Earthquake Engineering Dynamics. 48*, pp.1156-1173

Csiamerica.com. 2021. Features | Building Analysis and Design | ETABS. [Online] Available at: <https://www.csiamerica.com/products/etabs/features> [Accessed 28 April 2021].

Dai, S., Liu, X. and Nawnit, K., 2019. Experimental study on the fracture process zone characteristics in concrete utilizing DIC and AE methods. *Applied Sciences*, *9*(7), pp.1-12.

Davis, R., 1992. Pounding of buildings modelled by an impact oscillator, *Earthquake Engineering & Structural Dynamics. 21(3)*, pp.253-274

Denarie, E., Saouma, V.E., Iocco, A. and Varelas, D., 2001. Concrete fracture process zone characterization with fiber optics. *Journal of engineering mechanics*, *127*(5), pp. 494-502

Dogan, M., Gumaydin, A., 2009. Pounding of adjacent RC buildings during seismic loads, *Journal of Engineering and Architecture. 22*, pp.129-145

Doroudi, R. and Lavassani, S.H.H., 2021. Connection of coupled buildings: A state-of-the-art review. *Structures*. 33(1), pp. 1299-1326

Elnashai, A.S., Kim, S.J., Yun, G.J., Sidarta, D., 2007. The Yogyakarta earthquake of May 27, 2006. MAE Centre, CD Release 07-02

ETABS features 2020 Available at: https://www.csiamerica.com/products/etabs/features (Accessed: 28 January 2020).

Eurocode. 1998. Design of structures for earthquake resistance - Part 1: General rules, seismic actions and rules for buildings. London: EC8

Fan, W., Shen, D., Huang, X., Sun, Y., 2020. Reinforced concrete bridge structures under barge impacts: FE modelling, dynamic behaviours, and UHPFRC-based strengthening. *Ocean Engineering.* 216 (1), pp.1-17

Favvata, M.J., 2017. Minimum required separation gap for adjacent RC frames with potential inter-story seismic pounding. *Engineering Structures.* 152 (1), pp.643-659

Fatahi, B., Nguyen, Q.V., Xu, R., Sun, W.J., 2018. Three-dimensional response of neighbouring buildings sitting on pile foundations to seismic pounding. *International Journal of Geomechanics.* 18(4), pp.1-25

Filiatrant, A., Wagner, P., Cherry, S., 1996. An experimental study on the seismic pounding of buildings. *Proceedings in Eleventh World Conference on Earthquake Engineering,* Mexico, pp.1-8

Fujikake, K., Li, B. and Soeun, S., 2009. Impact response of reinforced concrete beam and its analytical evaluation. *Journal of structural engineering*, *135*(8), pp.938-950.

Ganel, R., Kochavi, R., Ben-Dor, G., 2016. Analytical and Finite Element Concrete Material Models- Comparison of Blast Response Analysis of One Way Slabs with Experimental Data. *An ACI Technical Publication from Ben-Gurion University of the Negev (BGU).* pp.1-17

Garcia, R., Hajirasouliha, I., and Pilakoutas, K., 2010. Seismic behaviour of deficient RC frames strengthened with CFRP composites. *Engineering Structures*, *32*(10), pp.3075-3085.

Godbole, S., Lam, N., Mafas, M.M.M. and Gad, E., 2021. Pounding of a modular building unit during road transportation. *Journal of Building Engineering*, *36*, p.102120.

GoldSmith, W., 1960. Impact: The Theory and Physical Behaviour of Colliding Solids, Edward Arnold, London, England.

Gomathi, K.A., Rajagopal, A., Reddy, K.S.S., Ramakrishna, B., 2020. Plasticity based material model for concrete subjected to dynamic loadings. International Journal of Impact Engineering. 142(1), pp.1-22

Guo, A., Cui, L., Li, H., 2012. Impact stiffness of the contact-element models for the pounding analysis of highway bridges: Experimental evaluation. *Journal of Earthquake Engineering,* 16(8), pp.1132-1160

Hao, Y., Hao, H. and Li, Z.X., 2010. Numerical analysis of lateral inertial confinement effects on impact test of concrete compressive material properties. *International Journal of Protective Structures*, 1(1), pp.145-167.

He, L.X., Shrestha, B., Hao, H., Bi, K.M, Ren, W.X., 2017. Experimental and three-dimensional finite element method studies on pounding responses of bridge structures subjected to spatially varying ground motions. *Advances in Structural Engineering.* 20(1), pp.105-124

Hong, J., Fang, Q., Chen, L. and Kong, X., 2017. Numerical predictions of concrete slabs under contact explosion by modified K&C material model. *Construction and Building Materials*, *155*, pp.1013-1024

Hun, M., Han, Q., Wen, J., Bai, Y., 2019. Seismic failure of multi-span simply supported RC slab on girder bridge in 2008 Wenchuan earthquake: Case study. *Engineering Failure Analysis.* 95(1), pp.140-153

Hunt, K.H., Crossley, F.R.E., 1975. Coefficient of restitution interpreted as damping in vibro-impact. ASME Journal of Applied Mechanics. 42, pp.440- 445

Hong, J., Fang, Q., Chen, L., Kong, X., 2017. Numerical predictions of concrete slabs under contact explosion by modified K&C material model. *Construction and Building Materials.* 155(1), pp.1013-1024

Ibrion, M., Mokhtari, M., Nadim, F., 2015 Earthquake Disaster Risk Reduction in Iran: Lessons and ‘‘Lessons Learned’’ from Three Large Earthquake Disasters—Tabas 1978, Rudbar 1990, and Bam 2003. *International Journal of Disaster Risk Science.* 6, pp.415-427

Iranian Standard Institution, 1988. Standard 2800: Design of structures against earthquake. 4th edition. Available at: http://dl.omranweb.com/2800-V4.pdf (Accessed: 9 April 2021)

Jaime, M.C., 2011. Numerical Modelling of Rock Cutting and Its Associated Fragmentation Process Using the Finite Element Method. Ph.D. thesis, University of Pittsburgh, Pennsylvania, United States

Jankowski, R., 2005. Non-linear viscoelastic modelling of earthquake-induced structural pounding. *Earthquake Engineering & Structural Dynamics*, 34(6), pp.595-611

Jankowski, R., 2006. Analytical expression between the impact damping ratio and the coefficient of restitution in the non-linear viscoelastic model of structural pounding, Earthquake Engineering and Structural Dynamics, 35, pp.517-524

Jankowski, R., 2007. Theoretical and experimental assessment of parameters for the non-linear viscoelastic model of structural pounding, Journal of theoretical and applied mechanics 45(4), pp.931- 942

Jankowski, R., 2009. Non-linear FEM analysis of earthquake-induced pounding between the main building and the stairway tower of the Olive View Hospital. *Engineering Structures.* 31(1), pp.1851-1864

Jankowski, R., 2010. Experimental study on earthquake-induced pounding between structural elements made of different building materials. *Earthquake Engineering and Structural Dynamics.* 39 (1), pp.343-354

Jankowski, R., Seleemah, A., El-Khoriby, S., Elwardany, H., 2015. Experimental study on pounding between structures during damaging earthquakes, Key Engineering Materials 627, pp.249-252

Jeng, V., Tzeng, W., 2000. Assessment of seismic pounding hazard for Taipei City, Engineering Structures, 22(5), pp.459-471

Jennings P. C., 1971. Engineering features of the San Fernando earthquake of February 9, 1971. EERL Report, No. 71-02. Earthquake Engineering Research Laboratory, California Institute of Technology, California, USA

Jia H.Y, Lan, X.L., Luo, N., Yang, J., Zheng, Sh.X., Zhang., Ch., 2019. Non-linear pounding analysis of multi-span and simply supported beam bridges subjected to strong ground motions. *Shock and Vibration.* 1(1), pp.1-11

Jiang, H., Wang, X. and He, S., 2012. Numerical simulation of impact tests on reinforced concrete beams. *Materials & Design*, *39*, pp.111-120.

Jiang, H. and Zhao, J., 2015. Calibration of the continuous surface cap model for concrete. *Finite Elements in Analysis and Design*, 97(1), pp.1-19.

Jiang, H., Wang, X. and He, S., 2012. Numerical simulation of impact tests on reinforced concrete beams. *Materials & Design*, *39*, pp.111-120.

Johnson, G., Cook, W., 1983. A constitutive model and data for metals subjected to large strains, high strain rates and high temperatures. *Florida Air force Armament Laboratory, pp.*1-7

Kasai, K., Maison, B.F., 1997. Building pounding damage during the 1989 Loma Prieta earthquake, *Engineering Structures*, 19 (3), pp.195-207

Kang, L., Fan, W., Liu, B., Liu, Y., 2021. Numerical efficient analysis of concrete-filled steel tubular columns under lateral impact loading. *Journal of Constructional Steel Research.* 179(1), pp.1-20

Khatiwada, S., 2014. A distributed-mass model with end-compliance effects for simulation of building pounding. Ph.D. thesis, The University of Auckland, Auckland.

Khatiwada, S. Chouw, N., 2014. Limitations in simulation of building pounding in earthquakes, International Journal of Protective Structures 5(2), pp.123-150

Khatiwada, S. Chouw, N., Butterworth, J.W., 2013. Evaluation of numerical pounding models with experimental validation, *Bulletin of the New Zealand Society for Earthquake Engineering* 46(3), pp.117-130

Khoe, Y., Weerheijim, J., 2019. Limitation of smeared crack models for dynamic analysis of concrete. [online] Netherlands, pp.1-14. Available at: <https://www.dynalook.com/conferences/12th-international-ls-dyna-conference/constitutivemodeling19-c.pdf> [Accessed 17 January 2021].

Kim, S.Y., Lee, J., Chung, C., Kim, S.P., Chung, Y.S., Lee, J., Jung, R., 2011. Numerical simulation of missile impacts on reinforced concrete plates- IRIS 2010 Benchmark Test, *IASMiRT.* 21(1), pp.1-8

Kang, H., Kim, J., 2017. Response of a steel column-footing connection subjected to vehicle impact. *Structural Engineering and Mechanics.* 63(1), pp.125- 136

Kong, X., Fang, Q., Chen, L. and Wu, H., 2018. Nonlocal formulation of the modified K&C model to resolve mesh-size dependency of concrete structures subjected to intense dynamic loadings. *International Journal of Impact Engineering*, *122*, pp.318-332.

Levi-Hevroni, D., Kochavi, E., Kofman, B., Gruntman, S. and Sadot, O., 2018. Experimental and numerical investigation on the dynamic increase factor of tensile strength in concrete. *International Journal of Impact Engineering, 114*, pp.93-104.

Li, Q.M. and Meng, H., 2003. About the dynamic strength enhancement of concrete-like materials in a split Hopkinson pressure bar test. *International Journal of solids and structures*, *40* (2), pp.343-360.

Lin, C.C.J., Hung, H.H., Liu, K.Y., Chai, J.F., 2010. Reconnaissance Observation on Bridge Damage Caused by the 2008 Wenchuan (China) Earthquake. *Earthquake Spectra.* 26(4), pp.1057- 1083

Lopez-Almansa, F., Kharazian, A., 2018 New formulation for estimating the damping parameter of the Kelvin-Voigt model for seismic pounding simulation. *Engineering Structures.* 175(1), pp.284-295

LS-DYNA, 2018. Keyword user's manual volume I R10. *Livermore Software Technology LST*, an ANSYS company. [Online]. Available: https://www.dynasupport.com/manuals/ls-dyna-manuals/lsdyna_manual_volume_i_r12.pdf

LS-DYNA, 2018. Keyword user's manual volume II R10. *Livermore Software Technology LST*, an ANSYS company. [Online]. Available: https://www.dynasupport.com/manuals/ls-dyna-manuals/ls dyna_manual_volume_ii_r12.pdf

Lu, X., Tian, Y., Sun, Ch., Zhang, Sh., 2019. Development and application of a high performance triangular shell elements and an explicit algorithm in Open Sees for strongly non-linear analysis. *Computer modelling in engineering and science.* 120(3), pp.561-582

Luccioni, B. and Aráoz, G., 2011. Erosion criteria for frictional materials under blast load. *Mecánica Computacional*, *30*(21), pp.1809-1831.

Ma, G.W., Dong, A. and Li, J., 2006. Modelling strain rate effect for heterogeneous brittle materials: 1st International Conference on Analysis and Design of Structures against explosive and Impact loads, 15-17 Sep., 2006, Tianjin China. Transaction of Tianjin University, 12(Suppl.), pp.70-82

Magallanes, J.M., 2008. Importance of concrete material characterization and modelling to predicting the response of structures to shock and impact loading. *Structures under shock an impact.* 98, pp.241- 250

Magallanes, J.M., Wu, Y., Malvar, L.J. and Crawford, J.E., 2010, June. Recent improvements to release III of the K&C concrete model. In *11th international LS-DYNA Users conference* (pp. 3-37). Livermore Software Technology Corporation Livermore, CA.

Mahin, S.A., Bertero, V.V., Chopra, A.K., Collins, R.G., 1976. Response of the Olive View hospital main building during the San Fernando earthquake. EERC Report No.76-22, Berkeley (USA): Earthquake Engineering Research Centre, University of California

Mahmud, S., 2008. Modified linear viscoelastic model for elimination of the tension force in the linear viscoelastic, the 14th World Conference on Earthquake Engineering. pp.17-18 October; Beijing, China

Maison BF, Kasai K., 1990. Analysis for type of structural pounding. *Journal of Structural Engineering (ASCE)*, 116: pp.957– 977

Malvar, L.J., Crawford, J.E., Wesevich, J.W. and Simons, D., 1997. A plasticity concrete material model for DYNA3D. *International journal of impact engineering*, 19(9-10): pp.847-873.

Malvar, L.J., Crawford, J.E., 1998 Dynamic increase factor. Proceedings of the twenty-eighth DoD explosive safety seminars Orlando, FL. pp.1-17

Mavronicola, E.A., Polycarpou, P.C., Komodromos, P., 2020. Effect of ground motion directionality on the seismic response of the base isolated buildings pounding against adjacent structures. *Engineering Structures.* 207(1), pp.1-12

Mazzoni, S., McKenna, F., Scott, M.H., Fenves, G., Jeremic, B., 2007. OpenSees command language manual. Pacific Earthquake Engineering Research Centre. University of California, Berkeley.

Meyers, M. A., 1994. Dynamic behaviour of materials. John Wiley & Sons, Inc.

Miari, M., Choong, K.K., Jankowski, R., 2019. Seismic pounding between adjacent buildings: Identification of parameters, soil interaction issues and mitigation measures, *Soil Dynamic Earthquake Engineering,* 121, pp.135-150

Moehle, J., Fenves, G., Mayes, R., Moehle, J., Priestley, N., Seible, F., Uang, C.M., Wermer, S., Ascheim, M., 1995. Highway bridges and traffic management. *Earthquake Spectra* 11, pp.287–372

Muthukumar, S., 2003. A contact element approach with hysteresis damping for the analysis and design of pounding in bridges. Ph.D. thesis, Georgia Institute of Technology, Atlanta, United States

Muthukumar, S., DesRoches. R., 2006. A Hertz contact model with non-linear damping for pounding simulation. *Earthquake engineering and structural dynamics,* 35(1), pp.811-828

Murray, Y.D., 2007a. Evaluation of LS-DYNA Concrete Material Model 159. *Report No.FHWA-HRT-05-063,* U.S. Department of Transportation, Federal Highway Administration, McLean, VA.

Murray, Y.D., 2007b. User's Manual for LS-DYNA concrete material model 159. *Report No.FHWA-HRT-05-062,* U.S. Department of Transportation, Federal Highway Administration, McLean, VA.

Olmati, P., Trasborg, P., Naito, C., Sgambi, L., Bontempi, F., 2016. Modelling the response of concrete slabs under blast loading. *Journal of the American Concrete Institute*. 1(1), *pp.*1-19

Oscar, P., Eduardo, R.L., 2008. Impact performance of advanced high strength steel thin-walled columns. *Proceedings of the world congress on engineering Vol II*. 2-4 July, London, UK. pp.1-6

Mahmud, S., 2008. Modified linear viscoelastic model for elimination of the tension force in the linear viscoelastic, the 14th World Conference on Earthquake Engineering. pp.17-18 October; Beijing, China

Pham, A.T., Tan, K.H, Yu, J., 2017b. Numerical investigations on static and dynamic responses of reinforced concrete sub-assemblages under progressive collapse. *Engineering Structures.* 149(1), pp.2-20

Pham, A.T., Lim, N.S. and Tan, K.H., 2017a. Investigations of tensile membrane action in beam-slab systems under progressive collapse subject to different loading configurations and boundary conditions. *Engineering Structures, 150*, pp.520-536.

Priestley M.N, Seible F, Calvi GM., 1996. Seismic design and retrofit of bridges. Wiley, New York

Polycarpou, P.C., Komodromos, P., 2012. A methodology for an efficient three-dimensional (3D) numerical simulation of earthquake-induced pounding of buildings. *15 WCEE Conference proceeding.* January; Nicosia, Cyprus

Rahbari, R., Tyas, A., Davison, J.B., Stoddart, E.P., 2014. Web shear failure of angle-cleat connections loaded at high rates. *Journal of Constructional Steel Research.* 103(1), pp.37-48

Rajaram, C., Kumar, R.P., 2012. Pounding between adjacent buildings: Comparison of Codal Provisions. *The Indian concrete journal.*1 (1), pp.49-59

Ranjan, R., Banerjee, S., Singh, R.K., Banerji, P., 2014. Local impact effects on concrete target due to missle: An empirical and numerical approach. *Annals of Nuclear Energy.* 68(1), pp.262-275

Remennikov, A.M., Kong, S.Y., 2012. Numerical simulation and validation of impact response of axially-restrained steel-concrete-steel sandwich panels. *Composite Structures.* 94(1), pp.3546- 3555

Rosenblueth, E. and Meli, R., 1986. The 1985 Earthquake: Causes and Effects in Mexico City. *Concrete International*, 8, pp.23-24.

Sadiq, M., Yun, Z.X., Rong, P., 2014. Simulation analysis of impact tests of steel plate reinforced concrete and reinforced concrete slabs against aircraft impact and its validation with experimental results. *Nuclear Engineering and Design*. 273 (1), pp.653- 667

Seifrued, W., Schiehlen, W., Eberhard, P., 2010. The role of the coefficient of restitution on impact problems in multi-body dynamics. *Proc. IMechE*, 224, pp.279-306

Saini, D., Shafei, B., 2018. Numerical investigation of CFRP-composite strengthened RC bridge piers against vehicle collision. Proceedings of the transportation research board 97th annual meeting. pp.1-16

Saini, D., Shafei, B., 2019. Concrete constitutive models for low velocity impact simulations. *International journal of impact engineering.* 132 (1), pp.1-13

Saini, D., Shafei, B., 2019. Investigation of concrete-filled steel tube beams strengthened with CFRP against impact loads. *Composite Structure.* 208 (1), pp.744-757

Saini, D., Shafei, B., 2019. Performance of concrete-filled steel tube bridge columns subjected to vehicle collision. *Journal of Bridge Engineering.* 24 (8), pp.1-13

Shi, Y., Li, Z.X. and Hao, H., 2010. A new method for progressive collapse analysis of RC frames under blast loading. *Engineering Structures*, *32*(6), pp.1691-1703.

Shrestha, B., Bi, K., 2016. An overview of the recent research advances in seismic pounding and unseating damages to bridge structures. 2nd Huixian International Forum on Earthquake Engineering for Young Researchers. Beijing, China, August 19-21

Shrestha, B. and Hao, H., 2018. Building pounding damages observed during the 2015 Gorkha earthquake. *Journal of Performance of Constructed Facilities*, *32*(2), p.04018006.

Schwer, L., 2020. Concrete models: Damage & Failure with mesh refinement & regularization.

Schwer, L.E. and Windsor, C.A., 2009. Strain rate induced strength enhancement in concrete: much ado about nothing. In *International Workshop on Structures Response to Impact and Blast* (No. 5-1).

Schwer, L., 2005. Simplified concrete modelling with *MAT_CONCRETE_DAMAGE_REL3. Anwenderforum, Baberg.

Tang, E.K.C., Hao, H., 2010. Numerical simulation of a cable-stayed bridge response to blast loads, part I: Model development and response calculations. *Engineering Structures.* 32(1), pp.3180-3192

Teng, T.L., Chu, Y.A., Chang, F.A., Shen, B.Ch., Cheng, D.Sh., 2008. Development and validation of numerical model of steel fibre reinforced concrete for high-velocity impact. *Computational Materials Science.* 42(1), pp.90-99

Tyas, A., Watson, A.J., 2000. Experimental evidence of Pochammer-Chree strain variations in elastic cylinders. *Experimental Mechanics.* 40(3), pp.331- 337

Vanmier, J.G.M., Pruijssers, A.F., Reinhardt, H.W., Monnier, T., 1991. Load-time response of colliding concrete bodies. *Journal of structural engineering*. 1, pp.354-374

Wang, D.S., Feng, Q.M. and Wang, G.X., 2004. Analysis model of pounding between adjacent bridge girders during earthquakes based on collinear impact between rods [J]. *Engineering Mechanics*, *21*(2), pp.157-166.

Kawashima, K., Watanabe, G., 2004. Effectiveness of cable-restrainer for mitigating rotation of a skewed bridge subjected to strong ground shaking. The 13th World Conference on Earthquake Engineering, Vancouver, Canada, August 1-6, Paper No. 789. Vancouver: University of British Columbia Press.

Weng, Y.H., Qian, K., Fu, F. and Fang, Q., 2020. Numerical investigation on load redistribution capacity of flat slab substructures to resist progressive collapse. *Journal of building engineering*, *29*, pp.101-109.

Wijeyewickrema, A., Bhagat, S., Buddika, H. A. D., Adhikari, R., 2015. Earthquake reconnaissance survey in Nepal of the magnitude 7.8 Gorkha Earthquake of April 25, Department of International Development Engineering Tokyo Institute of Technology.

Wolf, J.P., Skrikerud, P.E., 1980. Mutual pounding of adjacent structures during earthquakes, Nuclear Engineering and Design, 57(2), pp.253-275

Wu, Y., Crawford, J.E., Lan, S. and Magallanes, J.M., 2014, June. Validation studies for concrete constitutive models with blast test data. In *Proc., 13th Int. LS-DYNA® Users Conf., LSTC, Livermore, CA*.

Wu, J., Zhou, Y., Zhang, R., Liu, C., Zhang, Z., 2020. Numerical simulation of reinforced concrete slab subjected to blast loading and the structural damage assessment. Engineering Failure Analysis, pp.118, 1-13

Wu, K.C., Li, B. and Tsai, K.C., 2011. The effects of explosive mass ratio on residual compressive capacity of contact blast damaged composite columns. *Journal of Constructional Steel Research*, *67*(4), pp.602-612.

Xu, K. and Lu, Y., 2006. Numerical simulation study of spallation in reinforced concrete plates subjected to blast loading. *Computers & structures*, 84(5-6), pp.431-438.

Ye, K., Li, L., Zhu, H., 2009(a). A modified Kelvin impact model for pounding simulation of base-isolated building with adjacent structures, *Earthquake Engineering and Engineering Vibration*, 8(3), pp.443-446

Ye, K., Li, L., Zhu, H., 2009(b). A note on the Hertz contact model with non-linear damping for pounding simulation. *Earthquake and Structural Dynamics*, 38(9), pp.1135-1142

Yu, J., Luo, L. and Li, Y., 2018. Numerical study of progressive collapse resistance of RC beam-slab substructures under perimeter column removal scenarios. *Engineering Structures*, *159*, pp.14-27.

Yu, J., Gan, Y.P., Wu, J. and Wu, H., 2019. Effect of concrete masonry infill walls on progressive collapse performance of reinforced concrete infilled frames. *Engineering structures*, 191, pp.179-193.

Zhu P., Abe M., Fujino, Y., 2002. Modelling three-dimensional non-linear seismic performance of elevated bridges with emphasis on pounding of girders. *Earthquake Engineering and Structural Dynamics.* 31(11), pp.1891- 1913.

Zhou, X., Wang, X., Zhang, R. and Zhang, W., 2020. Experimental and numerical simulation studies of RC beams under the actions of equal energy impact loads. *Advances in Civil Engineering*, *2020*, pp.1-14.

APPENDIX A

A. Validation of FE simulations against drop weight impact test on concrete beam

To make the validation process of the FE model more complete, the behaviour of the concrete model (CSCM) has also been examined at element level through a set of drop weight impact tests on reinforced concrete series S1616 carried out by Fujikake et al. (2009) under four different impact velocities of 1.72, 2.425, 3.429, and 4.85 m/s. In these impact tests, a striker with a mass of 400 kg and a hemispherical tip of 180mm in diameter struck a simply supported concrete beam in the centre from different heights of 0.3, 0.6, 1.2, and 2.4m. Test set-up is shown in Figure. A.1.

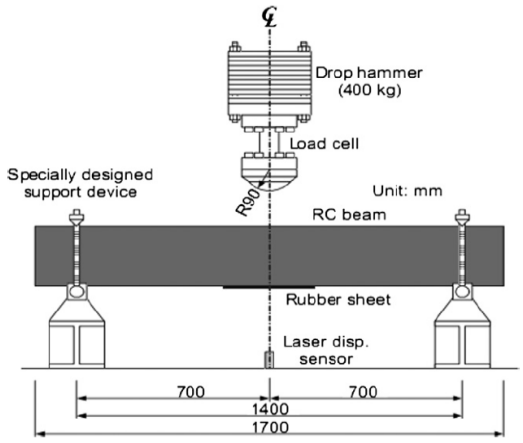

A. 1 Schematic drawing of drop weight impact test (Fujikake et al. 2009)

The concrete beam's length, width, and depth dimensions were 1700 × 150 × 250 mm^3 with concrete compressive strength of 42 MPa with a maximum aggregate size of 10mm. The concrete beam had four longitudinal bars of 16mm, two bars on top and two bars at the bottom, with a yield strength of 426 Mpa and was supported over a span of 1400mm as shown in Figure A. 2. Transversal bars were 10mm in diameter with interval of 75mm with a yield strength of 295 MPa. Concrete properties are illustrated in Table A. 1. The FE model of the drop-weight test is given in Figure A. 3.

APPENDIX A

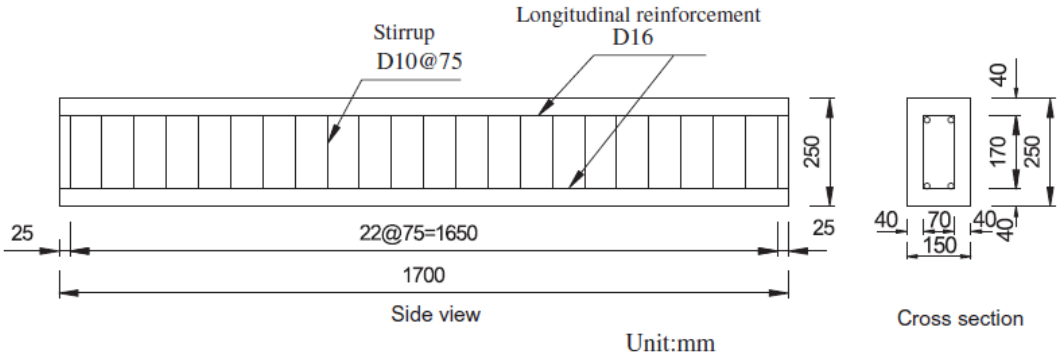

A. 2 Reinforcement detail of the concrete beam (Fujikake et al. 2009)

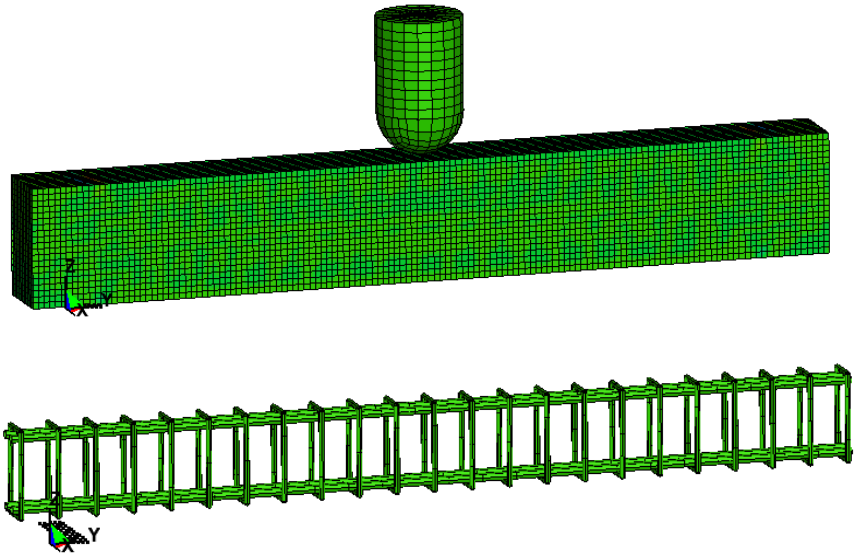

A. 3 FE model of drop-weight impact in LS-DYNA

APPENDIX A

Table A. 1 CSCM long input for concrete strength of 42 MPa

Section 1: Control parameters

MID	159
ρ	2340
NPLOT	1
INCRE	0
IRATE	1
ERODE	1.09
RECOV	10
IRETRC	1
PreD	0

(* Units are Newton, meter, kilogram, and seconds, and Pascal)

Section 2: Stiffness parameters

G_0 Shear Modulus	1.282E+10 (Pascal)
K_0 Bulk Modulus	1.404E+10 (Pascal)

Section 3: Shear surface hardening parameters

N_H	1
C_H	0

Section 4: Yield surface parameters

α	1.5700E+07 (Pascal)
θ	0.3362
λ	1.0510E+07 (Pascal)
β	1.9290E-08 ($Pascal^{-1}$ or 1 m s^2/kg)
α_1	0.7473
θ_1	7.8270E-10 ($Pascal^{-1}$ or 1 m s^2/kg)
λ_1	0.1700
β_1	5.603E-08 ($Pascal^{-1}$ or 1 m s^2/kg)
α_2	0.6600
θ_2	9.439E-10 ($Pascal^{-1}$ or 1 m s^2/kg)
λ_2	0.1600
β_2	5.603E-08 ($Pascal^{-1}$ or 1 m s^2/kg)

Section 5: Cap parameters

R	5.0
X_0	9.724E+07 (Pascal)
W	0.05
D_1	2.5000E-10 ($Pascal^{-1}$)
D_2	3.4920E-19 ($Pascal^{-2}$ or 1 m^2 s^4/kg^2)

Section 6: Damage parameters

b	100
d	0.1
G_{fc}	7.1820E+03 Pascal-meter
G_{ft}	7.1820E+01 Pascal-meter
G_{fs}	7.1820E+01 Pascal-meter
pwrc	5
pwrt	1
pmod	0

Section 7: Rate effects parameters

η_{co}	6.754E-04
N_c	0.78
η_{to}	2.713E-05
N_t	0.480
overc	2.805E+07 (Pascal)
overt	2.805E+07 (Pascal)
S_{rate}	1.0
repow	1.0

APPENDIX A

A.1 Mesh study

The FE model of the concrete beam for test 1 has been meshed in variable element sizes of 4, 6, 8, 10, and 12mm and the mid-span deflection- time histories have been compared and illustrated in Figure A. 4. Mesh size of 12 mm has been chosen to carry out the rest of the validation with.

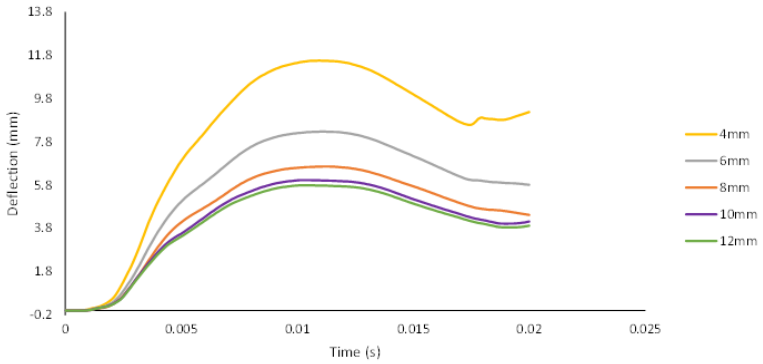

A. 4 Mesh convergence analysis for the FE model

A.2 FE validation results against drop weight experimental tests

Figure A. 5 to Figure A. 8 illustrate comparison between the experimental and FE simulations' deflection and impact force- time histories for 4 different drop heights of 0.15, 0.3, 0.6, and 1.2m under impact velocities of 1.72, 2.43, 3.43, 4.85 m/s. The results show that CSCM is capable of capturing the peak impact forces, the duration of the impact, and the post-peak vibration as well as the deflection of the concrete beam. Once the concrete beam has been impacted by the drop hammer, the mid-span deflection tends to increase with the concrete beam being moved downward and then gradually decreasing after reaching a peak value to form the main curve. After that, the mid span-deflection continue to decay and then increase again after attaining a minimum value forming a small curve as a result of the hammer rebound. This is the result of the concrete beam pushing back the drop weight slightly and then getting pushed back again by the weight until the deflection becomes horizontal. This is more pronounced in higher impact velocities as the higher the velocity the greater the degree of rebounds.

APPENDIX A

(a)

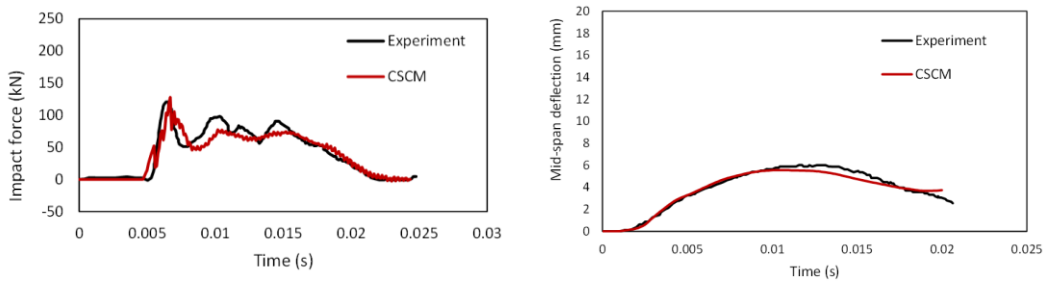

A. 5 Impact response of concrete under drop weight height of 0.15m

(b)

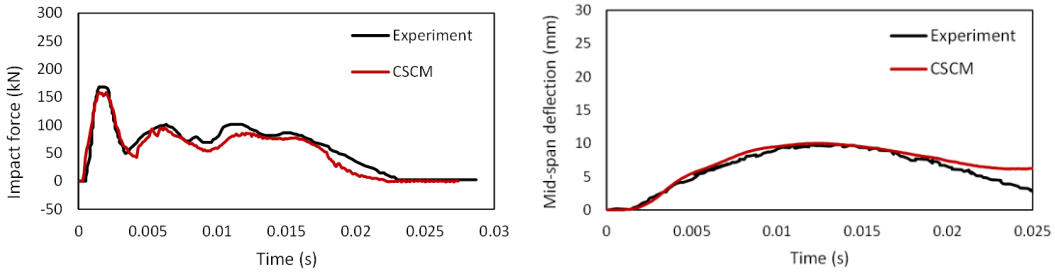

A. 6 Impact response of concrete under drop weight height of 0.3m

(c)

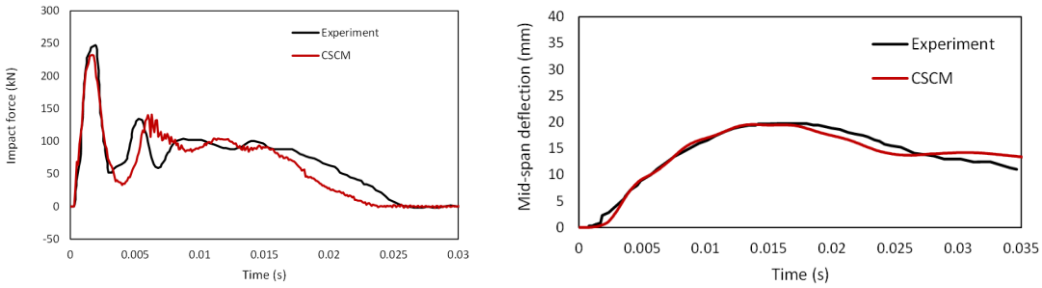

A. 7 Impact response of concrete under drop weight height of 0.6m

(d)

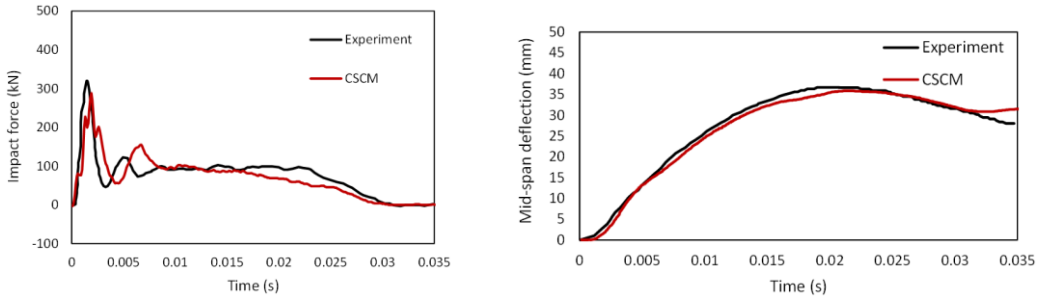

A. 8 Impact response of concrete under drop weight of 1.2m

APPENDIX A

Figure A. 9 depicts plastic deformation occurring in the concrete beam as a result of impact. Comparison of the numerical simulations with the experiments show that CSCM is capable of capturing the impact response of the concrete beams observed in the experiments.

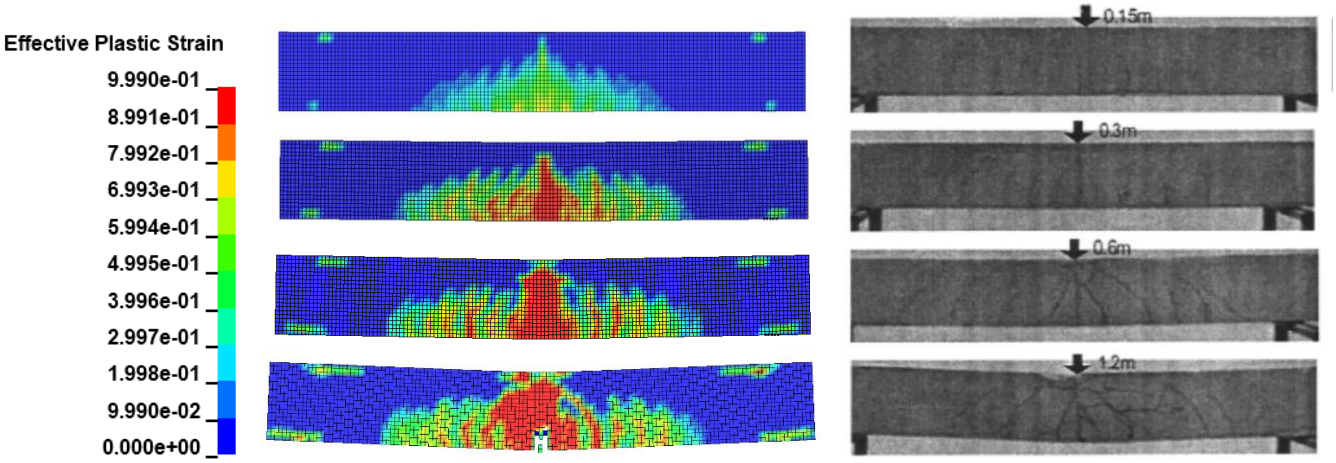

A. 9 Impact response of concrete beam versus FE simulation of the impact response for all drop heights

A.3 Summary

A new validation was carried out to complement the methodology used within this thesis to step by step validate the FE numerical models at material level, element level to structural level. Within this validation, four FE models of a dropping hammer on a concrete beam was simulated and were validated against experimental test carried out by Fujikake et al. (2009) under different impact heights. Force-time and deflection-time histories obtained from the FE model show to be in good agreement with the experiments using CSCM. Within this validation process, it has been observed that the CSCM model is capable of resembling the impact responses of structures/elements including cracking, spalling, and crushing of concrete.